2014

SOIL AND BIOSOLID NANO- AND MACRO-COLLOID PROPERTIES AND CONTAMINANT TRANSPORT BEHAVIOR

Jessique L. Ghezzi
University of Kentucky, jessighezzi@gmail.com

STUDENT AGREEMENT:

I represent that my thesis or dissertation and abstract are my original work. Proper attribution has been given to all outside sources. I understand that I am solely responsible for obtaining any needed copyright permissions. I have obtained needed written permission statement(s) from the owner(s) of each third-party copyrighted matter to be included in my work, allowing electronic distribution (if such use is not permitted by the fair use doctrine) which will be submitted to UKnowledge as Additional File.

I hereby grant to The University of Kentucky and its agents the irrevocable, non-exclusive, and royalty-free license to archive and make accessible my work in whole or in part in all forms of media, now or hereafter known. I agree that the document mentioned above may be made available immediately for worldwide access unless an embargo applies.

I retain all other ownership rights to the copyright of my work. I also retain the right to use in future works (such as articles or books) all or part of my work. I understand that I am free to register the copyright to my work.

REVIEW, APPROVAL AND ACCEPTANCE

The document mentioned above has been reviewed and accepted by the student's advisor, on behalf of the advisory committee, and by the Director of Graduate Studies (DGS), on behalf of the program; we verify that this is the final, approved version of the student's thesis including all changes required by the advisory committee. The undersigned agree to abide by the statements above.

Jessique L. Ghezzi, Student

Dr. A.D. Karathanasis, Major Professor

Dr. Mark Coyne, Director of Graduate Studies

SOIL AND BIOSOLID NANO- AND MACRO-COLLOID PROPERTIES AND CONTAMINANT TRANSPORT BEHAVIOR

DISSERTATION

A dissertation submitted in partial fulfillment of the
requirements for the degree of Doctor of Philosophy
in the College of Agriculture
at the University of Kentucky.

By

Jessique L. Ghezzi

Lexington, Kentucky

Director: Dr. A.D. Karathanasis, Professor of Soil Science

Lexington, Kentucky

ABSTRACT OF DISSERTATION

SOIL AND BIOSOLID NANO- AND MACRO-COLLOID PROPERTIES AND CONTAMINANT TRANSPORT BEHAVIOR

Despite indications that they are potential contaminant transport systems and threats to groundwater quality, very little effort has been invested in comparing contaminant transport behavior of natural environmental nanocolloids and their corresponding macrocolloid fractions in the presence of As, Se, Pb, and Cu contaminants. This study involved physico-chemical, mineralogical, stability and contaminant-transport characterizations of nano- (< 100 nm) and macro-colloids (100-2000 nm) fractionated from three Kentucky soils and one biosolid waste. Particle size was investigated with SEM/TEM and dynamic light scattering. Surface reactivity was estimated using CEC and zeta potential. Mineralogical composition was determined by XRD, FTIR, and thermogravimetric analyses. Sorption isotherms assessed affinities for Cu^{2+}, Pb^{2+}, AsO_3^-, and SeO_4^{-2} contaminants, while settling kinetics experiments of suspensions at 0, 2 and 10 mg/L contaminants determined stability and transportability potential. Undisturbed 18x30 cm KY Ashton Loam soil monoliths were also used for transport experiments, involving infusion of 50 mg L^{-1} colloid suspensions spiked with 2 mg L^{-1} mixed contaminant loads in unsaturated, steady state, unit gradient downward percolation experiments. Overall, nanocolloids exhibited greater stability over corresponding macrocolloids in the presence and absence of contaminants following specific mineralogy trends. Physicochemical characterizations indicated that extensive organic carbon surface coatings and higher Al/Fe:Si ratios may have induced higher stability in the nanocolloid fractions, in spite of some hindrance by nano-aggregation phenomena. In the transport experiments, nanocolloids eluted significantly higher concentrations of colloids, total, and colloid-bound metals than corresponding macrocolloids. Contaminant elutions varied by colloid type, mineralogy and contaminant, with the following sequences: soil-colloids>bio-colloids, smectitic>mixed≥kaolinitic>biosolid, and Se>Pb/Cu≥As. Our findings demonstrate that even though they behave more like nano-aggregates rather than individual nano-particles, nanocolloids may exhibit significantly higher mobility and contaminant transport potential over great distances in subsoil environments than their corresponding macrocolloid fractions.

KEYWORDS: nanocolloid, macrocolloid, biosolid, contaminant transport, nanoparticle

Jessique L. Ghezzi

May 6, 2014

SOIL AND BIOSOLID NANO- AND MACRO-COLLOID PROPERTIES AND CONTAMINANT TRANSPORT BEHAVIOR

By

Jessique L. Ghezzi

A.D. Karathanasis
(Director of Dissertation)

Mark Coyne
(Director of Graduate Studies)

May 6, 2014
(Date)

To Haley, Levi and Grandma Sandy. You've always been my greatest inspiration and motivational force. I love you.

ACKNOWLEDGEMENTS

I have many people to thank. First, I must thank Dr. K for being my fearless leader, you've given me the opportunity of a lifetime and many untold life lessons. You are, and continue to be the best mentor I could have ever asked for, thank you for believing in me and for pushing me to excel. Great thanks are due to my committee members Dr. Matocha, Dr. Unrine, and Dr. Lynn for your counsel and for your generous use of multiple pieces of lab equipment and chemicals. I was a complete pest and you endured my constant questioning with encouragement and a smile. Yvonne Thompson, thank you for untold amounts of help, I couldn't have done this without you! You are unbelievably patient and kind! Thank you to Dr. Wendroth and Jason Walton for allowing me the use of your infiltrometer equipment, without your help my monolith studies couldn't have been completed. Dr. McCulley, Dr. McNear, Joe Kupper, Elizabeth Carlisle and Jim Nelson, thank you also for granting me permission to use your lab equipment, I really appreciate your kindness. Thank you to Martin, Dr. Matocha's lab assistant for your help and assistance. Jim Crutchfield, thank you so much for the generous use of your lab.

Thank you to the Lyman T. Johnson Fellowship for funding me and providing me with the National MANRRS Organization for pushing me outside of my comfort zone and providing me with the professional development skills I needed to succeed.

Thanks are also due to Brian Murphy, the undergrad who assisted me with lab work for a semester. Dr. Mark Coyne, thank you for being the unsung hero of all graduate students. Not many people realize how much you do behind the scenes to ensure their success, please know that the graduate students appreciate your hard work and dedication.

Thank you to my family and friends back home and across the globe for your unwavering support. Grandma Sandy, thank you for being the greatest editor of all time, I love you. Mom and Dad, you keep asking me how many degrees I am going to get and continue to be the proudest, most supportive and amazing parents I could ever ask for, thank you. Haley and Levi, you are my greatest inspiration and the best siblings I could ever ask for, thank you. Last, but certainly not least, thank you to my fellow graduate students. You have been my family, my support and my greatest cheerleaders. I cherish the amazing friendships we've developed over the last 4 years and I look forward to a lifetime of memories.

Table of Contents

List of Tables

List of Figures

Chapter One - General Introduction

It has long been accepted that soil acts as a filtration medium between contaminants at the surface of the geosphere and groundwater. However, despite the role of soils as a filtration device, soil doesn't always remove all contaminants before they reach groundwater supplies. The transport of contaminants to groundwater and groundwater aquifers is a function of multiple processes, some of which include transport through soluble phases, via microorganisms, or through sorption processes onto environmental nanoparticles.

Environmental nanoparticles in general refer to those particles 'having at least one dimension less than 100 nm in size" (Maurice and Hochella, 2008; Theng and Yuan, 2008). Environmental nanoparticles are those nanoparticles formed in natural systems, they may include inorganic and organic nanoparticles such as clay minerals and colloids, metal (hydr)oxides, and humic substances (Theng and Yuan, 2008; Tsao et al., 2011). This study will focus on soil and biosolid derived nanoparticles. Soil nanoparticles are derived from the weathering products of minerals and fall within the clay fraction of soils (Tsao et al., 2011), while biosolid nanoparticles come from human or animal derived waste (Haering and Evanylo, 2006).

Kjaergaard, Hansen et al. (2004), indicated that both surface and subsurface soil colloids have considerable transport potential, depending on their mineralogy and physicochemical properties. While many have characterized, modeled, and predicted the movement of water dispersible colloids (Seta and Karathanasis, 1996; Seta and Karathanasis, 1997; Kaplan, Bertsch et al., 1997; Kjaergaard, Hansen et al., 2004; McCarthy and McKay, 2004), there is a lack of information comparing the stability of macro-sized (0.1-2.0 μm) to nano-sized colloids (<0.1 μm), of differing mineralogy from subsurface horizons, and their potential to transport contaminants such as Se, As, Cu, and Pb. Additionally, there is little to no information available on the role of nano-sized biosolid-derived colloids, despite studies showing larger sized bio-colloids enhancing contaminant transport through soil (Karathanasis, Johnson et al., 2005; Karathanasis and Johnson, 2006; Karathanasis, Johnson et al., 2007; Miller, Karathanasis et al., 2010).

Four contaminants that are of particular concern include arsenic (As), selenium (Se), copper (Cu), and lead (Pb), all of which are considered toxic to humans, wildlife and plants. While both As and Se are considered metalloids, and are usually present as oxy-anions, copper and lead are cationic metals (Signes-Pastor, Burlo et al., 2007; Su and Suarez, 2000). They may be readily transported into groundwater by naturally occurring soil and biosolid colloids.

This study will evaluate and compare the characteristics of soil and biosolid derived nano- (<100 nm) and macro- (100-2,000nm) particles in their natural state, their behavior with associated contaminants, and their transportability through undisturbed soil monoliths. We hypothesize that nanoparticles will have drastically different characteristics, behavior and transportability than macroparticles, including larger and more reactive surface areas coupled with more amorphous materials and highly weathered minerals, greater stability in suspension (in the presence and absence of selected metal contaminants), higher sorption affinities and greater transport potential for contaminants than corresponding macroparticles. Further hypothesis and detail will be discussed in each representative chapter of the study. In chapter one the physico-chemical and mineralogical characteristics of soil and biosolid nano- and macro-colloids

will be compared, in chapter two the stability potential in the absence and presence of As, Pb, Cu and Se will be compared, in chapter three the reactivity and sorptive potential of nano- and macro-colloids is explored and finally, in chapter four, the transport potential of As, Cu, Se and Pb is compared for nano- and macro-colloids.

Hoachella (2008) best described the study of nanoparticles when he theorized that the study of a single nanoparticle with a transmission electron microscope is the same as scaling the entire Earth down to a single light bulb. Nanoparticles are very small – smaller than or similar to the sizes of bacteria and viruses - but these tiny particles uphold the time old saying that dynamite comes in small packages.

Chapter Two - Characterization of Environmental Nano- and Macro-colloid Particles Extracted from Selected Soils and Biosolids

2.1 Introduction

It has long been accepted that soil acts as a filtration medium between contaminants at the surface of the geosphere and groundwater. However, despite the role of the soil as a "filter", a large portion of contaminants still reach groundwater supplies. The transport of contaminants to groundwater aquifers is a function of multiple processes, some of which include soluble phases, microorganisms, or sorption onto environmental colloids (McCarthy and Zachara, 1989; Christian et al., 2008; Karathanasis, 2010). The IUPAC defines colloids as dispersed media with average diameters of 1-1,000 nm (IUPAC, 1997). This definition includes nanoparticles, which by definition are particles with "at least one dimension equal to or less than 100 nm" (IUPAC, 1997; Christian et al., 2008; Hochella et al., 2008; Maurice and Hochella, 2008; Theng and Yuan, 2008). Although the properties and behavior of environmental colloids have been studied extensively, very little information exists on natural environmental nanocolloids and their differences from their corresponding larger macrocolloid fractions.

What differentiates nanoparticles (or nanocolloids) from their larger scale counterparts is that, in addition to and as a function of their smaller size, their mechanical, structural, and chemical characteristics change, making them drastically different from their corresponding macroparticles (or macrocolloids) (Hochella, 2008; Maurice and Hochella, 2008; Theng and Yuan, 2008; Waychunas and Zhang, 2008). In natural systems, soil nanocolloids may include inorganic and organic nanoparticles such as clay minerals and colloids, metal (hydr)oxides, and humic substances (Theng and Yuan, 2008; Karathanasis, 2010; Tsao et al., 2011). Biosolid nanocolloids come from anthropogenic or animal-derived wastes which are introduced into the environment through land application as fertilizers (Haering and Evanylo, 2006). Soil and biosolid nanocolloids are active in many environmental processes, including but not limited to soil genesis, dispersion/flocculation, nutrient cycling, bioavailability, contaminant transport and various remediation processes (Christian et al., 2008; Karathanasis, 2010).

Due to their smaller size there are likely differences in nanoparticle (nanocolloid) physicochemical, morphological, and mineralogical characteristics as compared to their corresponding macroparticles (macrocolloids). The changes in characteristics between nanoparticles (nanocolloids) and their corresponding larger fractions (macrocolloids) may include substantial differences in molecular and electronic structure, mechanical behavior, and chemical reactivity, with the greatest changes occurring at particle sizes of 10 nm or less (Waychunas and Zhang, 2008). It is at these smaller sizes that changes in surface bonding, shape, and energy considerations affect strain, reactivity, phase transformations and structure of the particles (Waychunas and Zhang, 2008). Because of their smaller size, nanocolloids are expected to have larger surface areas and depending on their mineralogy and organic content, higher surface charge and sorption capacities as compared to macrocolloids. This insinuates that nanocolloids may be a greater threat to groundwater quality due to their greater contaminant loading potential as compared to macrocolloids (Christian et al., 2008, Karathanasis, 2010).

On a morphological basis, nanoparticles are typically shaped differently than their larger counterparts due to the size limitation in at least one dimension, resulting in nano-sheets, -rods, or other particle shapes and surface constraints (Hochella, 2008; Hochella et al.,

2008; Maurice and Hochella, 2008). Mineralogically, previous studies performed on soil clays 80-200 nm in size have indicated size based composition trends, including decreased amounts of mica or hydroxyl-interlayered vermiculite, and increased amounts of kaolinite and gibbsite as compared to larger size fractions (Bryant and Dixon, 1963; Dixon, 1966; Kjaergaard et al., 2004a; Kjaergaard et al., 2004b). It is reasonable then, to expect nanoparticles or "nanocolloids" to show size separation trends (i.e. hydroxyl-interlayer vermiculite, mica vs. kaolinitic, gibbsite), as well as to contain more weatherable minerals and lower Si:Al ratios (excluding smectite) than their larger scale counterparts (Bryant and Dixon, 1963; Dixon, 1966; Kretzschmar et al., 1993; Kaplan et al., 1997; Shen, 1999). Studies have also shown that soil colloids with higher Al or Fe content than Si have greater potential to sorb humic acids to their surfaces, and will display greater reactivity, stability, and mobility potentials (Shen, 1999). Higher quantities of amorphous phases found in the fine-clay fraction (<200 nm) may also contribute to higher chemical reactivity and sorption capacities to nanocolloids over that of their larger sized counterparts (Bryant and Dixon, 1963; Dixon, 1966). The combination of surface constraints, particle morphology, and enhanced chemical reactivity based on mineralogy may drastically alter nanocolloid sorption characteristics as compared to that of their larger size macrocolloid particles.

Since soil colloids have been shown to carry contaminants, they are of particular interest in environmental pollution, water quality, and remediation processes (Kaplan et al., 1993; Ouyang et al., 1996). In the past, environmental colloid research focused on their physico-chemical, mineralogical, and morphological characterization, as well as their mobility, and contaminant transport potential. While it has been well documented that natural colloids derived from soil and biosolid systems are capable of transporting contaminants into surface and ground waters (Kaplan et al., 1993; Ouyang et al., 1996; Kretzschmar et al., 1999; Kjaergaard et al., 2004; McCarthy and McKay, 2004), currently, very little information exists that distinguishes the characteristics and behavior of nano- and macro-colloid sized particles in natural environments. It is anticipated that nanocolloids may have drastically different physical, chemical, morphological and mineralogical characteristics than macrocolloids: (i) physically, nanocolloids are likely to have larger and more reactive surface areas than macrocolloids, (ii) chemically, nanocolloids may have greater chemical reactivity, as evidenced by greater surface charges and exchange capacities than macrocolloids, (iii) morphologically and mineralogically, nanocolloids could contain more amorphous materials and highly weathered minerals than macrocolloids. Therefore, nanocolloids may have a greater potential than macrocolloids to negatively impact groundwater supplies. The objectives of this study were to evaluate and compare differences in physico-chemical, morphological, and mineralogical characteristics of nano- and macro-colloid fractions separated from three soils with diverse mineralogy and one anaerobically digested biosolid waste material.

2.2 Materials and Methods

2.2.1 Colloid Generation

Mineral colloids were generated from Bt horizons of three Kentucky soils of differing mineralogy: Caleast-variant (fine, smectitic, mesic mollic Hapludalf), Tilsit (fine-silty, mixed, mesic Typic Fragiudult), and Trimble (fine-loamy, siliceous, mesic Typic Paleudult), which will be referred to as smectitic, mixed, and kaolinitic, respectively. An

aerobically digested municipal sewage sludge was obtained from Jessamine County, Kentucky and utilized to fractionate the biosolid colloids. To fractionate, 15 grams of moist bulk soil/biosolid sample was mixed with 200 mL of deionized water (resistivity of 1 μΩcm at 25°C) in plastic bottles (without addition of dispersing agent), shaken overnight, followed by 5 minutes of ultrasonification, and then centrifuged. Colloids were fractionated using centrifugation into two size classes (nanocolloids <100 nm and macrocolloids 100-2000 nm) using a Centra GP8R Model 120 centrifuge (ThermoIEC). Centrifugation was performed at 107 RCF for 3.5 minutes to separate the clay fraction from the bulk soil, and then the nanocolloids were separated from the macrocolloids via centrifugation at 4387 RCF for 46 minutes (Karathanasis, 2010; Karathanasis et al., 2005). Stokes law was used to determine centrifugation times with a rotor radius of 170 mm, a speed of 4387 RCF, a density difference from water of 1650 kg m^{-3}, and viscosity of 0.0008904 Pas, while the separation of the clay fraction from the bulk soil was calculated using a rotor radius of 170 mm, using 107 RCF, a density difference of 1650 kg m^{-3}, and viscosity of 0.0008904 Pas.

2.2.2 Particle Size, Morphology, and Surface Area Analysis

A Malvern Instruments Zetasizer Nano ZS (Malvern, United Kingdom) was used to determine intensity weighted mean particle hydrodynamic diameters (z-average diameter) of triplicate sample suspensions with concentrations of 50 mg colloid L^{-1} using dynamic light scattering (173° backscatter analysis method). Primary particle size of nanocolloid crystallites was determined using high resolution transmission electron microscopy (Jeol 2010F, Tokyo, Japan). TEM-EDS grids were prepared with nanocolloids after vortexing 40 mL of 50 mg colloid L^{-1} de-ionized water suspensions, spreading 1 mL aliquots out on parafilm-backing paper, then swabbing a 400 mesh Cu grid (No. 01824 Ted Pella, Redding, CA, USA) through the suspension. Images were collected using a JEOL 2010F electron microscope with an ultra-high resolution pole piece operating at 200keV with a field emission gun attached to an Oxford EDS detector (Zhu and Lu, 2010; Nemeth et al., 2011). Primary particle size of macrocolloid crystallites was determined using scanning electron microscopy (SEM; Hitachi S-4300, Tokyo, Japan) (Zhu and Lu, 2010; Nemeth et al., 2011). SEM-EDS stubs were prepared with macrocolloids after vortexing 40 mL of 2,500 mg colloid L^{-1} de-ionized water suspensions, spreading 1 mL aliquots onto parafilm paper, and then swabbing the carbon tape through the suspension. The carbon tape was then attached to an Al holder and sputter coated with Au/Pd. Images were collected on a Hitachi S-4300 scanning electron microscope equipped with a Princeton Gamma-Tech EDS Microanalysis system (Goldstein et al., 1992; Deng et al., 2009). All samples were dried in a laminar flow hood for 48 hours prior to TEM- or SEM-EDS analysis. The average diameters were calculated using ImageJ software to measure the minimum diameter of 300 representative particles (until the mean and standard deviation stabilized) from three to eight separate representative images of each colloid (ImageJ 1.46r, Wayne Rasband, National Institutes of Health, USA). The morphology of nano- and macro-colloid fractions was evaluated using HRTEM-EDS and SEM-EDS, respectively. Surface area analysis was performed in triplicates on both the nano- and macro-colloids using the Ethylene Glycol Monoethyl Ether (EGME) method (Carter et al., 1965).

2.2.3 Chemical Characterization

Colloid suspension concentrations were determined by oven drying triplicate samples at 100°C for 24 hours. Concentrations allowed for determination of water dispersible colloid (WDC) percentages for each size fraction prior to diluting all suspensions to 50 mg L^{-1} concentrations for further analyses. The electrical conductivity and pH of the nano- and macro-colloid suspensions was determined using a Denver Instruments Model 250 pH*ISE*electrical conductivity meter (Arvada, CO). Electrical conductivities were multiplied by 0.0127 to estimate ionic strength (Griffin and Jurinak, 1973). Triplicate samples of the nano- and macro-colloids were analyzed for cation exchange capacity (CEC) using an adapted version of the ammonium acetate method (where ratios of reagents were adapted to reflect the 50 mg L^{-1} colloid concentrations) and reported as a sum of the base cations Ca^{2+}, Mg^{2+}, K^{+}, and Na^{+}. The base cation concentrations were analyzed with a Varian Spectr AA 50B atomic absorption spectrometer (NRCS, 1996). Organic Carbon was derived by subtracting dissolved organic carbon from total carbon as measured on a Flash EA 1112 Series NC Soil Analyzer (Thermo Electron Corporation) with a Mettler Toledo MX5 microbalance. Due to low pH conditions and the typical absence of carbonates in the region, inorganic carbon contributions were assumed to be minimal. Surface and point of zero charge (PZC) analyses were accomplished by converting electrophoretic mobility measurements taken on a Malvern Zetasizer Nano ZS to zeta potentials using the Smoluchowski approximation. Zeta potentials were measured on suspensions with a 0.001M NaCl background electrolyte where pH was adjusted to 4, 6, 8, and 10 using 0.01N NaOH and HCl (Malvern, United Kingdom).

2.2.4 Mineralogical Characterization

A combination of X-ray diffraction (XRD), Thermogravimetric analysis (TG), and Diffuse reflectance infrared Fourier-transform (DRIFT) spectroscopy was used for mineralogical characterization. For XRD analysis, K, Mg, and Mg-glycerol saturated samples were collected on glass slides and analyzed on a Philips PW 1840 diffractometer and PW 1729 x-ray generator (Mahwah, NJ) fitted with a cobalt X-ray tube and run at 40 kV and 30 mA using a Bragg-Bretano design goniometer at a scanning rate of 0.05°2θ per minute from 2° to 40° with a scattering slit of 0.1°. Philips Automated Powder Diffraction software (version 3.5B) was used to analyze the XRD patterns (Mahwah, NJ). K-saturated slides underwent heat treatments to verify the presence of kaolinite, as well as to differentiate hydroxy-interlayered minerals from smectite and vermiculite. Mg-saturated colloids were also used for TG analysis on a Thermal Analyst 2000 (TA Instruments) equipped with a 951 Thermogravimetric Analyzer (DuPont Instruments) with a heating rate of 20˚C/min under N_2 atmosphere (Karathanasis et al., 2005; Karathanasis, 2008). TG Analysis was performed using the General DuPont 2000 software program (version 4.1C, DuPont Instruments). The TG Analysis was used to verify the presence of kaolinite, as well as goethite and gibbsite, and to compliment quantification interpretations derived from the XRD patterns (Karathanasis et al., 2005; Karathanasis, 2008). DRIFT spectroscopy was used for mineralogical characterization of the macro- and nano-colloids and their complexes with soil organic matter (White, 1971; Farmer, 1974; Madejova, 2003; Deng et al., 2009). DRIFT spectroscopy was performed on a Nicolet 6700 FT-IR Model spectrometer with a Thermo Fisher Smart Collector Diffuse Reflectance accessory, using a 600-4000 cm^{-1} reciprocal range obtained at 4 reciprocal cm^{-1} resolution, with the co-addition of 200 scans using a liquid N_2 cooled

MCT detector. The DRIFT samples were prepared by homogenizing oven-dried colloids combined with spectroscopic grade KBr at a 5% ratio, then poured into a sample cup of about 1 mm depth and 3mm diameter to obtain random orientation. The OMNIC32 software (Thermo Electron Corporation, Madison, WI) was used to analyze spectra obtained from the nano- and macro-colloids.

2.2.5 Statistical Analysis

The accepted error levels for all duplicate and triplicate measurements were ≤ 15%. Significant differences between means were tested using Analysis of Variance (ANOVA) (SAS PROC GLM) and Fisher's protected least significant difference test (LSD) in SAS 9.3 (SAS Institute Inc., Cary, NC, USA). The statistical significance level used was $\alpha = 0.05$.

2.3 Results and Discussion

2.3.1 Particle Size and Surface Area Analysis

The average intensity weighted (Z-average) hydrodynamic diameter (d_h) of nanocolloid particles measured by DLS was nearly double the ideal maximum size 100 nm for the mineral fractions (regardless of mineralogy), and 3.5 times greater for the biosolid fractions (Table 2.1). This may suggest incomplete separation of nano-sized particles but it may also reflect on the diversity of the shape of the particles. Environmental nanoparticles are seldom spherical and occur in a variety of shapes (Hochella et al., 2008). Considering that nanoparticles by definition have a size range of < 100 nm in at least one dimension, they may have sizes > 100 nm in other dimensions. Since the DLS measures the intensity weighted average, the calculated hydrodynamic diameter represents the average size of the particles. This explanation was supported by TEM analysis indicating the majority of individual nanoparticles to be in the < 100 nm size range. This does not preclude some limited aggregation that may have occurred after centrifugation, particularly with the biosolid fraction. Even a small mass of aggregates in this case may have large effects on the intensity weighted d_h because it is heavily weighted towards the larger size particles (Kretzschmar et al., 1999; Kjaergaard et al., 2004). Dynamic light scattering analysis of macrocolloid mineral particles indicated Z-average d_h between 487-596 nm, with the smaller size representing smectitic mineralogy (Table 2.1). Biosolid macrocolloid particles averaged larger d_h than the mineral counterparts, potentially reflecting aggregation through organic ligand interactions (Table 2.1).

A significant finding of the SEM/TEM analysis was that a considerable number of macrocolloid particles had nanoparticles adhered onto their surfaces (Fig. 2.1). This observation may insinuate that the initial separation of nano- and macro-colloid fractions via centrifugation without a dispersive agent may have been inadequate for lack of effective dispersion. SEM/TEM images showed a variety of platy or rod-like images suggesting that the spherical particle shape assumption used by Stokes law would obviously obscure size separation via centrifugation (Fig. 2.1 and 2.2). The use of a dispersing agent to induce further dispersion was purposely avoided in order to better represent natural conditions and eliminate artifacts.

Table 2.1. Physical and chemical characteristics of nano- and macro-colloids

Properties	Colloids							
	Smectitic		Mixed		Kaolinitic		Biosolid	
Size Class	Macro	Nano	Macro	Nano	Macro	Nano	Macro	Nano
DLS † Mean Hydrodynamic Diameter (d_h) ±SD ‡ (nm)	487± 10	181±3	596± 21	205±4	545±25	187±4	4456±599	353±8
SEM/TEM ¶ Mean Smallest Particle Size ±SD ‡ (nm)	328±144	37±13	549±394	7±5	288±184	41±19	363±338	50±19
Surface Area ($m^2\ g^{-1}$) ±SD ‡	708±137	879±76	420±105	466±10	333±37	389±44	1674±70	1303±63
% Water Dispersible Colloid Recovered from Bulk Sample	33.41	0.67	37.17	0.33	11.00	0.07	4.95	0.03
Electrical Conductivity (mmhos cm^{-1})	$3.93x10^{-3}$	$6.07x10^{-3}$	$2.91x10^{-3}$	$3.09x10^{-2}$	$2.87x10^{-3}$	$3.80x10^{-3}$	$1.56x10^{-2}$	$4.69x10^{-2}$
Ionic Strength § (mol L^{-1})	$4.99x10^{-5}$	$7.71x10^{-5}$	$3.70x10^{-5}$	$3.92x10^{-4}$	$3.64x10^{-5}$	$4.83x10^{-5}$	$1.97x10^{-4}$	$5.96x10^{-4}$
Natural pH	4.92	5.12	5.07	4.92	4.91	5.38	5.39	5.25
CEC ($cmol_c\ kg^{-1}$) #	35.05±12.84	42.19±15.12	8.89±1.62	10.51±1.67	6.94±1.85	13.12±2.84	37.61±14.85	70.99±22.98
Ca^{2+} ($cmol_c\ kg^{-1}$)	27.60	32.64	3.80	4.00	4.40	7.12	31.60	51.68
Mg^{2+} ($cmol_c\ kg^{-1}$)	6.27	8.00	3.40	3.47	1.60	3.73	3.60	12.13
K^{+} ($cmol_c\ kg^{-1}$)	0.57	0.78	1.15	2.80	0.45	1.23	1.64	3.98
Na^{+} ($cmol_c\ kg^{-1}$)	0.61	0.77	0.54	0.24	0.49	1.04	0.77	3.20
SAR ††	0.15	0.17	0.28	0.12	0.28	0.45	0.18	0.57
OC (mg kg^{-1}) ‡‡	658	897	645	774	430	647	1.3K	16K
N (mg kg^{-1}) §§	228	332	315	612	230	282	1.5K	62K

† DLS = Dynamic Light Scattering was used to measure the mean intensity weighted hydrodynamic diameters (z-average diameter, d_h).

‡ SD = Standard Deviation was calculated based on the averages of duplicate or triplicate measurements (see Methods section).

§ Ionic Strength (IS) = Estimated using Griffin and Jurinak's equation where IS (mol L^{-1}) = 0.0127 x Electrical Conductivity (millimhos cm^{-1}) (1973).

¶ SEM = Scanning Electron Microscopy, TEM= Transmission Electron Microscopy data represent the average smallest dimension of 300 representative particles from three to eight images of each size fraction as measured until the average and standard deviation values had less than 10% variation.

CEC = Cation Exchange Capacity by sum of cations.

†† SAR = Sodium Adsorption Ratio

‡‡ OC = Organic Carbon was derived by subtracting dissolved organic carbon from total carbon measurements. Due to low pH conditions and the typical absence of carbonates in the region, Inorganic carbon contributions were assumed to be minimal.

§§ N = Nitrogen

Figure 2.1. SEM Images of the a) smectitic, b) mixed, c) kaolinitic, and d) biosolid macrocolloid aggregates.

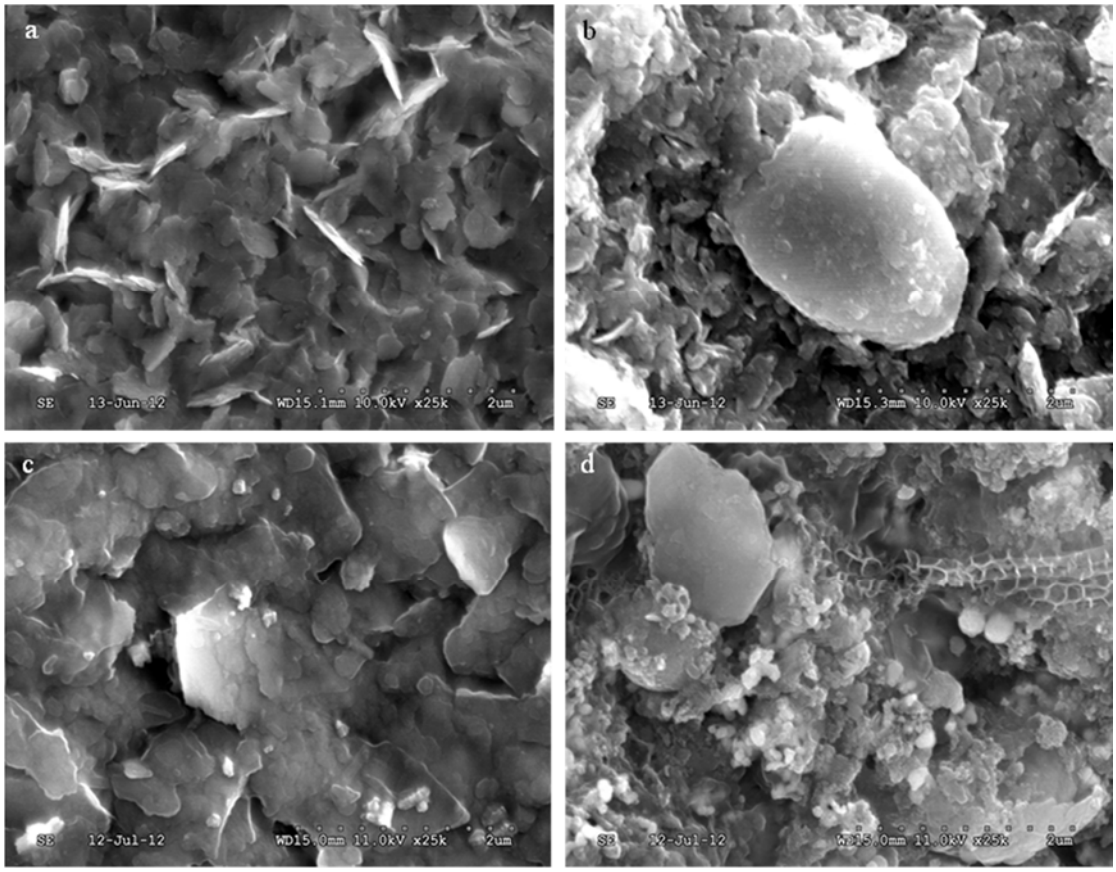

Figure 2.1. TEM images of a) smectitic nanocolloids (Fe-interbedded), b) mixed nanocolloid aggregates (HIV/vermiculite and Fe-interbedded), c) hexagonal kaolinitic particles (Fe-interbedded), and d) a biosolid nanocolloid aggregate.

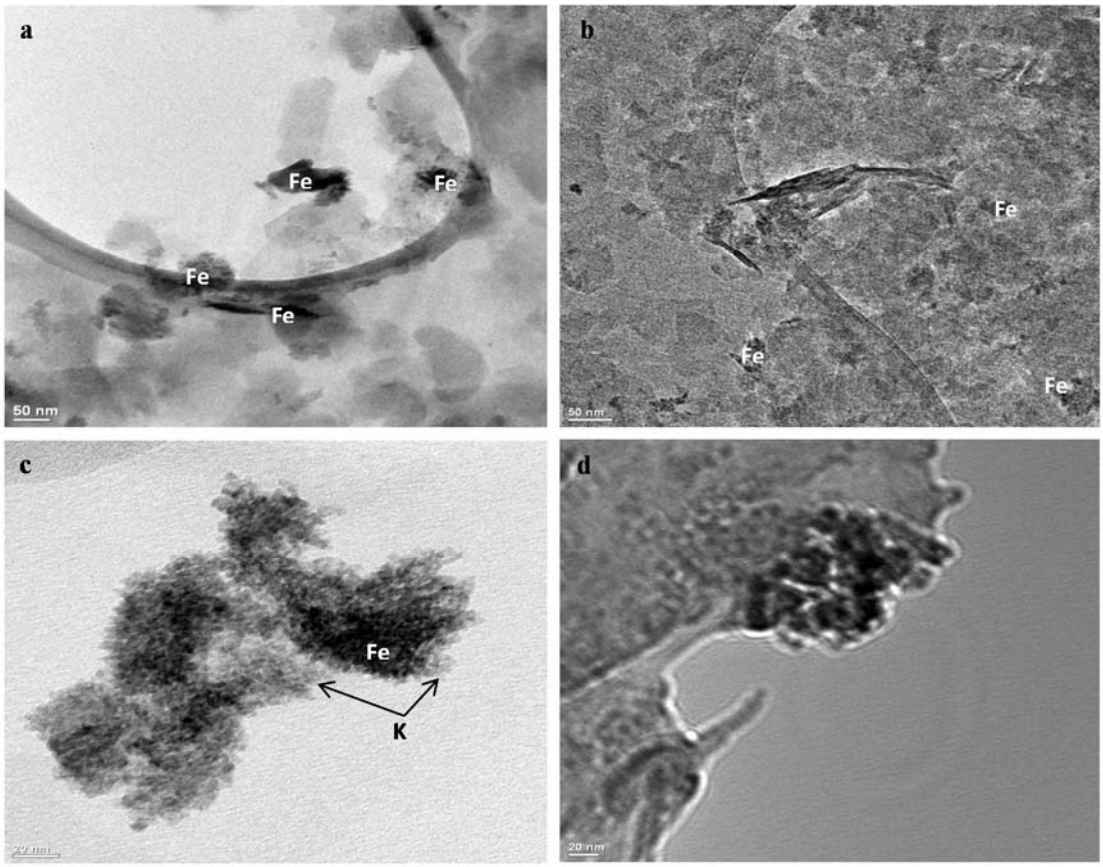

The adhesion of nanoparticles onto colloid surfaces may have also obscured the mineralogical composition of macrocolloid fractions due to segregation phenomena, and enhanced their surface reactivity and sorption capacity (Table 2.1). Particle size analysis by TEM indicated the majority of nanoparticles to have a smaller size range dimension of 7 to 50 nm, while SEM of the macrocolloid fractions showed a range between 288 and 549 nm (Table 2.1, Fig. 2.2). These observations confirm that the centrifugation based primary particle size estimates may have been somewhat misleading even though some aggregation impacts may not be discounted.

In spite of the adhesion of some nanoparticles onto macrocolloid surfaces, the mineral nanocolloids exhibited overall greater surface area than the macrocolloids (Table 2.1). The surface areas measured varied amongst colloid type, with the largest values associated with the biosolid, followed by the smectitic, mixed, and kaolinitic colloids (Table 2.1). The large surface area of the biosolid colloids is apparently associated more with the extent of organic functional groups and acids associated with their composition rather than their size. Smectitic mineralogies typically have greater surface availability than kaolinitic or mixed mineralogies due to the larger percentage of expanding 2:1 minerals present (Carter et al., 1986).

2.3.2 Morphological Characteristics

The morphology of the smectitic macrocolloids was typical of montmorillonite, showing a honeycomb like appearance with edge-face interactions in the SEM images (Fig. 2.1a). The TEM-EDS data from the smectitic nanocolloids also showed an increase in iron minerals (Fig. 2.2a) as opposed to their larger macrocolloid counterparts (Zhu and Lu, 2010). The mixed mineralogy macrocolloids also showed some aggregated honeycomb morphology, but mostly granulated platy clusters in SEM images (Fig. 2.1b). The TEM images of the mixed mineralogy nanocolloids showed multiple particle shapes ranging from tubes/rods to plates and hexagons, suggesting increased shape deformation with decreasing size (Fig. 2.2b). Similar images were shown by Nemeth et al. (2011) for HIV with associated iron minerals. The SEM images of the kaolinitic macrocolloids showed the typical hexagonal shapes displayed by kaolinitic minerals (Fig. 2.1c). Kaolinitic nanocolloid TEM images involved much smaller hexagonal shapes with noted increases in iron minerals embedded within and binding the hexagonal aggregates (Fig. 2.1c) (Zhu and Lu, 2010). SEM images of biosolid macrocolloids included mainly aggregated organic material in various forms coating the surfaces of quartz grains (Fig. 2.1d), while TEM images of the biosolid nanocolloids showed aggregated organic material, with much more dissolution of particle shape and less sample integrity (Fig. 2.2d). Overall, the macrocolloids appeared to have better crystallinity and shape integrity than the nanocolloids. Similar findings were reported by Zhu and Lu (2010), who also found increases of iron minerals in nanoparticles as opposed to larger size mineral classes. The TEM images in this study also showed nanocolloid structures with increased interlayering and disorder in their structures and embedded iron minerals (Fig. 2.3) (Zhu and Lu, 2010) that may cause greater shape and surface constraints in the nanocolloids as compared to the macrocolloids (Maurice and Hochella, 2008).

Figure 2.2. TEM images of the a) montmorillonite and b) mixed nanocolloids showing some disorder of atoms, and the c) kaolinitic nanocolloids showing hexagonal morphology.

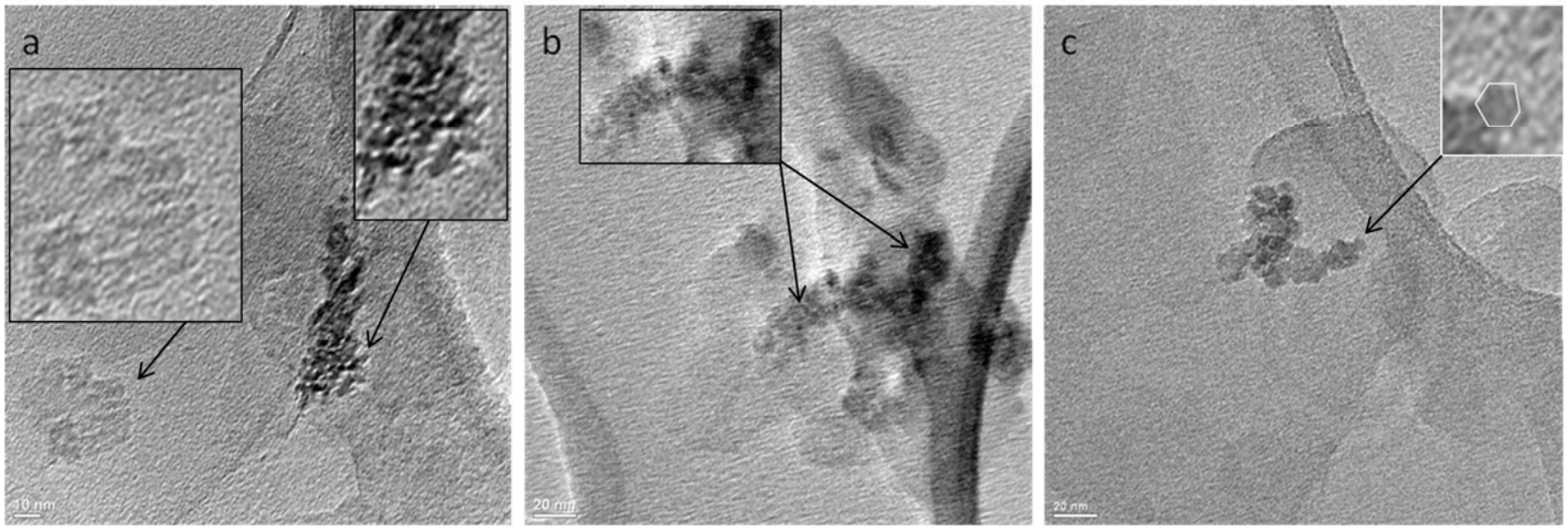

2.3.3 Chemical Characteristics

2.3.3.1 Characteristics of Water Dispersible Colloids

The percentage of water dispersible colloids (WDC) recovered from the bulk Bt horizon samples indicated greater quantities of macro- WDC than nano- WDC in all three soil types (Table 2.1). This agrees with Kjaergaard et al. (2004), who fractionated two size classes of WDC, <0.2 μm and 0.2-2.0 μm, and recovered greater amounts of WDC in the latter. The mixed and smectitic colloids produced greater amounts of WDC when compared with kaolinitic colloids (Table 2.1). This indicates the important role of clay mineralogy in dictating WDC content. Past studies have noted that soils with increasing amounts of kaolinite are less prone to disperse (Seta and Karathanasis, 1996). The WDC percentages may be useful for predicting the amount of potentially mobile colloids in a soil profile.

The original pH of soil colloids is also an important factor in dictating WDC content, with acidic conditions promoting flocculation (Seta and Karathanasis, 1997). The unadjusted pH of the nanocolloids had a range of 4.92 to 5.38 (mixed and kaolinitic colloids, respectively) and the macrocolloids had a pH range of 4.91 to 5.39 (kaolinitic and biosolid colloids, respectively) (Table 2.1). This relatively narrow range suggests that original pH values did not strongly influence WDC content in the three soil types. Despite low overall electrical conductivity (EC) and ionic strength (IS) values (all values below $5x10^{-3}$ mmhos cm^{-1} and $6x10^{-4}$ mol L^{-1}, respectively), the EC and IS values for the nanocolloids were higher than that of their corresponding macrocolloids, with the biosolid colloids showing greater EC and IS suspensions than the mineral colloids (Table 2.1). The higher ionic strengths for each of nanocolloids might have contributed to the lower amounts of WDC recovered when compared to the macrocolloids. Higher ionic strength tends to promote flocculation rather than dispersion (Hesterberg and Page, 1990).

The nanocolloids exhibited greater cation exchange capacity than did the macrocolloids, likely due to their smaller particle size and greater surface area (Table 2.1). The smectitic colloids had the highest CEC amongst the mineral colloids, as expected, followed by the mixed mineralogy and the kaolinitic colloids (Table 2.1). The biosolid colloids exhibited the greatest CEC as compared to the mineral colloids, likely due to their higher organic carbon content. At their natural pH, or the pH measured in suspension without any chemical adjustments, there were larger exchangeable Ca^{2+} and Mg^{2+} concentrations in the nanocolloids than in their corresponding macrocolloid fractions (Table 2.1). The presence of these divalent cations might be an additional reason why nanocolloids were less dispersible than the macrocolloids, as divalent cations such as Ca^{2+} promote flocculation (Kjaergaard et al., 2004).

The nanocolloids had greater organic carbon (OC) and nitrogen content than did the macrocolloids, with OC decreasing in the following order:
biosolid>smectitic>mixed>kaolinitic (Table 2.1). The impact of OC on WDC content is not straightforward; some studies show a positive correlation between OC and WDC content (Kaplan et al., 1993; Kaplan et al., 1997; Kjaergaard et al., 2004; Christian et al., 2008; Hassellov and Von der Kammer, 2008; Ottofuelling et al., 2011) whereas others have reported weak correlations (Seta and Karathanasis, 1996). Given that WDC in the nanocolloid fraction was always lower than that of the corresponding macrocolloids implies that OC might be promoting flocculation rather than dispersion.

2.3.3.2 Zeta Potential

Nano- and macrocolloids exhibited negative zeta potentials which became more negative with an increase in pH from all three soil types (Fig. 2.4). The mineral nanocolloid zeta potentials were more negative than their corresponding macrocolloids, particularly as pH increased above 6 for the smectitic and mixed soil types. The kaolinitic nanocolloids showed more negative zeta potentials than the macrocolloids across the entire pH range (Fig. 2.4c). Assuming that zeta potential measurements approximate the charge residing in the diffuse layer of the electrical double layer (Sposito, 1984), our results indicate that all colloids bear net negative surface charge. Thus, a more negative zeta potential with increasing pH is ascribed to the deprotonation of edge sites on phyllosilicates, making these sites more negatively charged (Frey and Lagaly, 1979).

Despite the predominance of kaolinite in the macro- and nanocolloid fractions from the kaolinitic soil type, there was never a point where the zeta potential (estimated from particle mobility) was zero (Fig. 2.4c). This suggests that the isoelectric point, defined as the pH of zero mobility (Sposito, 1984; Essington, 2004), is <4. Pure kaolinite exhibits an isoelectric point at pH 4.25 (Carroll-Webb and Walther, 1988). The fact that an isoelectric point was not reached under our experimental conditions for kaolinitic colloids might be due to the presence of other minerals (Table 2.2) and organic carbon (Table 2.1). An isoelectric point was not reached for the smectitic colloids either, which is not surprising given the low values typically reported (< pH 2.5) (Fig. 2.4a).

The increase in negative zeta potential with pH in all colloid types is also due to the presence of organic carbon. Organic carbon has been proposed to coat naturally occurring colloids, imparting negative surface charge and enhancing dispersion (Kaplan et al., 1993; Chorover and Sposito, 1995; Bertsch and Seaman, 1999; Kjaergaard et al., 2004; Christian et al., 2008). Where carboxyl groups are present, an increase in pH promotes deprotonation and would contribute to the negative zeta potentials (Fig. 2.4).

The biosolid colloids showed different trends than the mineral colloids, with the bio-nanocolloids having less negative zeta potentials (-11.60 to -3.30 mV) than their corresponding bio-macrocolloids (-11.7 to -33.0 mV) (Fig. 2.4d). Additionally, the bio-nanocolloids became less negative with increasing pH, while the bio-macrocolloid zeta potentials became more negative with increasing pH (Fig. 2.4d). Organic surface functional groups that may be dominating the bio-macrocolloid zeta potentials are likely carboxyl groups, which offer negative surface charge (depending on the full structural formation) above pH's 2.5 and 6 (Essington, 2004). Overall, the biosolid colloids exhibited more positive zeta potentials than the mineral colloids which might be due to their greater ionic strength (Table 2.1).

Figure 2.3. Nano- and macro-colloid zeta potential as a function of pH (mean values of triplicate soil colloid samples with background electrolyte of 0.001M NaCl). Error bars represent standard deviation between triplicate measurements.

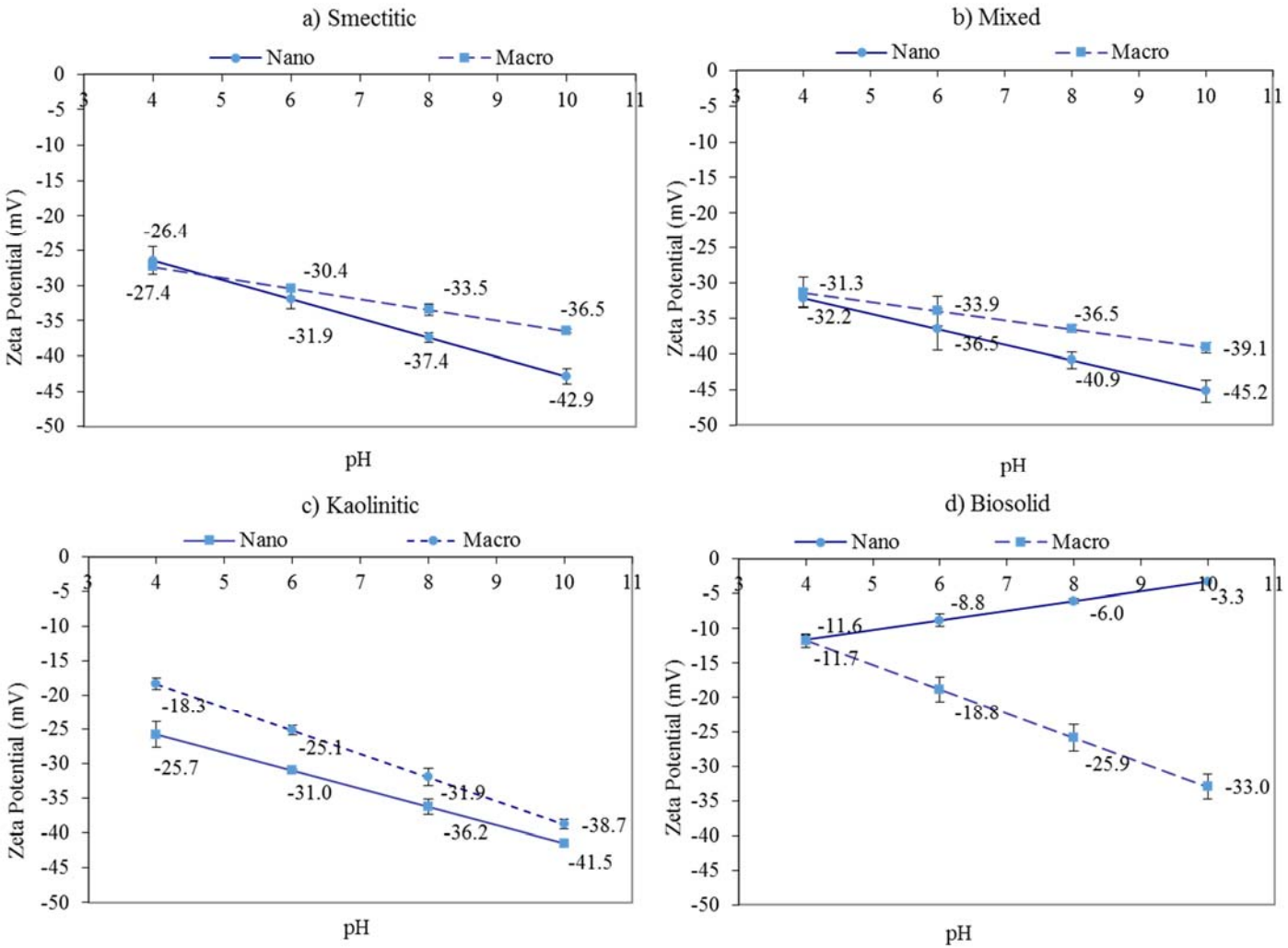

Table 2.2. Mineralogical composition of nano- and macro-colloids

Properties	Colloids							
	Smectitic		Mixed		Kaolinitic		Biosolid	
Size Class	Macro	Nano	Macro	Nano	Macro	Nano	Macro	Nano
Kaolinite (%) ‡	29	30	42	46	52	55	NA §	NA §
Goethite (%) ‡	7	9	5	7	12	15	NA §	NA §
Gibbsite (%) ‡	0	0	0	0	5	6	NA §	NA §
Quartz (%) ‡	6	4	5	3	4	2	NA §	NA §
Mica (%) ‡	10	6	31	30	3	3	NA §	NA §
Smectite (%) ‡	48	51	0	0	0	0	NA §	NA §
MVI ¶ (%) ‡	0	0	7	7	0	0	NA §	NA §
HIV# (%) ‡	0	0	10	7	24	19	NA §	NA §

‡ Mineral percentage as determined using X-Ray Diffraction and Thermogravimentric Data (Karathanasis, 2008).

§ NA = Not Applicable

¶ MVI = Mica-Vermiculite Interstratified

HIV = Hydroxyinterlayered Vermiculite

2.3.4 Mineralogical Characteristics

2.3.4.1 XRD and TG

XRD analysis of the smectitic nano- and macro-colloids indicated montmorillonite to be the dominant mineral (>50%), with 001 peaks at 1.4 nm under Mg treatments, expansion to 1.6 nm under Mg-glycerolated conditions, and a collapse to 1.0 nm with K-heat treatments (Table 2.2). The kaolinitic nano- and macro-colloids contained >50% kaolinite with 001 peaks at 0.7 nm under Mg treatments, no expansion with Mg-glycerolation, and a disappearance of the 0.7 nm peak under K-heat treatments of 550°C (Table 2.2). The mixed mineralogy nano- and macro-colloids contained kaolinite, hydroxyl-interlayered vermiculite (HIV) and mica as the most abundant minerals. The presence of HIV was indicated through the resistance of collapse of the 1.4 nm peak during K heat treatments (100°C heat treatment showed collapse to 1.3 nm, 350°C heat treatment showed collapse to 1.2 nm and 550°C heat treatment showed partial collapse to 1.1 nm with a partial peak resisting collapse at 1.2 nm). The presence of mica was indicated in all samples by peaks at 1.0 nm under all treatment conditions (Table 2.2). TG analysis confirmed XRD compositions and showed slight increases of kaolinite, goethite, and gibbsite in the nanocolloid fractions as compared to the macrocolloids (Table 2.2). Multiple studies have shown mineral fractions with diameters less than 200 nm to be enriched in kaolinite, gibbsite, and Fe oxides, and to exhibit decreases in mica and hydroxyl-interlayered vermiculite than their corresponding larger clay size fractions (Bryant and Dixon, 1963; Dixon, 1966; Kretzschmar et al., 1993; Kaplan et al., 1997) Surprisingly, the combined XRD and TG quantitative analysis showed only slight mineralogical differences between the nano- and macro-colloid fractions, including noted decreases in quartz content, and increases in some phyllosilicate minerals and goethite within the nano-colloid fractions (Table 2.2). The lack of expected drastic differences may be due to adhesion of nanoparticles to macrocolloid surfaces, as evidenced in the SEM images (Fig. 2.1), rendering mineralogical differences inscrutable. However, more significant differences were observed in elemental percentages of individual particles obtained from the EDS data. Generally, nanocolloids had on average 9.25% more Si than Al, and 9% more Fe than Si (LSD=4.92, CV=1.96, α=0.05). The macrocolloids had an average of 17% more Si than Al, and 19% less Fe than Si (LSD=2.74, CV=1.96, α=0.05 as calculated using Fisher's protected LSD). These trends, in addition to increased kaolinite and goethite within the nanocolloid fractions (Table 2.2), insinuate that the nanocolloids have a decreased ratio of Si:Al and an increase in Fe as compared to the macrocolloids, which demonstrates a higher degree of weathering and greater goethite content. The SEM and TEM images also indicated an increase in iron minerals with decreased size as well as a more prominent platy morphology in the nanocolloid fractions (Figs. 2.1 and 2.2). Additionally, the XRD patterns displayed a discernible loss of crystallinity in the nanocolloids as compared to their corresponding macrocolloids, suggesting a higher presence of amorphous and poorly-crystalline materials which may greatly affect both stability and surface reactivity of the colloids (Fig. 2.5).

Figure 2.4. Mg-saturated XRD patterns of the (a, b) smectitic, (c, d) mixed and (e, f) kaolinitic nano- and macro-colloids.

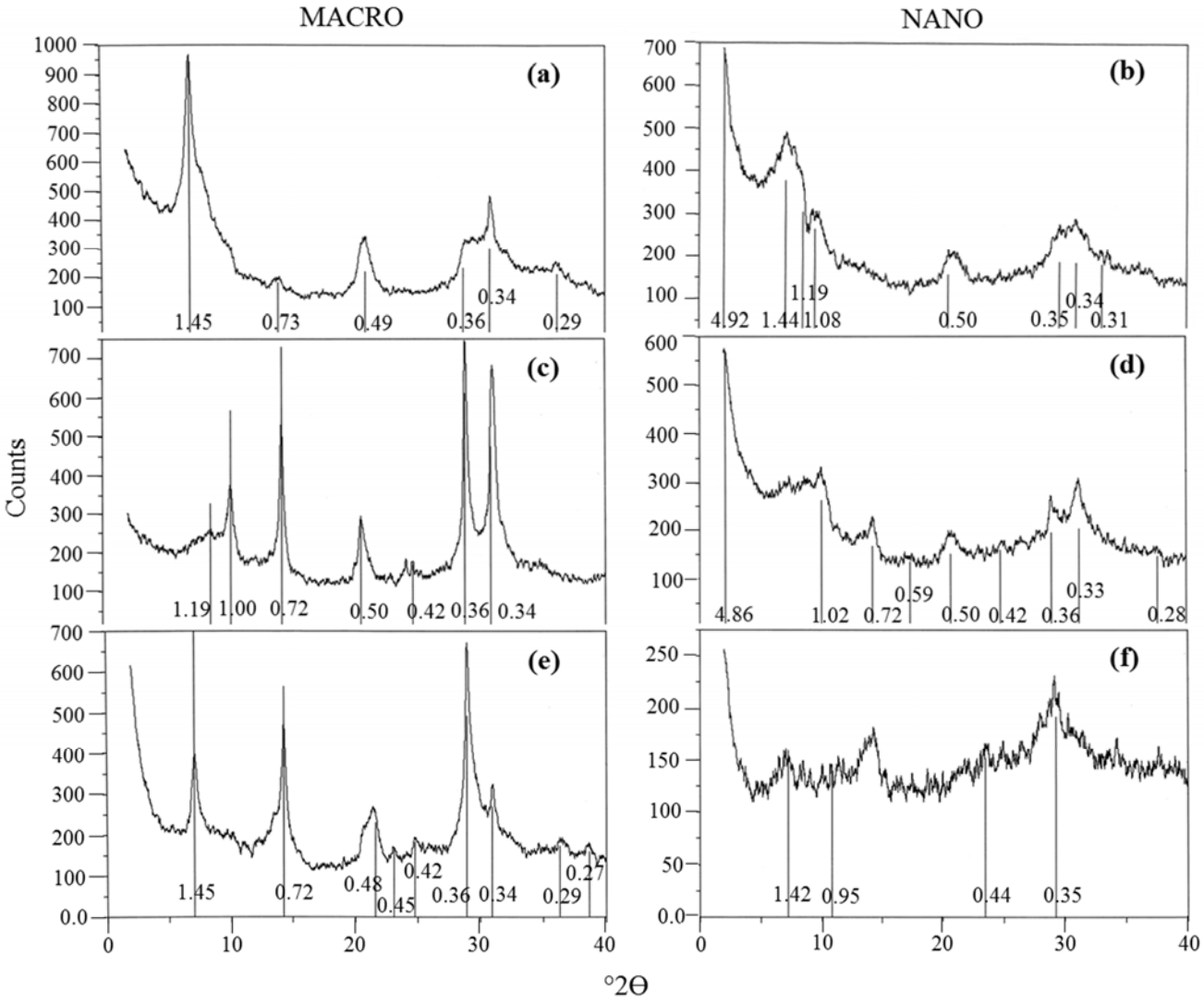

2.3.4.2 IR Characterization

The DRIFT spectra of the mineral nano- and macro-colloids (Figs. 2.6-2.8) indicated the presence of O-H stretching vibrations between 3700 and 3000 cm^{-1}, and O-H bending vibrations from 950 to 650 cm^{-1} due to the presence of structural O-H in minerals (Farmer, 1974). Peaks located between 900 and 1200 cm^{-1} correspond to Si-O stretching. A broad peak centered at 1404 to 1425 cm^{-1} is attributed to the presence of carboxyl groups, while broad peaks at 1634 cm^{-1} are likely a combination of three features; C=O stretching of amide functional groups (referred to amide I), aromatic C=C stretching, and asymmetric COO^- stretching (Baes and Bloom, 1989) (Figs. 2.6-2.8). Additionally, the appearance of a shoulder at 1720 cm^{-1} occurred in each mineral spectra, which is assigned to the C=O stretch of COOH groups (Figs. 2.6-2.8).

DRIFT data from the smectitic nano- and macro-colloids (Fig. 2.6) complimented the XRD findings and confirmed a small amount of kaolinite (3697 cm^{-1}) in both size fractions. The nanocolloid DRIFT pattern also indicated greater amounts of quartz (through stronger intensities at 697, 780 and 800 cm^{-1}), and biotite mica (stronger intensities at 1000 and 750 cm^{-1}; Fig. 2.6) than the macrocolloid pattern (Dupuy and Douay, 2001, Farmer, 1974, Madejova, 2003, Shroeder, 2002, White, 1971). The mixed nano- and macro-colloid DRIFT patterns (Fig. 2.7) indicated kaolinite (3696, 3620, 1008 and 914 cm^{-1}), HIV and vermiculite (combination of 3550 with broad 3400-3200 cm^{-1} peaks), with a noted decrease in the breadth of expression in the nanocolloid pattern for the HIV and vermiculite peaks.

In the kaolinitic nano- and macro-colloids, the presence of kaolinite was confirmed by the O-H stretching peaks located at 3696, 3668, 3650, and 3620 cm^{-1}, while the bands at 3527, 3449, and 3395 cm^{-1} are assigned to gibbsite (Fig. 2.8). In both the nano- and macro-colloids, the peaks at 939 and 914 cm^{-1} correspond to O-H bending vibrations of kaolinite. The broad band around 3200-3400 cm^{-1} in the kaolinitic macrocolloids (Fig. 2.8) also corresponds to an O-H stretching vibration due to phenolic O-H, confirmed by the shoulder at 1266 cm^{-1} which is the diagnostic C-OH stretch of phenolics (Baes and Bloom, 1989), whereas the nanocolloid pattern has the O-H stretching region merged into one broad band centered at roughly 3395 cm^{-1} with appearances of kaolinite peaks as small shoulders at 3696 and 3650 cm^{-1} (Fig. 2.8). In addition, there was appearance of a sharp peak at 1384 cm^{-1} in the nanocolloid pattern, which is assigned to either surface carboxyl-Fe groups (1380 cm^{-1}) or nitrate.

Figure 2.5. Smectitic nano- and macro-colloid FTIR characterization

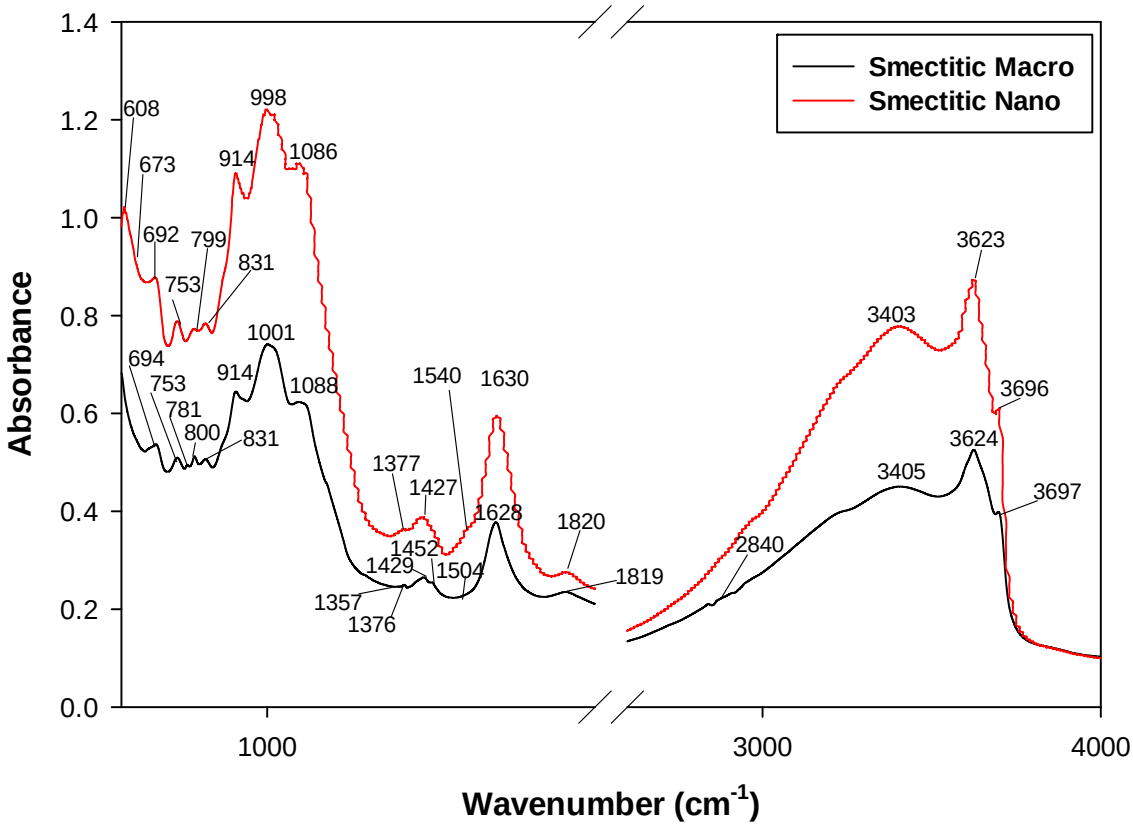

Figure 2.6. Mixed mineralogy nano- and macro-colloid FTIR characterization

.

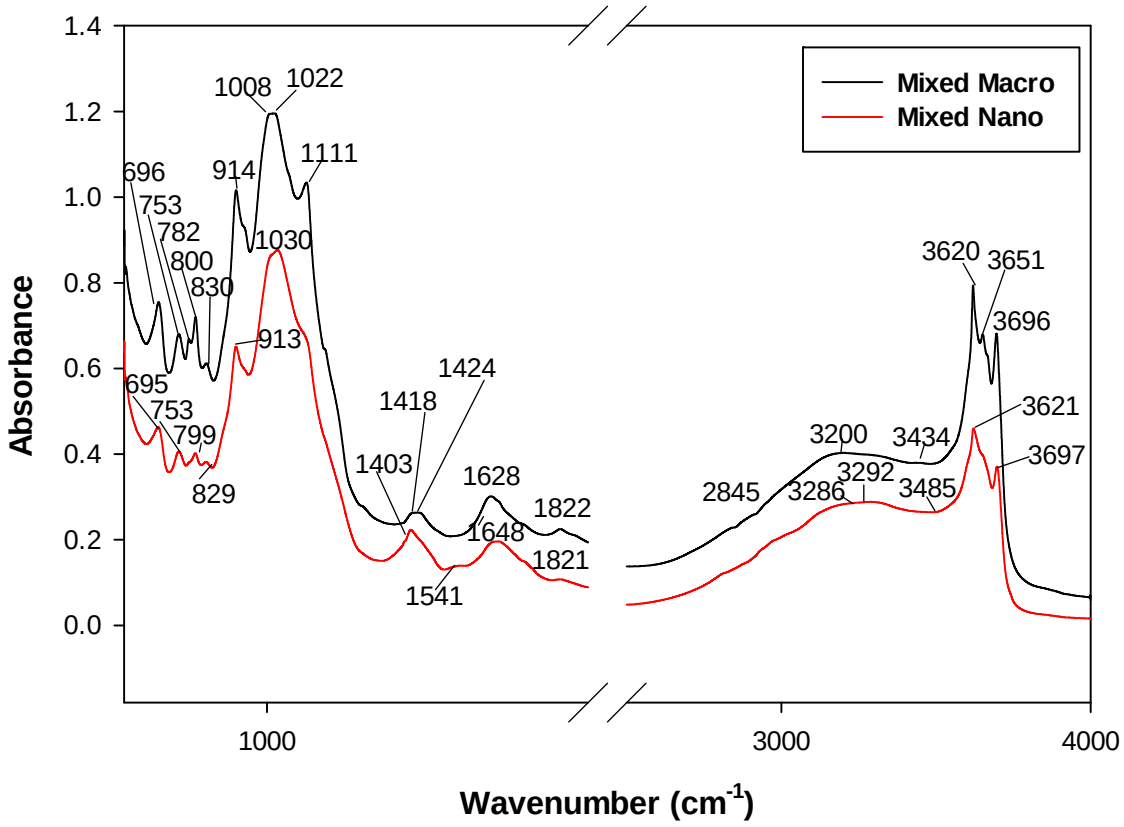

Figure 2.7. Kaolinitic nano- and macro-colloid FTIR characterization

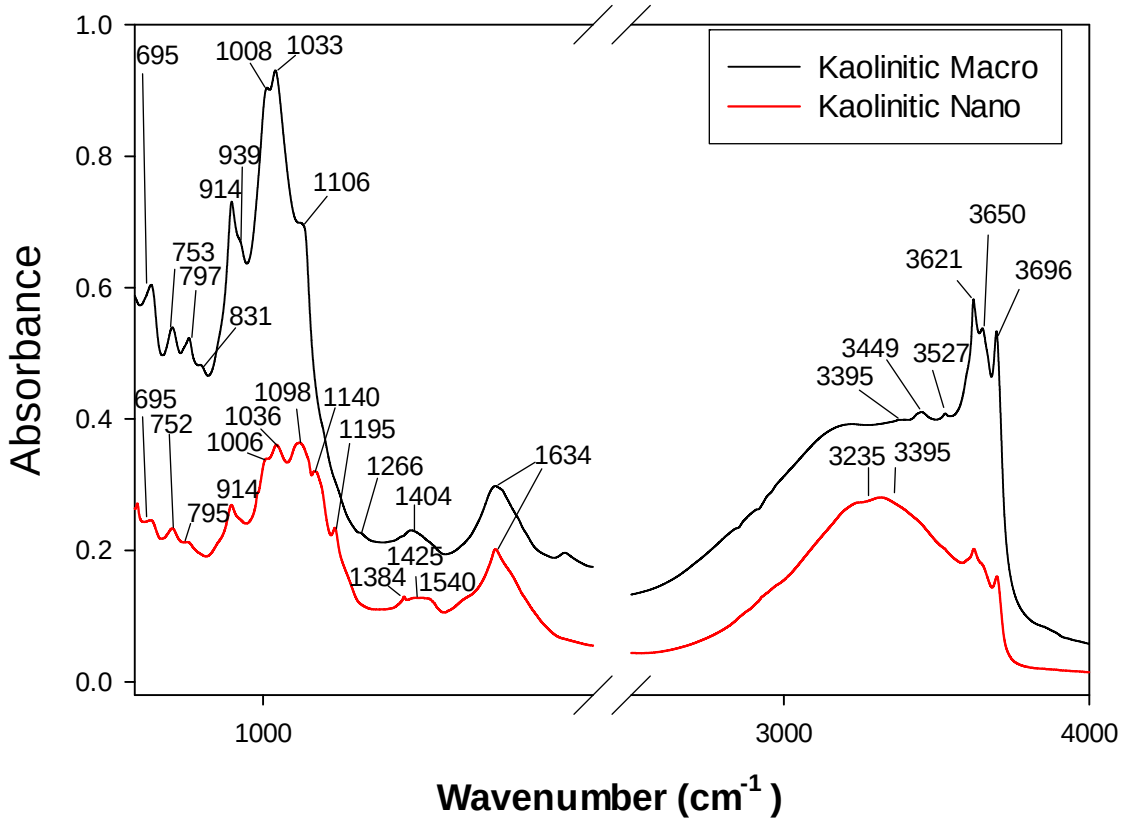

Within all nanocolloid soil types, the DRIFT spectra revealed the presence of a shoulder near 1540 cm^{-1} (Fig. 2.6-2.8), which is assigned to the amide II peak (Baes and Bloom, 1989, Cheshire, et al., 2000). This feature was not present in the macrocolloids. The presence of amide functional groups in the nanocolloids agrees with Calabi-Floody, et al. (2011), who noted amide groups in nanoclays and not in coarser clay fractions. This is especially significant since all three soil samples were removed from B horizons. Within the biosolid colloids (Fig. 2.9) there were signatures of phenol groups (broad peaks at 1250, and between 3600 and 3000 cm^{-1}, aliphatic C-H groups (2950 cm^{-1}) and other methyl groups (2950, 2410, 2420 cm^{-1}), as well as carboxyl groups (1700, 1660, and 1400 cm^{-1}) in both the nano- and macro-colloid fractions (Chefetz, et al., 1996). Both size fractions had shoulder peaks representing Amide II bonds at 1550 cm^{-1}, with prominent nitrate peaks at 1384 cm^{-1}, while the C-O stretch of polysaccharides were represented by peaks between 950 and 1170 cm^{-1} (Fig. 2.9) (Chefetz, et al., 1996, Dupuy and Douay, 2001, Farmer, 1974, Madejova, 2003, Niemeyer, et al., 1992, Shroeder, 2002, White, 1971). The bio-nanocolloid pattern indicated a greater prevalence of carboxyl, phenolic, amide and methyl groups than did the bio-macrocolloids through greater absorption values (Fig. 2.9). Additionally, the bio-nanocolloids had peaks at 2398, 2232 and 1843 cm^{-1}, indicating a greater presence of aromatic C=C bonds than the bio-macrocolloids (Fig. 2.9) (Chefetz, et al., 1996). The bio-nanocolloid pattern also indicated a greater presence of CO_2H groups through the shift and occurrence of a greater intensity shoulder peak at 1767 cm^{-1}, whereas the bio-macrocolloid pattern showed a smaller shoulder peak at 1732 cm^{-1} (Fig. 2.9) (Chefetz, et al., 1996). The extensive organic functional groups characterized in the bio-colloids DRIFT spectra provide ample surface area for reactivity with contaminants as indicated by the larger surface area measured within the bio-colloids over that of the mineral colloids (Table 2.1).

Figure 2.8. Biosolid nano- and macro-colloid FTIR characterization

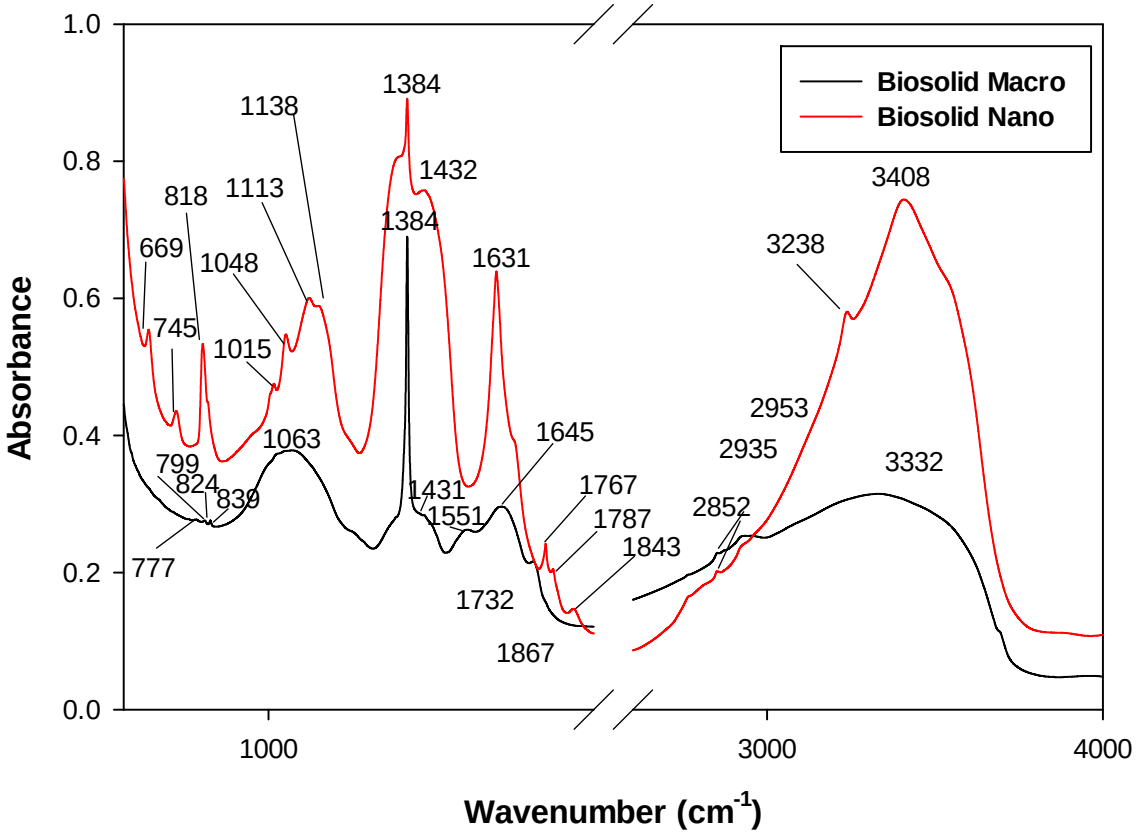

2.4 Conclusions

Nanocolloids fractionated by centrifugation appeared to have a larger average size range (> 100 nm) than typical nanoparticles due to irregular shape and or limited aggregation. Nanoparticles were also found to be attached to the surfaces of some macrocolloid fractions, suggesting macro-nano aggregate behavior. The occurrences of nanoparticle clusters within the nanocolloids and of macro-nano aggregates in the macrocolloids may have modified somewhat the behavior of the different sized fractions, obscuring some of the expected differences between the two size classes. Nevertheless, nanocolloids exhibited greater surface reactivity, as evidenced by higher negatively charged surfaces and larger surface areas. The higher negatively charged surfaces and sodium adsorption ratios of the nanocolloids over their corresponding macrocolloids also indicated greater potential for colloidal stability. In contrast, the biosolid nanocolloids showed less stability than corresponding macrocolloids due to shifts towards a more positive surface charge with pH changes. The presence of siloxane, aluminol, and carboxylic surface functional groups on the nano- and macro-colloids may provide surface sites that can interact and potentially sorb contaminants depending on the conditions in the subsurface environment. Mineralogical differences between the nano- and macro-colloids may have been obscured by the attachment of nanoparticles to macrocolloid surfaces, but generally the nanocolloids displayed poor crystallinity in comparison to their corresponding macrocolloids, which may further enhance their surface reactivity and sorption potential. Further, TEM images indicated morphological shape changes with decreased size, which may alter nanocolloid surface free energy, reactivity and surface area availability for contaminant sorption. Overall, this study showed that nanocolloids - due to their physico-chemical and morphological differences from corresponding macrocolloids – may have the potential for greater chemical reactivity, sorption, and transport of contaminants than macrocolloids. This has important ramifications in water pollution and remediation processes. However, due to their heterogeneous nature, predictions of their physicochemical behavior in natural environments and associated risks based exclusively on size separations may be different from what was originally anticipated.

Chapter Three - Stability Characteristics of Soil and Biosolid Nanocolloid and Macrocolloid Particles in the Absence and Presence of Arsenic, Selenium, Copper and Lead

3.1 Introduction

Water dispersed colloids (WDC) are known to disperse from soil aggregates and remain mobile in subsurface environments (Seta and Karathanasis, 1996; Seta and Karathanasis, 1997). They have average diameters between 1 and 1,000 nm (IUPAC, 1997), which includes nanoparticles, with one dimension equal to or less than 100 nm (IUPAC, 1997; Christian et al., 2008; Maurice and Hochella, 2008). These naturally derived nanocolloids are prevalent in the environment and play various roles in environmental processes such as the cycling of nutrients, remediation procedures, contaminant transport and soil genesis (Karathanasis, 2010).

Nanoparticle stability can be used as an indicator of potential transport into groundwater supplies. The tendency for particles to aggregate or remain stable in solution may be affected by the complex mineralogical and physico-chemical attributes of the particle, including particle size, surface chemistry, and the aqueous environment surrounding transport (Maurice and Hochella, 2008; Karathanasis, 2010). Even though the small size of nanoparticles may promote long-range stability and transport due to the proportionality of their displacement to the inverse square root of their radius, their high surface energy may also result in multiple interparticle collisions and aggregation, especially at increased ionic strengths (Bradford, et al., 2007; Bradford and Torkzaban, 2008; Karathanasis, 2010). Colloid stability can be influenced by solution ionic strength and composition, particle surface coatings and functional groups, pH, and zeta potential (Kretzschmar et al., 1999; Karathanasis, 2010). Stability can also be a function of the mineralogical composition of the particles. Studies have shown that kaolinitic particles tend to flocculate, while smectitic particles tend to remain dispersed or stable over time (Dixon, 1989; Seta and Karathanasis, 1996; Lado and Ben-Hur, 2004). An important consideration in natural systems includes their complex composition, which consists of mixed colloidal phases. This encompasses the interactions with other nanocolloids and solutes in the system, particularly since nanoparticle mobility is controlled mainly by Brownian motion and not by gravitational settling like their larger counterparts (Tsao et al., 2011).

Nanoparticles and nanocolloids can carry contaminants, illustrating their potential role in environmental pollution, water quality, and remediation processes (Kaplan et al., 1993; Ouyang et al., 1996). Four contaminants that are of particular concern include arsenic (As), selenium (Se), copper (Cu), and lead (Pb), all of which are considered toxic to humans, wildlife and plants at sufficiently high concentrations. All four of these contaminants are accumulated in the environment from anthropogenic sources/industrial runoff, including car batteries, where arsenic is used to strengthen copper and lead alloys (Grund et al., 2005), or from naturally occurring sources like seleniferous and arsenopyrite containing soils (Su and Suarez, 2000; Signes-Pastor et al., 2007). They may be readily transported into groundwater by naturally occurring soil and biosolid colloids. While many have characterized, modeled, and predicted the movement of water dispersible colloids (Seta and Karathanasis, 1996; Seta and Karathanasis, 1997; Kaplan et al., 1997; Kjaergaard et al., 2004; McCarthy and McKay, 2004), there is a lack of information comparing the stability of macro-sized (0.1-2.0 μm) to nano-sized colloids

(<0.1 μm) of differing mineralogy from subsurface horizons, and their potential to transport contaminants such as Se, As, Cu, and Pb. Additionally, there is little to no information available on the role of nano-sized biosolid-derived colloids, despite studies showing that larger sized bio-colloids enhance contaminant transport through soil (Karathanasis and Johnson, 2006; Karathanasis et al., 2007; Miller et al., 2010). The objectives of this study were to evaluate and compare the stability of water suspended nano- and macro-colloids derived from Bt horizons of 3 Kentucky soils with kaolinitic, montmorillonitic, and mixed mineralogies, as well as from an aerobically digested biosolid with three levels of Cu, Pb, As, and Se contaminant loads.

3.2 Materials and Methods

3.2.1 Colloid Generation and Recovery

Mineral colloids were fractionated from the Bt horizons of three Kentucky soils with differing mineralogy: Caleast-variant (fine, smectitic, mesic mollic Hapludalf), Tilsit (fine-silty, mixed, mesic Typic Fragiudult), and Trimble (fine-loamy, siliceous, mesic Typic Paleudult). The recovered colloids are referred to as smectitic, mixed, and kaolinitic nano- or macro-colloids, respectively. An aerobically digested municipal sewage sludge, obtained from Jessamine County, Kentucky, was fractionated to obtain the biosolid nano- and macro-colloids. Centrifugation was used to fractionate the water dispersible colloids (WDC) into two size classes (nanocolloids <100 nm and macrocolloids 100-2000 nm) using a Centra GP8R Model 120 centrifuge (ThermoIEC) in deionized water (resistivity of 1 μΩ/cm at 25°C). The clay fraction was separated from the bulk soil using centrifugation at 107 g for 3.5 minutes, and then at 4387 RCF for 46 minutes to separate the nano- from the macro-colloids (Karathanasis et al., 2005; Karathanasis, 2010). Centrifugation times were determined using Stokes' law, and separation of nano- from macro-colloids was performed on a centrifuge with a rotor radius of 170 mm, a speed of 4387 g, a density difference from water of 1650 kg m^{-3}, and viscosity of 0.0008904 Pas. In separating the clay fraction from the bulk soil, centrifuge times were calculated using a rotor radius of 170 mm, using 107 g, a density difference of 1650 kg m^{-3}, and viscosity of 0.0008904 Pas. To quantify WDC recovery from the differing size fractions as compared to the bulk soil, as well as to determine the concentration of suspended colloids in each generated suspension, triplicate 50 mL aliquots of the nano- and macro-colloid suspensions were oven dried at 100°C for 24 hours, weighed and expressed as a percentage of the bulk soil. All collected sample suspensions were then diluted to 50 mg L^{-1} concentrations for additional analysis.

3.2.2 Stability Experiments

Settling kinetics experiments were used to determine the stability of the nano- and macro-colloids over time. Duplicate 400 mL suspensions of 50 mg colloid L^{-1} in de-ionized water (D-H_2O) were used to generate stability graphs based on sampled concentrations at times 0, 30 minutes, 1, 2, 4, 8, 24 and 48 hours. Additional stability experiments were performed using the same procedure with the addition of 2 and 10 mg L^{-1} mixed contaminant concentrations of Pb, Cu, As, and Se [prepared as aqueous solutions from: $PbCl_2$ (98% purity, Aldrich Chemicals, Milwaukee, WI), $CuCl_2$ (>99% purity, Sigma Chemical Company, St. Louis, MO), arsenic acid $Na_2HAsO_4 \cdot 7H_2O$ (98% purity, Sigma Chemical Company, St. Louis, MO), and sodium selenate decahydrate $Na_2SeO_4 \cdot 10H_2O$ (99.9% purity, Sigma Chemical Company, St. Louis, MO)]. The suspended colloid

concentrations were determined using a colorimetric procedure on a Molecular Devices Versa Max Microplate Reader at 450 nm (Seta and Karathanasis, 1997).

3.2.3 Particle Size, Morphology, and Surface Area Analysis

Primary particle size of nanocolloid particles was determined using a high resolution transmission electron microscope attached to an Oxford energy dispersive spectrometer (TEM-EDS; JEOL 2010F, Tokyo, Japan). Primary particle size of macrocolloid particles was determined using a S-4300 scanning electron microscope, equipped with a Princeton Gamma-Tech EDS (SEM-EDS; Hitachi S-4300, Tokyo, Japan). The average diameters were calculated using ImageJ software (ImageJ 1.46r, Wayne Rasband, National Institutes of Health, USA). A Malvern Instruments Zetasizer Nano ZS (Malvern, United Kingdom) was used to obtain intensity weighted mean particle hydrodynamic diameters (z-average diameter, d_h) on suspensions of 50 mg colloid L^{-1} using dynamic light scattering (173° backscatter analysis method). This procedure also allowed estimates of nano- and macro-colloid aggregation potentials in the absence and presence of 2 mg L^{-1} additions of As, Cu, Pb and Se contaminants. Surface area analysis was performed on both the nano- and macro-colloids using the Ethylene Glycol Monoethyl Ether (EGME) method.

3.2.4 Mineralogical Characterization

A combination of X-ray diffraction (XRD) and thermogravimetric analysis (TG) was employed for mineralogical characterization. For XRD analysis, K, K-heat treated, Mg, and Mg-glycol saturated samples were collected on glass slides and analyzed on a Phillips PW 1840 diffractometer and PW 1729 x-ray generator (Mahwah, NJ) fitted with a cobalt X-ray tube and run at 40 kV and 30 mA using a Bragg-Bretano design goniometer at a scanning rate of 0.05°2θ per minute from 2° to 40° with a scattering slit of 0.1°. Mg-saturated colloids were also used for TG analysis on a Thermal Analyst 2000 (TA Instruments) equipped with a 951 Thermogravimetric Analyzer (DuPont Instruments) with a heating rate of 20˚C/min under N_2 atmosphere (Karathanasis, 2008). The TG analyses were used to verify the presence of kaolinite, as well as goethite and gibbsite, and to compliment quantification interpretations derived from the XRD patterns (Karathanasis, 2008).

3.2.5 Chemical Characterization

A Denver Instruments Model 250 pH*ISE*electrical conductivity meter (Arvada, CO) was used to measure pH and electrical conductivity of the nano- and macro-colloid suspensions. Ionic strength was derived by multiplying electrical conductivities by 0.0127 (Griffin and Jurinak, 1973). A Varian Spectr AA 50B atomic absorption spectrometer was used to determine the base cation concentrations (Ca^{2+}, Mg^{2+}, K^+, and Na^+), which were summed and used to report the cation exchange capacity (CEC) from triplicate samples of the nano- and macro-colloids using an adapted version of the ammonium acetate method. Concentrations of Ca^{2+}, Mg^{2+}, and Na^+ were used to calculate sodium adsorption ratios (SAR) (Harron et al., 1983). A Flash EA 1112 Series NC Soil Analyzer (Thermo Electron Corporation) with a Mettler Toledo MX5 microbalance was used to determine organic C (OC). Zeta potential measurements were used to estimate surface and point of zero charge (PZC), as well as suspension stability at adjusted pH values of 4, 6, 8, and 10 using 0.01N NaOH and HCl. The Smoluchowski approximations determined zeta potentials from electrophoretic mobilities on suspensions in 0.001M NaCl background electrolyte as measured on a Malvern Zetasizer Nano ZS

(Malvern, United Kingdom). Additionally, zeta potentials were measured in the presence of 2 and 10 mg L^{-1} additions of Cu, Pb, As and Se.

3.2.6 Statistical Analysis

The accepted error levels for all duplicate and triplicate measurements were ≤ 15%. The data were analyzed using analysis of variance (ANOVA) (SAS PROC GLM) and Fisher's protected least significant difference test (LSD) in SAS 9.3 (SAS Institute Inc., Cary, NC, USA). The statistical significance level used was $\alpha = 0.05$.

3.3 Results and Discussion

3.3.1 Colloid Recovery

The percentage of WDC recovered from bulk soil Bt horizon samples indicated greater quantities of macro-WDC than nano-WDC, with values ranging from 5-37% and 0.03-0.7% recovered, respectively (Table 3.1) (Kjaergaard et al., 2004). Higher recovery would have been obtained if a dispersing agent had been used, but previous studies have shown that the use of a dispersing agent enhances stability potentials outside of a soil's natural behavior (Seta and Karathanasis, 1996). The highest amount of WDC came from the mixed macrocolloids (37%), followed by the smectitic (33%), kaolinitic (11%), and biosolid (5%) macrocolloids (Table 3.1). Lower WDC values were obtained from the nanocolloids, showing less than 1% recovered from the smectitic (0.7%), mixed (0.3%), kaolinitic (0.1%), and biosolid (0.03%) NCs (Table 3.1). Greater amounts of WDC were recovered from the soils with mixed and smectitic mineralogy as compared to the kaolinitic and biosolids (Tables 3.1 and 3.2), highlighting the importance of clay mineralogy in dictating WDC content. Generally, soils with increasing amounts of kaolinite, Fe- and Al-oxides are less prone to disperse, whereas those higher in smectitic and other 2:1 minerals are more dispersive (Seta and Karathanasis, 1997). Nano-WDC had greater organic carbon associations than the macro-WDC (Table 3.3). The literature suggests that the role of OC on the recovery of WDC can have variable effects, but most report increased recovery with increasing OC content (Kaplan et al., 1993; Kaplan et al., 1997; Kjaergaard et al., 2004; Christian et al., 2008; Ottofuelling et al., 2011). In our study, the higher OC values appeared to decrease WDC recovery of the NCs (Tables 3.1 and 3.3) (Seta and Karathanasis, 1997). Differences in WDC recovery were not necessarily indicative of their stability behavior and probably reflect different soil physicochemical properties and mineralogical effects on soil dispersivity (Fig. 3.1, Tables 3.1-3.3).

Table 3.1. Physical characteristics of nano- and macro-colloids.

Properties	Colloids							
	Smectitic		Mixed		Kaolinitic		Biosolid	
Size Class	Macro	Nano	Macro	Nano	Macro	Nano	Macro	Nano
% Water Dispersible Colloid Recovered from Bulk Sample	33.41	0.67	37.17	0.33	11.00	0.07	4.95	0.03
SEM/TEM § Mean Smallest Particle Size ±SD ‡ (nm)	328±144	37±13	549±394	7±5	288±184	41±19	363±338	50±19
Surface Area (m^2 g^{-1}) ±SD ‡	708±137	879±76	420±105	466±10	333±37	389±44	1674±70	1303±63

‡ SD = Standard Deviation was calculated based on the averages of duplicate or triplicate measurements (see Methods section).

§ SEM = Scanning Electron Microscopy, TEM= Transmission Electron Microscopy data represent the average smallest dimension of 300 representative particles from three to eight images of each size fraction as measured until the average and standard deviation values had less than 10% variation.

Table 3.2. Mineralogical compositions of nano- and macro-colloids.

Properties	Colloids							
	Smectitic		Mixed		Kaolinitic		Biosolid	
Size Class	Macro	Nano	Macro	Nano	Macro	Nano	Macro	Nano
Kaolinite (%) ‡	29	30	42	46	52	55	NA §	NA §
Goethite (%) ‡	7	9	5	7	12	15	NA §	NA §
Gibbsite (%) ‡	0	0	0	0	5	6	NA §	NA §
Quartz (%) ‡	6	4	5	3	4	2	NA §	NA §
Mica (%) ‡	10	6	31	30	3	3	NA §	NA §
Smectite (%) ‡	48	51	0	0	0	0	NA §	NA §
MVI ¶ (%) ‡	0	0	7	7	0	0	NA §	NA §
HIV# (%) ‡	0	0	10	7	24	19	NA §	NA §

‡ Mineral percentage as determined using X-Ray Diffraction and Thermogravimentric Data (Karathanasis, 2008).

§ NA = Not Applicable

¶ MVI = Mica-Vermiculite Interstratified

HIV = Hydroxyinterlayered Vermiculite

Table 3.3. Chemical characteristics of nano- and macro-colloids.

Properties	Colloids							
	Smectitic		Mixed		Kaolinitic		Biosolid	
Size Class	Macro	Nano	Macro	Nano	Macro	Nano	Macro	Nano
Electrical Conductivity (mmhos cm^{-1})	$3.93x10^{-3}$	$6.07x10^{-3}$	$2.91x10^{-3}$	$3.09x10^{-2}$	$2.87x10^{-3}$	$3.80x10^{-3}$	$1.56x10^{-2}$	$4.69x10^{-2}$
Ionic Strength § (mol L^{-1})	$4.99x10^{-5}$	$7.71x10^{-5}$	$3.70x10^{-5}$	$3.92x10^{-4}$	$3.64x10^{-5}$	$4.83x10^{-5}$	$1.97x10^{-4}$	$5.96x10^{-4}$
Natural pH	4.92	5.12	5.07	4.92	4.91	5.38	5.39	5.25
CEC ($cmol_c$ kg^{-1}) # ±SD ‡	35.05±12.84	42.19±15.12	8.89±1.62	10.51±1.67	6.94±1.85	13.12±2.84	37.61±14.85	70.99±22.98
Ca^{2+} ($cmol_c$ kg^{-1})	27.60	32.64	3.80	4.00	4.40	7.12	31.60	51.68
Mg^{2+} ($cmol_c$ kg^{-1})	6.27	8.00	3.40	3.47	1.60	3.73	3.60	12.13
K^{+} ($cmol_c$ kg^{-1})	0.57	0.78	1.15	2.80	0.45	1.23	1.64	3.98
Na^{+} ($cmol_c$ kg^{-1})	0.61	0.77	0.54	0.24	0.49	1.04	0.77	3.20
SAR ††	0.15	0.17	0.28	0.12	0.28	0.45	0.18	0.57
OC (mg kg^{-1}) ‡‡	658	897	645	774	430	647	1.3K	16K

‡ SD = Standard Deviation was calculated based on the averages of duplicate or triplicate measurements (see Methods section).

§ Ionic Strength (IS) = Estimated using Griffin and Jurinak's equation where IS (mol L^{-1}) = 0.0127 x Electrical Conductivity (millimhos cm^{-1}) (1973).

CEC = Cation Exchange Capacity by sum of cations.

†† SAR = Sodium Adsorption Ratio

‡‡ OC = Organic Carbon was derived by subtracting dissolved organic carbon from total carbon measurements. Due to low pH conditions and the typical absence of carbonates in the region, inorganic carbon contributions were assumed to be minimal.

Figure 3.1. Stability of the macro- and nano-colloids in the presence and absence of equal parts (0, 2, and 10 mg L^{-1}) mixtures of each contaminant (As, Se, Cu and Pb). Stability is represented for the nano- and macro-colloids as percent colloid in solution after 48 hours. Error bars represent standard error between duplicates. Nanocolloids were more stable than the macrocolloids as determined using Fisher's protected least significant difference test at a probability level of 0.05, with LSD=11.52, CV=3.18. Upper case letters represent significant differences (α=0.05) between mineralogy at the same level of contaminant concentration. Lower case letters represent trends within the same mineralogy across the 0, 2, and 10 mg L^{-1} contaminant additions.

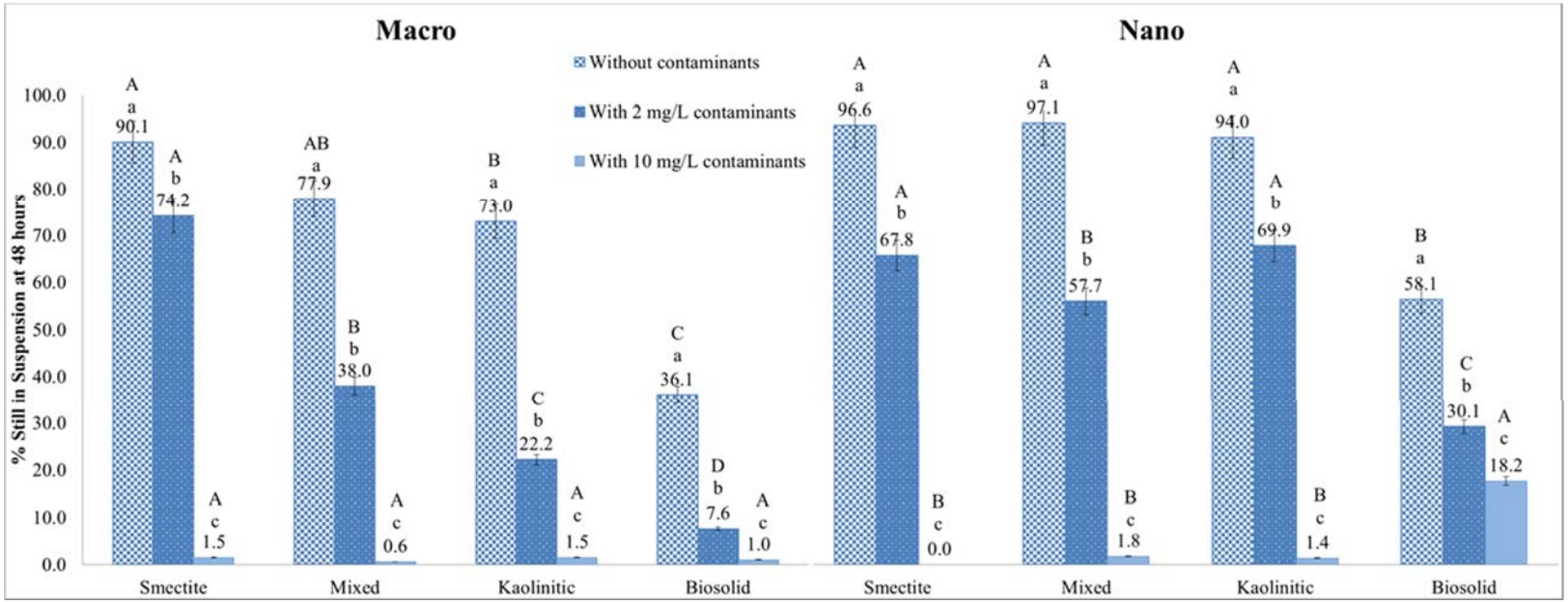

3.3.2 Colloid Stability

3.3.2.1 Effect of Particle Size

Stability settling characteristics of WDC as affected by size and contaminant load are shown in Fig. 3.1. A particle is considered stabile if it tends to remain dispersed in suspension (Seta and Karathanasis, 1997). Particle size analysis by SEM indicated size ranges between 288 and 549 nm for the macrocolloids, while TEM portrayed size ranges between 7 and 50 nm for the nanocolloids (Table 3.1). Based on size alone, the settling experiments (Fig. 3.1) showed nanocolloids to be more stable in solution after 48 hours than the macrocolloids (LSD=11.52, CV=3.18, p-value <0.001) in the presence and absence of contaminants. Mineral macro- and nano-colloids had an average of 45 and 65% of colloids in suspension after 48 hours, respectively, in comparison to the biosolid macro- and nano-colloids having only 1 and 18% still in suspension after 48 hours, respectively (Fig. 3.1). This highlights two things: first, the enhanced mobility and contaminant transport potential of the nanocolloids over their corresponding macrocolloids, with nanocolloids (smectitic, mixed, kaolinitic, and biosolid NCs at both 2 and 10 mg L^{-1} contaminant levels) showing as much as 20% more colloids in suspension in the presence of contaminants (Fig. 3.1). Second, even though the mineral colloids had an average of 42% more colloids in suspension than the bio-colloids in the presence of 2 mg L^{-1} contaminants, the bio-nanocolloids had as much as 18% more colloids in suspension in the presence of 10 mg L^{-1} contaminants than the mineral colloids.

The average intensity weighted (Z-average) hydrodynamic diameters (d_h) complemented the stability findings, showing similar trends in the absence of contaminants for the smectitic, kaolinitic, and mixed nanocolloids and a lower stability with increasing d_h for the bio-nanocolloids (Fig. 3.1 and 3.2). For the macrocolloids, the anomaly was the kaolinitic fraction, which showed the smallest d_h, but with lower stability than the smectitic and mixed macrocolloid fraction (Fig. 3.1 and 3.2). Other than the macrocolloid kaolinitic fraction, the smectitic colloids showed consistently small d_h values and high stability in the settling studies compared to other colloid compositions (Fig. 3.1 and 3.2). Since d_h is related to aggregate sizes formed by the colloids, the smaller values indicate smaller aggregate size thus more dispersive colloids. The d_h values in the absence of contaminants suggested that the macrocolloids were nearly four-times larger than the nanocolloids, with an average d_h of 842 nm for the macrocolloids and 224 nm for the nanocolloids (Fig. 3.1). The d_h also showed compositional trends, with mean comparisons showing the bio-colloids to be significantly larger than the mineral colloids (LSD=362.54, CV=2.16, p-value=0.03). While the larger d_h values (as measured by DLS) compared to the crystallite diameters (as measured by TEM/SEM) may indicate some aggregation on both size fractions, the larger DLS measurements may also be partially explained from the influence larger particles present within the samples, which have a disproportionate influence on the Z-average diameter as compared to smaller particles (Fig. 3.3 and 3.4), or by potential surface coatings on the particles (Kretzschmar et al., 1999; Kjaergaard et al., 2004).

Figure 3.2. Dynamic Light Scatter (DLS) intensity weighted hydrodynamic diameters (Z-Average diameters, d_h) in the absence and presence of 2 mg/L contaminants after 12 and 24 hour reaction times for the mineral and biosolid a) macrocolloids and b) nanocolloids. Error bars represent standard error of the mean.

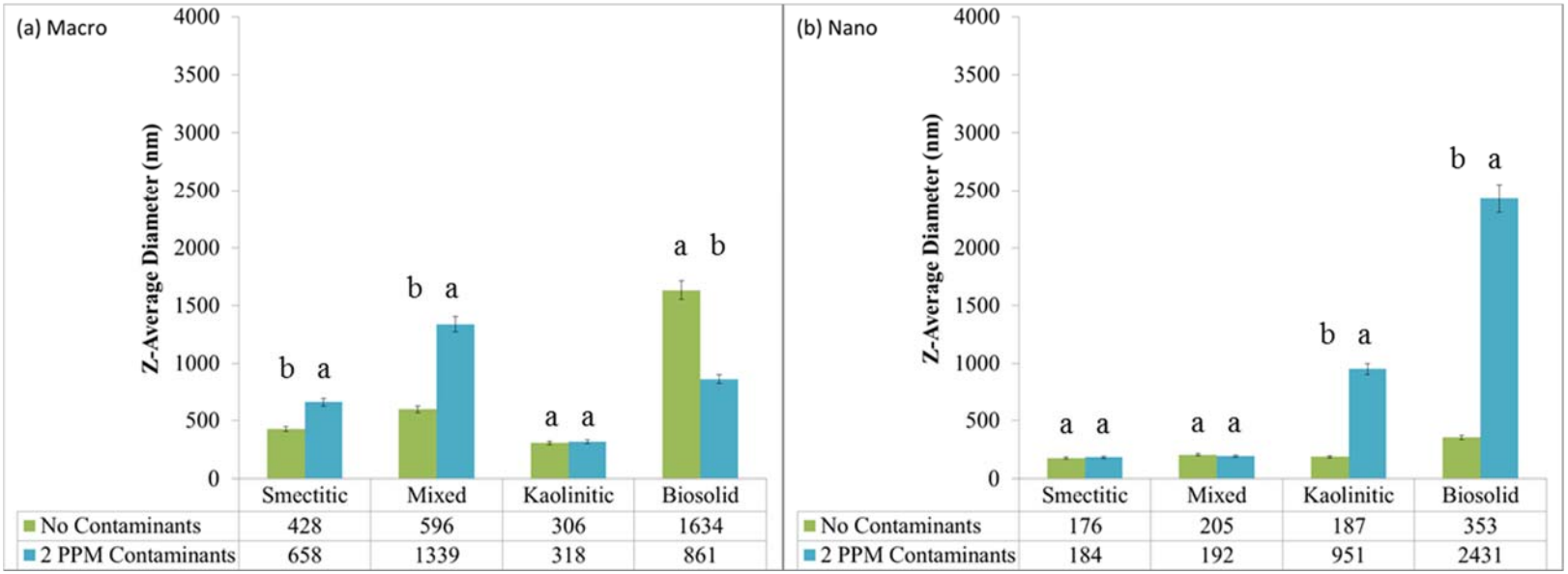

Figure 3.3. SEM images of the a) smectitic, b) mixed, c) kaolinitic, and d) biosolid macrocolloid aggregates.

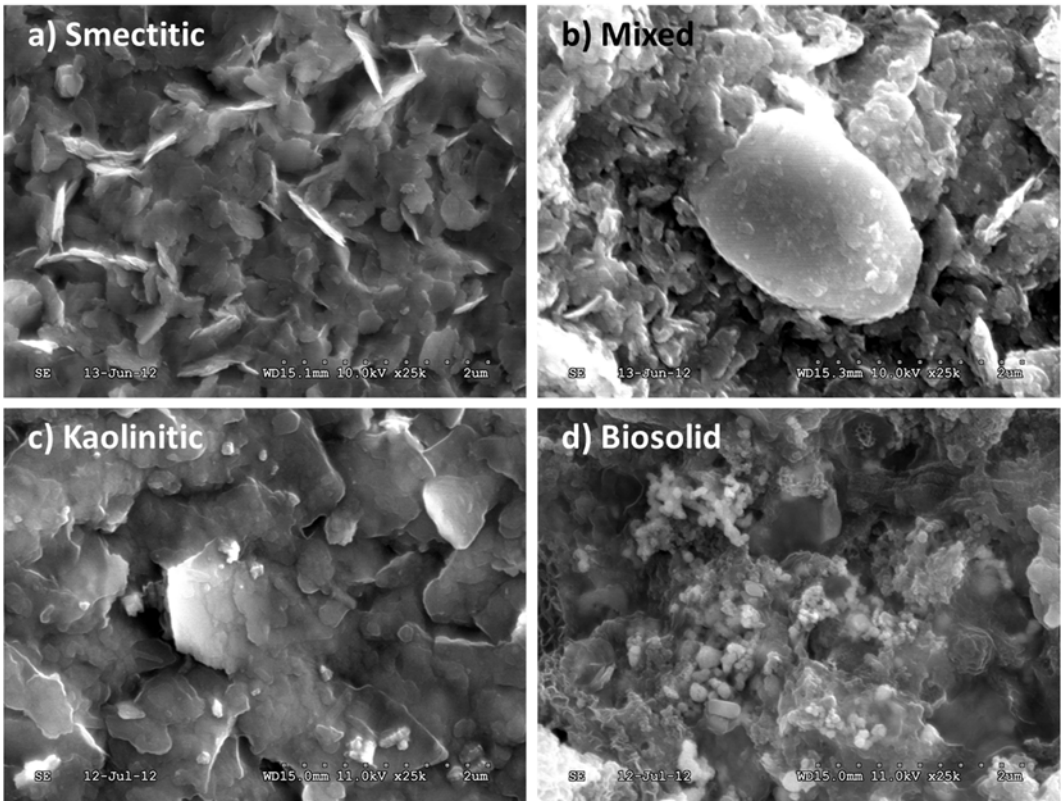

Figure 3.4. TEM images of a) smectitic nanocolloids with interbedded iron-minerals, b) mixed mineralogy nanocolloid aggregates showing HIV/vermiculite and interbedded iron- minerals, c) an aggregate of small hexagonally shaped kaolinitic particles with interbedded iron, and d) a biosolid nanocolloid aggregate (mineralogy as verified by morphology and XRD/TG Analysis).

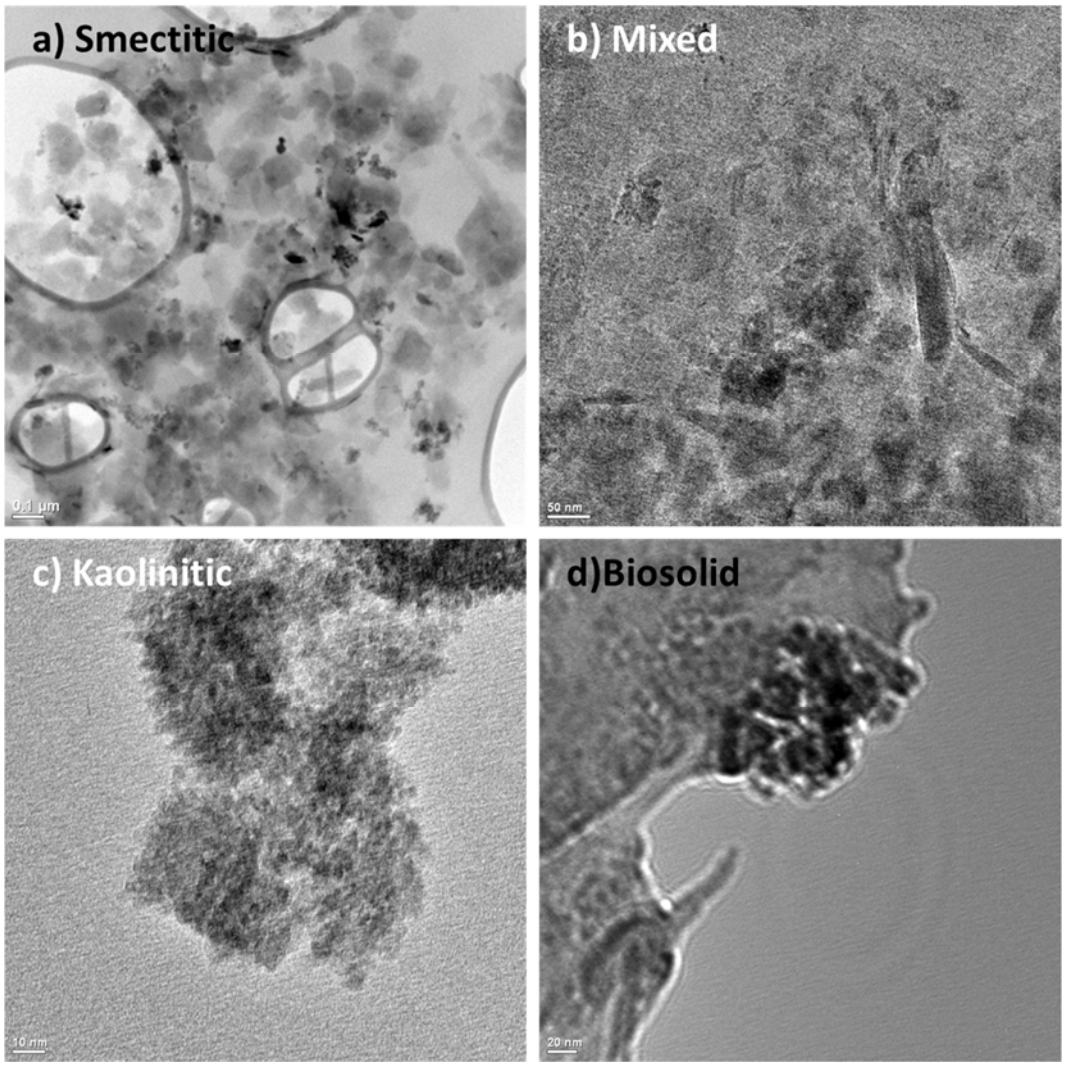

The d_h values in the presence of contaminants were similar as compared to d_h values in the absence of contaminants for the kaolinitic macrocolloids, the smectitic and mixed nanocolloids, but increased significantly for the smectitic macrocolloids, and the kaolinitic, and biosolid nanocolloids. Surprisingly, the biosolid macrocolloids experienced a considerable reduction in size in the presence of contaminants (Fig. 3.1). In spite of a size increase of about 230 nm, the smectitic macrocolloid fraction showed a slight reduction in stability comparable to that of the nanocolloid fraction. In contrast, the stability of the kaolinitic, mixed, and biosolid macrocolloid fraction decreased significantly regardless of the d_h size changes (Fig. 3.1) following the mixed > kaolinitic > biosolid trend. The addition of the 2 mg L^{-1} contaminant load caused a consistent stability reduction across all nanocolloids following the sequence smectitic = kaolinitic > mixed > biosolid. However, the stability of the nanocolloids was generally higher than that of the macrocolloids under the 2 mg L^{-1} contaminant load, with the exception of the smectitic macrocolloids which showed similar stability to the smectitic nanocolloids. Increased d_h values in the presence of contaminants indicates enhanced aggregation (Kretzschmar et al., 1999; Kjaergaard et al., 2004) likely due to the increase in ionic strength due to addition of polyvalent ions (Fig. 3.1). Macrocolloids showed greater aggregation potentials in the presence of contaminants than nanocolloids through larger shifts in d_h values, especially in the biosolid and mixed macrocolloids (Fig. 3.1). The largest d_h shifts with contaminant additions occurred in the kaolinitic and biosolid nanocolloids and the mixed and biosolid macrocolloids (Fig. 3.1). Greater contaminant loading potential of cationic contaminants onto larger surface areas could cause aggregation of other negatively charged colloids nearby, thus creating pseudo-aggregates that increase the measured Z-average diameter (Fig. 3.1) (Kretzschmar et al., 1999; Kjaergaard et al., 2004).

3.3.2.2 Effects of Mineralogy

Mineralogy appears to have played a partial role in the stability processes of the macro- and nano-colloids (Table 3.2). In the absence of contaminants, the smectitic macrocolloids had greater stability than the kaolinitic and biosolid macrocolloids, but equal stability to the mixed macrocolloids (Fig. 3.1). In the absence of contaminants, the smectitic, mixed and kaolinitic nanocolloids were more stable than the biosolid nanocolloids (Fig. 3.1). After additions of 2 mg L^{-1} contaminants the mineral colloids showed more surface repulsion than the biosolid colloids. The smectitic and kaolinitic nanocolloids were more stable than the mixed and biosolid colloids, while within the macrocolloid fraction, the smectitic and mixed macrocolloids were more stable than the kaolinitic and biosolid colloids (Fig. 3.1). With the exception of the bio-nanocolloids, the addition of 10 mg L^{-1} contaminants overwhelmed the available surface area of the colloids and induced significant flocculation (Fig. 3.1). The greater stability (Fig. 3.1) of the smectitic colloids over that of other mineralogies is likely due to higher surface charge potential, with the greater charge densities in smaller sized colloids resulting in greater repulsion (Table 3.1, Fig. 3.1) (Goldberg and Glaubig, 1987; Seta and Karathanasis, 1996). Lower stability in colloids containing kaolinite are likely due to the tendency of kaolinite to remain flocculated at pH less than 7.5 (Seta and Karathanasis, 1996; Lado and Ben-Hur, 2004). Additionally, smaller sized fractions that are high in kaolinite, Al and Fe hydroxides may have enhanced surface charge density contributing to destabilization potentials (Kretzschmar et al., 1993; Seta and Karathanasis, 1997).

This is evidenced by the attachment of smaller nanoparticles to several macrocolloid surfaces (Fig. 3.3). Additionally, the presence of hydroxyl-interlayered vermiculite may have released Al and promoted flocculation processes in the mixed and kaolinitic colloid fractions (Fig. 3.1 and 3.2; Table 3.2) (Seta and Karathanasis, 1997). In the stability kinetics experiments, mixed macrocolloids were more stable than kaolinitic macrocolloids after the addition of 2 mg L^{-1}, with a reversed stability sequence for the nanocolloids (Fig. 3.1). The mixed nanocolloids were less stable than the kaolinitic nanocolloids in the presence of 2 mg L^{-1} contaminants, probably due to their higher Fe-hydroxide content (Fig. 3.1, Table 3.2). One confounding observation is that there are higher quantities of flocculating agents (Fe and Al hydroxides, geothite, and gibbsite) in the nanocolloids, yet they remain more stable than their corresponding macrocolloids (Table 3.2, Fig. 3.1). The answer to this dilemma may lie in the EDS data which indicated greater (Al+Fe):Si ratios in the nanocolloids than in their corresponding macrocolloids. Both Shen (1999) and Kjaergaard et al. (2004) showed that increased (Al+Fe):Si ratios enhance humic acid sorption capacities which can stabilize colloid suspensions.

3.3.2.3 Effects of Particle Morphology

The smectitic macrocolloids showed typical montmorillonitic honeycomb shapes with edge-face interactions (Fig. 3.3a). Montmorillonite can be more dispersive than other minerals because weak Van der Waals' forces between oriented tactoids allow penetration between layers by water and exchangeable cations, which may inhibit stable aggregate formation (van Olphen, 1977; Singer, 1994; Lado and Ben-Hur, 2004). The smectitic nanocolloids indicated less particle to particle attachment than the macrocolloids (Fig. 3.4a).

Morphologies displayed by the mixed mineralogy macrocolloids showed tightly aggregated honeycomb-like plates (Fig. 3.3b), while the mixed nanocolloids had various shapes encompassing tubes, rods, plates and hexagons within a tightly aggregated mineral matrix (Fig. 3.4b). The variable shapes in the mixed nanocolloids indicate some surface deformation, which may explain the greater morphological variation evidenced in TEM images (Fig. 3.4b, 3.5b). Similar HIV images were shown with associated iron minerals by Nemeth et al. (2011). Kaolinitic macrocolloid SEM images had the typical kaolinitic hexagonal shapes (Fig. 3.3c), while TEM images of the nanocolloids showed much smaller hexagonal shapes with a noted increase in iron minerals (Fig. 3.4c) (Zhu and Lu, 2010). Kaolinitic minerals tend to flocculate below pH 7, which is representative of the colloid suspension pHs (Table 3.1; Lado and Ben-Hur, 2004).

The morphological compositions of the biosolid macrocolloids, as shown in their SEM images, displayed various aggregations of organic materials with some quartz grains present (Fig. 3.3d), while the nanocolloid TEM images lacked distinct particle shapes or displays of individual particle morphology, indicating less integrity of sample and potential dissolution (Fig. 3.4d). Overall, within the mineral colloids, macrocolloid SEM images insinuated more tightly held aggregates (Fig. 3.3), which may explain their greater flocculation potential (Fig. 3.1) as opposed to the more loosely held aggregates offered within the corresponding nanocolloid TEM images (Fig. 3.4). Additionally, TEM images suggest potential particle morphology alterations from surface disorder, which may have altered nanocolloid stability behavior (Fig. 3.5).

Figure 3.5. TEM images of the a) montmorillonite nanocolloids showing some interlayering/disorder of the individual atoms, b) mixed mineralogy nanocolloids showing some interlayering/disorder of the individual atoms, c) kaolinitic nanocolloids showing kaolinitic hexagonal morphology.

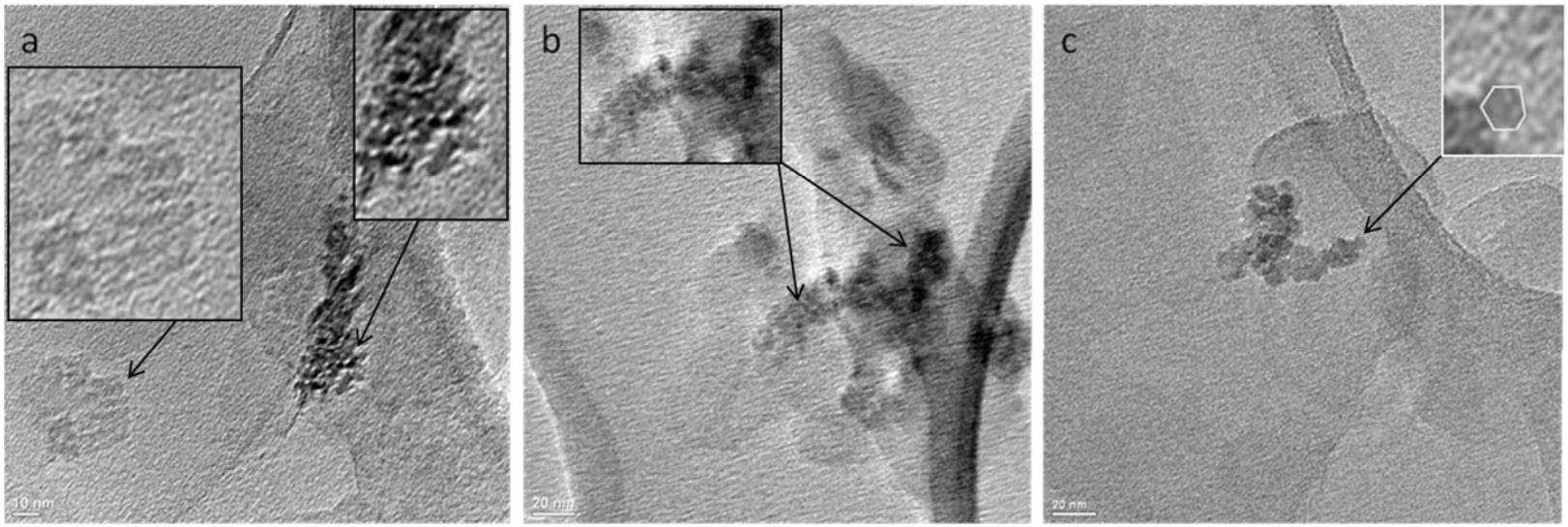

This may be evidenced within the smectitic nanocolloids (Fig. 3.5a) where two particles appear to have connected through oriented attachment (Waychunas et al., 2005; Maurice and Hochella, 2008). The lattice fringes suggest that the sheets have oriented at misplaced angles, forming two mis-matched "boxes" in the highlighted particle on the left as well as forming a rod-like particle on the right (Fig. 3.5a) (Waychunas et al., 2005; Maurice and Hochella, 2008). EDS spectra suggest that the black concretions in the rod-like particle on the right are embedded iron minerals (Fig. 3.5a). TEM images of the mixed nanocolloids indicated similar disorder (Fig. 3.5b), showing two rod/cylinder shaped particles that appear to be adhering to each other to display extended and oblong morphology. The cause of such abnormalities has been suggested to be impurities or oriented aggregation resulting from forced structural incorporation of previously sorbed species that could alter surface sites and influence stability and reactivity characteristics (Tsunekawa et al., 2000; Gilbert et al., 2004; Qu et al., 2004; Waychunas et al., 2005; Maurice and Hochella, 2008).

3.3.2.4 Surface Area Effects

With the exception of the biosolids, nanocolloids had greater surface area than the macrocolloids despite the SEM indications of nanoparticle adhesion to macrocolloid surfaces (Table 3.1) (Waychunas et al., 2005; Maurice and Hochella, 2008; Karathanasis, 2010). Surface area showed trends by composition, with the largest coming from the biosolid materials, followed by the smectitic, mixed, and kaolinitic colloids, respectively (Table 3.1). In addition to size effects, increased surface area values measured in the nanocolloids could be the result of organic surface coatings or the presence of iron hydroxides maximizing sorption of the EGME (Schwertmann and Taylor, 1989; Pennell et al., 1995). The larger surface areas in the nanocolloids also indicate greater potential for contaminant sorption and increased repulsion of similarly charged particles, thus enhancing stability potentials.

3.3.2.5 Effect of Chemical Characteristics

Unadjusted pH values ranged from 4.9 to 5.4 for both the nano- and macro-colloid fractions (Table 3.3). Such a narrow pH range evinces that pH values may not have promoted differences in stability between the differing colloid compositions or sizes, but may have contributed to a greater overall flocculation tendency (Table 3.3, Fig. 3.1) (Seta and Karathanasis, 1997). However, in spite of this narrow pH range, there were significant differences in stabilization potentials (Fig. 3.1) across most of the studied colloid fractions. The same colloids in higher pH environments would likely be even more dispersive, as evidenced by the zeta potential titrations above pH 6 (Fig. 3.6).

The electrical conductivity (EC) and ionic strength (IS) of the colloids were relatively low (Table 3.3) with the nanocolloids showing higher overall values than their corresponding macrocolloids (Table 3.3). Additionally, the bio-colloids had greater EC and IS values than most mineral colloids except for the mixed nanocolloids (Table 3.3). Higher IS values for the nanocolloids could decrease stability (Hesterberg and Page, 1990) and may have contributed to lower fractional recoveries as compared to macrocolloids (Tables 3.1 and 3.3). However, at the natural range these higher EC and IS values of the nanocolloid suspensions did not appear to significantly deter the overall stability of the nanocolloids as shown in Fig. 3.1.

Figure 3.6. Zeta potential titrations of the nano- and macro-colloids.

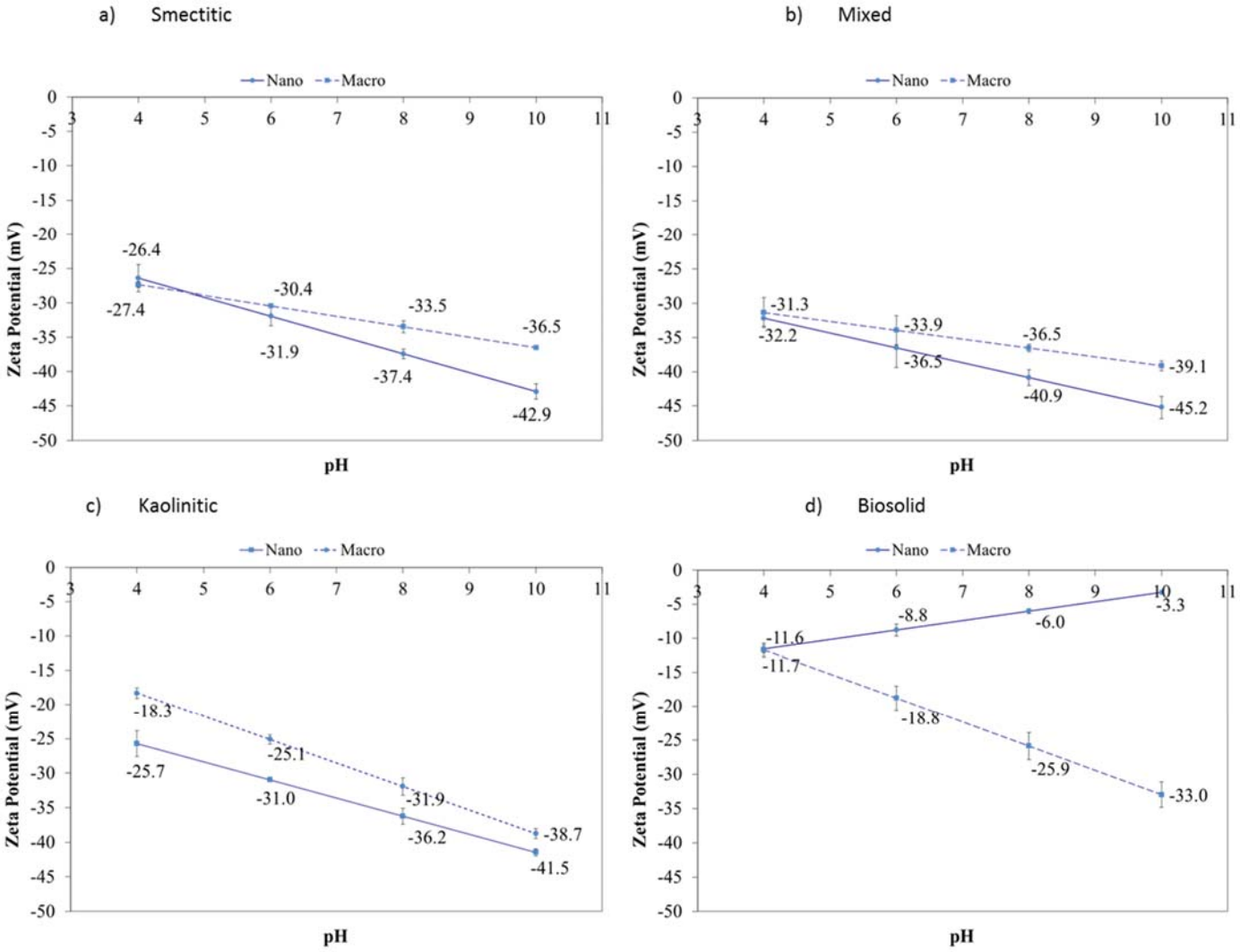

Increased ionic strength effects from contaminant additions resulted in lower nano- and macro-colloid stability, likely due to flocculation in the presence of contaminants, with greater flocculation at higher contaminant concentrations (Fig. 3.1) (Kjaergaard et al., 2004; Karathanasis, 2010). Increased ionic strength has been shown to reduce the effectiveness of Coulomb repulsion by shielding the charge of two approaching particles (Karathanasis, 2010). This effect on Coulomb repulsion may explain the stability findings after contaminant additions of 10 mg L^{-1}, where significantly lower colloid suspension concentrations indicated flocculation in all but the bio-nanocolloid fractions (Fig. 3.1). Coulomb repulsions appeared to overcome ionic strength effects at 2 mg L^{-1} contaminant concentrations.

The higher SAR values of the nanocolloids over that of the macrocolloids are more consistent with their stability trends than the IS values, indicating greater dispersion potentials in the nanocolloids over their corresponding macrocolloids (Table 3.3). The higher CEC values of the nanocolloids over the macrocolloids are also complimentary to their larger and likely more reactive surface areas (Table 3.3). As expected, the smectitic colloids had the greatest CEC within the mineral colloids (Dixon, 1989), followed by the mixed mineralogy and kaolinitic colloids (Table 3.3). The higher OC content of the bio-colloids may have contributed to their higher CEC over that of the mineral colloids (Table 3.3). There were higher exchangeable Ca^{2+} and Mg^{2+} concentrations in the nanocolloids than the corresponding macrocolloid fractions (Table 3.3). Divalent cations can promote flocculation and may explain why nanocolloids were found attached to macrocolloid surfaces likely due to bridging effects (Table 3.3, Fig. 3.3) (Kjaergaard et al., 2004).

Nanocolloids also contained higher OC content than their corresponding macrocolloids which may have enhanced their stability over corresponding macrocolloids (Fig. 3.1, Table 3.3) (Kaplan et al., 1993; Kretzschmar et al., 1993; Seta and Karathanasis, 1997). While some studies indicated enhanced dispersibility and stability with increased OC content due to both charge and stearic stabilization (Kaplan et al., 1993; Kaplan et al., 1997; Kjaergaard et al., 2004; Christian et al., 2008; Hassellov and Von der Kammer, 2008; Ottofuelling et al., 2011), other findings suggested weak correlations (Seta and Karathanasis, 1996). It is likely that the presence of differing OC functional groups caused a different behavior. Referring back to the d_h findings (Fig. 3.1), the greatest aggregation potentials with contaminant additions occurred in the biosolid colloids that had a combination of greater OC content and surface area (Tables 3.1 and 3.3). Correlations between amount of C measured per unit surface area (SA) showed that the greatest aggregation potentials occurred in the colloids with the highest C:SA ratios (kaolinitic and biosolid nanocolloids, respectively) (Fig. 3.1, Tables 3.1 and 3.3). The difference in OC functional group as well as C:SA ratio may also explain differences in stability findings (Tables 3.1 and 3.3; Fig. 3.1). It is also possible that OC bridges together micro-nano-aggregates that are more stable in suspension than individual particles. Despite higher OC and potential formations of micro-nano-aggregates, nanocolloids were generally still more stable in the absence and presence of contaminants than were macrocolloids (Fig. 3.1).

3.3.2.6 Zeta Potential Effects

Nanocolloid zeta potentials were more negative than that of their corresponding macrocolloids, with both sizes showing increasingly negative zeta potentials with

increased pH (Fig. 3.6). Mineral nanocolloids exhibited more negative zeta potentials than their corresponding macrocolloid counterparts and the bio-colloids, especially above pH 6 (Fig. 3.6). Based on the assumption that zeta potentials approximate the charge residing in the diffuse layer of the electrical double layer, the negative zeta potential values suggest that all colloids bear a net negative surface charge (Sposito, 1984). The increased negative charge with increasing pH is ascribed to the deprotonation of phyllosilicate edge sites (Frey and Lagaly, 1979), and indicates repulsion energies of the particles, suggesting increased stability potential of nanocolloids over corresponding macrocolloids (Fig. 3.6), especially in negatively charged subsurface environments (McCarthy and Zachara, 1989).

In the mineral colloids, there is never a point where the zeta potential reached zero (Fig. 3.6), suggesting the isoelectric point (the pH of zero mobility) was <4 for all colloids (Sposito, 1984; Essington, 2004). This was especially surprising in fractions where mineral compositions included kaolinite, which has an isoelectric point of pH 4.25 (Carroll-Webb and Walther, 1988). This suggested altered isoelectric points are likely due to the presence of other minerals or organic carbon surface coatings (Table 3.3) (Bertsch and Seaman, 1999).

The biosolid colloids had differing trends from the mineral colloids, where the bio-nanocolloids became less negative with increasing pH as opposed to bio-macrocolloids that showed an increased negative charge with increasing pH (Fig. 3.6d). This may suggest a lower stability potential in the bio-nanocolloids than in the bio-macrocolloids, which is the opposite of what was seen in stability kinetics experiments (Fig. 3.1). The less negative zeta potentials exhibited by the bio-colloids than the mineral colloids may be due to the greater ionic strength of the bio-colloids, especially those of the bio-nanocolloids (Table 3.3), whose higher ionic strength likely overwhelmed potential negative surface charges generated by carboxyl groups above pH's 2.5 and 6 (Essington, 2004).

In the single point zeta potential measurements, additions of 2 and 10 mg L^{-1} mixed contaminants resulted in nanocolloid zeta potentials which were still more negative than those of their corresponding macrocolloids, with both sizes showing trends based on composition (Fig. 3.7). This display of greater stability in the nanocolloids over the macrocolloids complements the stability kinetics studies, suggesting that their stabilization potentials overcame their supposed high surface energy, even in the presence of up to 2 mg L^{-1} contaminants (Karathanasis, 2010). It is noted here that in order to mimic natural conditions, the pH of the zeta potential measurements varied (Fig. 3.7), so the change in zeta potential is likely a reference to colloidal stability potential.

Overall, the mineral colloids indicated greater stability over bio-colloids through higher negative zeta potentials in the presence of 0, 2 and even 10 mg L^{-1} contaminant concentrations, although evidence of flocculation was more prevalent after 10 mg L^{-1} contaminant additions (Fig. 3.7). While some aggregation was implied with increasing ionic strengths of contaminants by slight shifts towards less negative zeta potentials (Fig. 3.7), corresponding to increased d_h values in the presence of contaminants (Fig. 3.1), the nanocolloids indicated significantly greater stability potentials over their corresponding macrocolloids.

Figure 3.7. Zeta potentials and pH for each zeta potential measurement for the nano- and macro-colloids in the presence and absence of equal parts (0, 2, and 10 mg L^{-1}) mixtures of each contaminant (As, Se, Cu and Pb; the sum of each contaminant totaled 2 and 10 mg L^{-1}). Error bars represent standard error between triplicate measurements taken on duplicate samples.

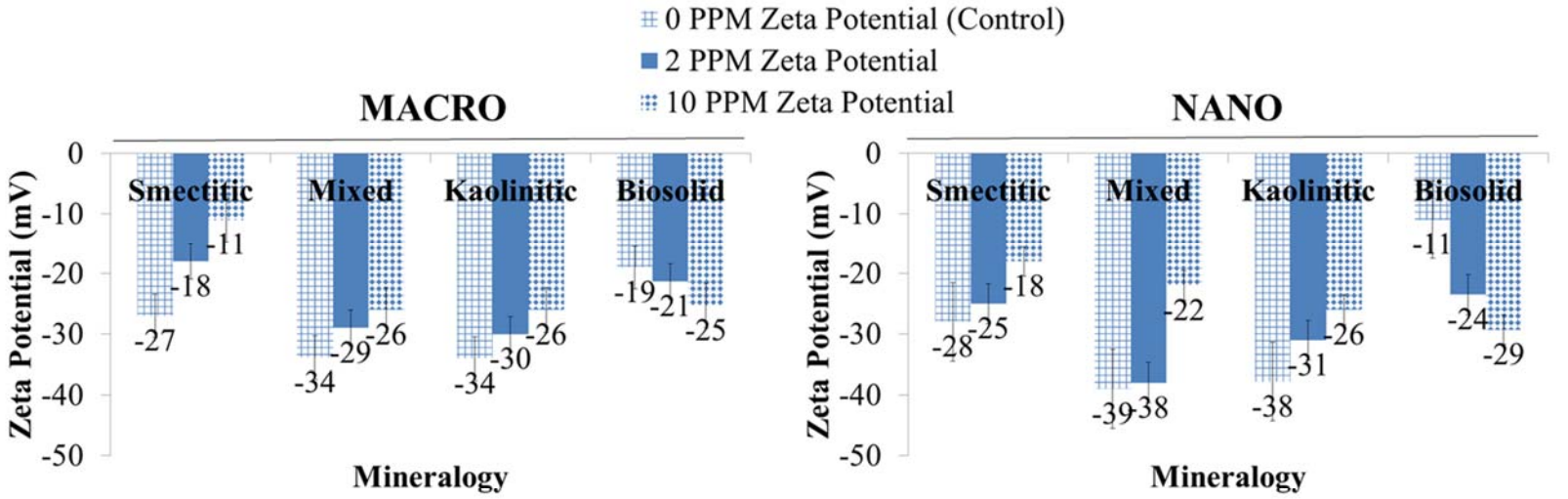

Macrocolloid pH of Zeta Potential Samples

	Smectitic	Mixed	Kaolinitic	Biosolid
0 PPM	4.60	5.50	4.98	5.11
2 PPM	4.67	4.45	4.96	5.42
10 PPM	4.38	4.24	4.40	5.18

Nanocolloid pH of Zeta Potential Samples

	Smectitic	Mixed	Kaolinitic	Biosolid
0 PPM	5.11	4.84	4.90	5.25
2 PPM	5.02	4.61	4.79	5.79
10 PPM	4.56	4.33	4.55	5.69

Kjaergaard et al. (2004) suggested that the colloids with the most negative zeta potential had the largest resistance to flocculation, which was true for the smectitic, mixed, kaolinitic and biosolid nanocolloids in the absence and presence of 2 and 10 mg L^{-1} contaminants (Fig. 3.7). The macrocolloids did not show the same stability trends based on composition, and surprisingly, the smectitic macrocolloids were the least stable upon contaminant additions as compared to the other mineral (and even the biosolid) macrocolloids (Fig. 3.7). The lack of stability indicated by lower negative zeta potentials in the smectitic macrocolloids upon addition of contaminants (despite their higher initial zeta potential) may be a function of their smaller C:SA ratio (Tables 3.1 and 3.3), and the greater shifts in their zeta potentials (-27 mV without contaminants shifting to -18, then -11 mV with 2 and 10 mg L^{-1} contaminant additions, respectively) materialized by greater cation contaminant attraction to their high initial negative charge and to larger surface area availability (Fig. 3.7). Despite this large shift in the smectitic macrocolloid zeta potential, the stability kinetics studies indicated that smectitic macrocolloids were more stable than any of the other mineral and biosolid macrocolloids (Fig. 3.1). The disparity of the zeta potential data to that of the stability kinetics data suggests that while the zeta potentials are consistent in predicting colloid stability of minerals versus biosolids, they may be inconsistent in predicting stability trends based on mineralogy.

The implications may be that colloid stability may not be accurately predicted from zeta potential and d_h measurements in the presence of contaminants. Also, it emphasizes placing more weight on stability settling experiments than chemical data alone for transport predictions (although chemical characterization should still be considered important for explaining portions of the overall model). Finally, this showcases how irrelevant the average surface charge of colloids may become in contaminant transport behavior because of spatial heterogeneity and the importance of considering additional multiple relevant factors to achieve reliable assessments of environmental risks (McCarthy and McKay, 2004).

3.4 Conclusions

This study filled a previous void on the stability behavior of natural soil and biosolid water dispersible nanocolloids and their differences from their corresponding larger macrocolloid fractions. The findings demonstrated that soil and biosolid nanocolloids are more stable in the absence and presence of up to 2 mg L^{-1} As, Se, Cu and Pb contaminants than corresponding macrocolloids. Only the bio-nanocolloids showed considerable stability at higher contaminant loads. The importance of mineralogy in stability was best shown by the macrocolloids, where the smectitic and mixed colloids were more stable than the kaolinitic and biosolid compositions. In the nanocolloids, the mineral colloids were more stable than the bio-colloids. Kaolinitic nano- and macro-colloids showed surprisingly high stability potentials, even in the presence of goethite and gibbsite minerals, likely due to stearic stabilization effects of surface OC functional groups. Overall, nanocolloids, regardless of mineralogy, where shown to have as much as 20% more colloids in suspension after 48 hours in the absence and presence of As, Se, Cu and Pb contaminants. While size played a very important role in the colloid stability behavior, nanocolloids were also found to enhance aggregation of macrocolloids via surface attachment on their surfaces. Further study is needed to better understand the causes of this nano-mediated aggregation behavior, but the presence of OC surface

coatings and increased Al/Fe:Si ratios of nanocolloids may have contributed to macrocolloid coagulation. Overall, the findings of this investigation demonstrated that sub-horizon nanocolloids - through a combination of physical, chemical, mineralogical and morphological properties that contribute to enhanced stability in natural environments possess a higher potential to transport contaminants to greater distances than their corresponding larger size macrocolloid fractions. This potential was even greater with the bio-nano-colloids at higher contaminant loads. However, coagulation phenomena through nano-macro-colloid interactions may complicate their behavior in natural environments and result in misleading predictions. Therefore, multiple physicochemical and mineralogical parameters need to be considered in contaminant transport models in order to accurately assess environmental pollution risks and develop efficient remediation strategies.

Chapter Four - Sorption Behavior of Lead, Copper, Arsenic and Selenium by Soil and Biosolid Nano- and Macro-colloids

4.1 Introduction

Major environmental concerns have risen within the past decade in regard to large-scale contamination of natural resources. The vast devastation experienced from catastrophic events such as hurricanes Sandy (2012) and Katrina (2005) have highlighted an ongoing water quality issue, which is the transport or mass influx of contaminants into groundwater supplies following storm events. Remediators need information on contaminant interactions at the soil-water interface and how these interactions affect contaminant plume movement and contaminant transport in surface and ground waters. One potential vector of contaminant transport that should be further investigated is that of naturally occurring environmental nanoparticles, such as those derived from soils or biosolids (IUPAC, 1997; Christian et al., 2008; Hochella, 2008; Maurice and Hochella, 2008; Theng and Yuan, 2008). Soil nanoparticles include humic substances, clay minerals/colloids, and metal (hydr) oxides (Theng and Yuan, 2008; Karathanasis, 2010; Tsao et al., 2011). Biosolid nanoparticles are present in the environment after human and animal wastes are land applied as fertilizers (Haering and Evanylo, 2006).

Recent research has also highlighted the potential dangers of the movement and biotoxicity of engineered nanoparticles in the environment and the development of engineered nanoparticles for remediation of contaminant plumes (Lowry et al., 2006; Saleh et al., 2007; Unrine et al., 2008; Judy et al., 2011). With regard to their behavior in environmental media, both as potential contaminant transport systems and as a model for manufactured nanoparticles (IUPAC, 1997; Christian et al., 2008; De Momi and Lead, 2008; Hochella et al., 2008; Maurice and Hochella, 2008; Theng and Yuan, 2008), research on naturally occurring environmental nanoparticles is limited.

Soil and biosolid nanocolloids, with their large surface area and greater reactivity, have the potential to sorb and transport larger quantities of heavy metals into groundwater supplies than macrocolloids. As particle size decreases, stability and surface area increase, which translates into greater potential for sorption and transport of contaminants than larger size fractions (Maurice and Hochella, 2008; Bolea et al., 2010; Karathanasis, 2010). Both mineral and biosolid derived nanocolloids can form inner- and outer-sphere complexes with heavy metals via surface siloxane, aluminol, carboxylic, and phenolic groups (Echeverria et al., 1998; Cruz-Guzman et al., 2003). The type of bonding between nanocolloid surfaces and contaminants will also dictate the likelihood of re-suspension of the contaminant in different ionic or pH environments, further demonstrating the need for a better understanding of the solid-solution interface between nanocolloids and potential contaminants (Echeverria et al., 1998; Bolea et al., 2010).

Environmental contaminants such as Pb, Cu, As, and Se are of considerable environmental concern (Echeverria et al., 1998; Weng et al., 2001; Cruz-Guzman et al., 2003). Studies of their interactions with various clay minerals suggested that sorption processes are controlled by the competition between ions in solution and those on the colloidal surface, pH, ionic strength, and colloid mineralogy (Echeverria et al., 1998; Covelo et al., 2007). Metal sorption processes on clay and organic surfaces may include: the presence in and competition for high-affinity binding sites from organic functional groups, the formation of ternary metal-organic surface complexes, and the alteration of surface charge from organic moieties during sorption to mineral surfaces (Heidmann et

al., 2005). However, very little is known about the interaction and sorption behavior of these contaminants with environmental nanoparticles since most of the investigations involved clay size fractions.

The objectives of this study were to evaluate and compare the sorption behavior of environmental nano- and macro-colloids with different composition for Pb, Cu, As and Se contaminants. We hypothesized that (i) nanocolloids will have higher sorption affinities for contaminants than the corresponding macrocolloids, (ii) cationic metals (Pb, Cu) will have stronger binding affinities to the soil and biosolid colloids likely due to innersphere bond formations as compared to that of the oxy-anions (As, Se), which will likely undergo outersphere bonding, and (iii) biosolid-derived colloids will have higher sorption affinities for selected contaminants than will mineral colloids. The findings of this study will be useful for water quality professionals and environmental consulting agencies undertaking remediation tasks involving contaminant movement in subsurface media and groundwater as well as to developers of engineered nanoparticles who seek to better understand and model the interaction and potential behavior of nanoparticles in the environment.

4.2 Materials and Methods

4.2.1 Colloid Generation

The Bt horizons of three Kentucky soils of differing mineralogy were used to generate the mineral colloids: Caleast-variant (fine, smectitic, mesic mollic Hapludalf), Tilsit (fine-silty, mixed, mesic Typic Fragiudult), and Trimble (fine-loamy, siliceous, mesic Typic Paleudult), referred to herein as smectitic, mixed, and kaolinitic, respectively. Biosolid colloids were fractionated from an aerobically digested municipal sewage sludge obtained from Jessamine County, Kentucky. Centrifuge fractionations using Stokes law allowed separation of the two size classes (nanocolloids <100 nm and macrocolloids 100-2000 nm) using a Centra GP8R Model 120 centrifuge (ThermoIEC). Clay fractions were separated from bulk soils by centrifugation at 107 RCF for 3.5 minutes, as calculated using a rotor radius of 170 mm, 107 RCF, a density difference of 1650 kg m^{-3}, and viscosity of 0.0008904 Pas. Nanocolloids were then separated from corresponding macrocolloids at 4387 RCF for 46 minutes, as calculated using a rotor radius of 170 mm, a speed of 4387 RCF, a density difference from water of 1650 kg m^{-3}, and viscosity of 0.0008904 Pas (Karathanasis, 2010, Karathanasis, et al., 2005). The colloids were generated with de-ionized water (resistivity of 1 μΩcm at 25°C).

4.2.2 Sorption Isotherms

The following reagents were used to prepare all contaminant concentrations used in this study: Aqueous solutions of Pb, Cu, As and Se were prepared from $PbCl_2$ (98% purity, Aldrich Chemicals, Milwaukee, WI), $CuCl_2$ (>99% purity, Sigma Chemical Company, St. Louis, MO), arsenic acid $Na_2HAsO_4 \cdot 7H_2O$ (98% purity, Sigma Chemical Company, St. Louis, MO), and sodium selenate decahydrate $Na_2SeO_4 \cdot 10H_2O$ (99.9% purity, Sigma Chemical Company, St. Louis, MO). Nano- and macro-colloid affinities for these contaminants were evaluated in mono-metal adsorption isotherms using duplicate colloid suspensions of 50 mg colloid L^{-1} de-ionized water, and spiked with contaminants to make solutions of 0.2, 0.5, 1, 2, 5 and 10 mg L^{-1} of either Cu and Pb-chloride salts, selenate or arsenic acid. Mixed-metal adsorption isotherms were also generated to evaluate the competitive affinity of each nano- and macro-colloid for Cu, Pb, Se, and As contaminants as a mixed system. MINEQL$^+$ indicated the predominant species were as follows: 99.9%

Pb^{2+}, 99.9% Cu^{2+}, 99.7% SeO_4^{-2}, and 98.6% H_2AsO_4, showing under-saturated conditions with respect to contaminant-bearing solid phases at even the highest initial contaminant concentrations, with the exception of the bio-colloids which had some over-saturation of chloropyromorphite. To reach equilibrium, the isotherms were shaken for 24 hours at room temperature (25 ˚C) in polyethylene tubes with pH measurements occurring at time 0 and at 24 hours. After shaking, nitrocellulose filters of 0.025 µm were used to separate the supernatant from the colloidal fraction. Supernatant fractions were preserved with 1% nitric acid, stored in polyethylene vials, and analyzed within 24 hours via inductively coupled plasma mass spectroscopy (ICP-MS). To best mimic a natural system the colloids were used as a natural buffer and the electrolyte matrix was composed of de-ionized water (resistivity of 1 µΩcm at 25°C). Experimental blanks and controls helped minimize error. Mass of contaminant sorbed per mass of colloid was calculated (Eq. 1) and plotted using the Freundlich equation (Eq. 2; Essington, 2004). Mass of contaminant sorbed was also calculated per unit surface area (Smith et al., 2002) and organic carbon (Eq. 3) of the respective nano- and macro-colloids and plotted using the Freundlich equation (Essington, 2004).

$$q = \frac{V \times (Cin - Co)}{M} = \mu mol\ kg^{-1}$$

Equation 1. Where q is the mass of contaminant sorbed per mass of soil, V is the volume used in the sorption isotherm experiment, Cin is the amount of contaminant put into solution, Co is the amount of contaminant measured at equilibrium and M is the mass of the sorbent (Essington, 2004).

$$\mathrm{Log}q = N\ \mathrm{Log}C_{eq} + \mathrm{Log}K_f$$

Equation 2. Plotting Log$q$ (y-axis variable) and LogC_{eq} (x-axis variable) yields a straight line with N slope and y-intercept LogK_f (Essington, 2004).

$$q = \frac{V \times (Cin - Co)}{M} = \frac{\mu mol}{km^2\ surface\ area}, \ or\ \frac{\mu mol}{kg\ Carbon}$$

Equation 3. Where q is the mass of contaminant sorbed [V x (Cin – Co)] per unit (M) surface area, or organic carbon (Essington, 2004, Smith, Naidu, et al., 2002).

4.2.3 Physico-chemical and Surface Characterizations

All analyses were performed on suspensions of 50 mg colloid L^{-1} in de-ionized water. A Malvern Instruments Zetasizer Nano ZS (Malvern, United Kingdom) measured suspensions for intensity weighted mean particle hydrodynamic diameters (z-average diameter) using dynamic light scattering (173° backscatter analysis method). Nano- and macro-colloid crystallite sizes were determined using transmission electron microscopy (TEM; JEOL 2010F, Tokyo, Japan) and scanning electron microscopy (SEM; Hitachi S-4300, Tokyo, Japan), respectively (Goldstein et al., 1992; Zhu and Lu, 2010; Nemeth et al., 2011). ImageJ software was used to calculate average minimum diameters (ImageJ 1.46r, Wayne Rasband, National Institutes of Health, USA). Surface area was measured using the Ethylene Glycol Monoethyl Ether (EGME) method. Electrical conductivity and pH were measured on a Denver Instruments Model 250 pH*ISE*electrical conductivity meter (Arvada, CO), and ionic strength was estimated by multiplying electrical conductivities by 0.0127 (Griffin and Jurinak, 1973). Cation exchange capacity was determined using an adapted version of the ammonium acetate method and reported as a sum of the base cations Ca^{2+}, Mg^{2+}, K^+, and Na^+, as measured with a Varian Spectr AA 50B atomic absorption spectrometer. Organic carbon was measured on a Flash EA 1112 Series NC Soil Analyzer (Thermo Electron Corporation) with a Mettler Toledo MX5

microbalance. Zeta potentials in the presence of 0 and 2 mg L^{-1} Pb, Cu, As, and Se were converted from electrophoretic mobility measurements using the Smoluchowski approximation on a Malvern Zetasizer Nano ZS (Malvern, United Kingdom).

4.2.4 Mineralogical Characterization

Mineralogical characterizations were completed using X-ray diffraction (XRD) and Thermogravimetric analysis (TG) on a Phillips PW 1840 diffractometer and PW 1729 x-ray generator (Mahwah, NJ), and a Thermal Analyst 2000 (TA Instruments) equipped with a 951 Thermogravimetric Analyzer (DuPont Instruments), respectively (Karathanasis et al., 2005; Karathanasis, 2008).

4.2.5 Statistical Analysis

The standard accepted error level for all duplicate and triplicate samples was 15%. Mean differences in sorption Freundlich coefficients (LOG K_f) and changes in the isotherm pH were calculated using the general linear model (PROC GLM). Mean differences (overall and based on mineralogy, size, and contaminant) were developed using Fisher's protected least significant difference test (LSD) in SAS using probability levels of 0.05, unless otherwise noted. Competitive sorption relationships were analyzed between colloid properties and sorption coefficients using multiple regression analysis using probability levels of 0.05 in SAS 9.3 (SAS Institute Inc., Cary, NC, USA).

4.3 Results and Discussion

4.3.1 Mono-metal Isotherms

Mono-metal isotherms were generated for each colloid size and composition studied (smectitic, kaolinitic, mixed and biosolid nano- and macro-colloids) and normalized to colloid mass (Table 4.1), surface area, and organic carbon (surface area and organic carbon data not shown) for the four contaminants studied (As, Se, Cu, Pb). Aside from soil pH, organic carbon, and surface area have been shown in many studies to be key factors in understanding sorption patterns (McKenzie, 1980; McBride, 1994; Naidu et al., 1997; Echeverria et al., 1998; Peak and Sparks, 2002; Lair et al., 2006; Seo et al., 2008). The effects on sorption of each contaminant are detailed in the next few sections.

4.3.1.1 Mono-metal Isotherms Normalized to Colloid Mass

Isotherms of As, Se, Cu and Pb sorption by colloid fractions were prepared by plotting equilibrium solution concentrations of contaminants (μmol L^{-1}) against calculated amounts of solid phase sorbed contaminants (μmol kg $colloid^{-1}$). The data conformed well to the Freundlich equation, showing R^2 values between 0.93 and 0.99 (Table 4.1), with differing sorption trends for each contaminant.

Generally, As sorption coefficients were the lowest among the contaminants studied (Fig. 4.1, Table 4.1). Arsenic was likely present as the oxy-anion arsenate in this study, which tends to form outer sphere complexes, yet inner sphere complexes as well. Inner sphere complexes are usually formed with goethite (Gao, 2008), or indirectly with organic groups through bridging on Al and Fe hydrolytic species (Violante, 2013). Outer sphere complexes can be formed with variable charge minerals and phyllosilicate edges (Violante, 2013). Macrocolloid As sorption affinities ranged from 1.67 to 3.48, with the highest affinity representing the mixed mineralogy and the lowest the biosolid colloids (Fig. 4.1, Table 4.1). Sorption affinities for As within the nanocolloids ranged from 1.85 to 3.60, with the highest affinity associated with the kaolinitic and the lowest with the biosolid colloids (Fig. 4.1, Table 4.1).

Table 4.1. Freundlich equation parameters and statistical fitness for monometal isotherms normalized by colloid mass (LOG Data).

		LOG Kf (L kg^{-1})				1/*n*				R^2			
Colloid	Size	As	Se	Cu	Pb	As	Se	Cu	Pb	As	Se	Cu	Pb
Smectitic	Macro	3.13	3.09	4.41	5.14	0.82	1.22	0.85	0.43	0.97	0.97	0.99	0.98
	Nano	3.30	2.06	4.54	5.02	0.70	1.53	0.76	0.50	0.96	0.98	0.99	0.93
Mixed	Macro	3.48	3.49	4.25	4.32	0.44	0.80	0.83	0.49	0.99	0.96	0.98	0.97
	Nano	2.53	3.53	4.29	4.33	0.86	0.56	0.85	0.44	0.99	0.99	0.99	0.95
Kaolinitic	Macro	2.78	3.21	3.72	3.96	0.43	1.05	1.14	0.52	0.99	0.99	0.98	0.98
	Nano	3.60	2.74	4.29	4.61	0.52	1.23	0.86	0.25	0.98	0.96	0.99	0.92
Biosolid	Macro	1.67	3.21	4.62	5.51	1.30	0.94	0.87	0.41	0.98	0.99	0.99	0.98
	Nano	1.85	3.39	4.18	6.20	1.77	0.79	1.13	0.88	0.95	0.99	0.98	0.99

Figure 4.1. Mono-metal Kf values for (a) arsenic, (b) selenium, (c) copper, and (d) lead. Error bars represent standard error between compositions of each size fraction.

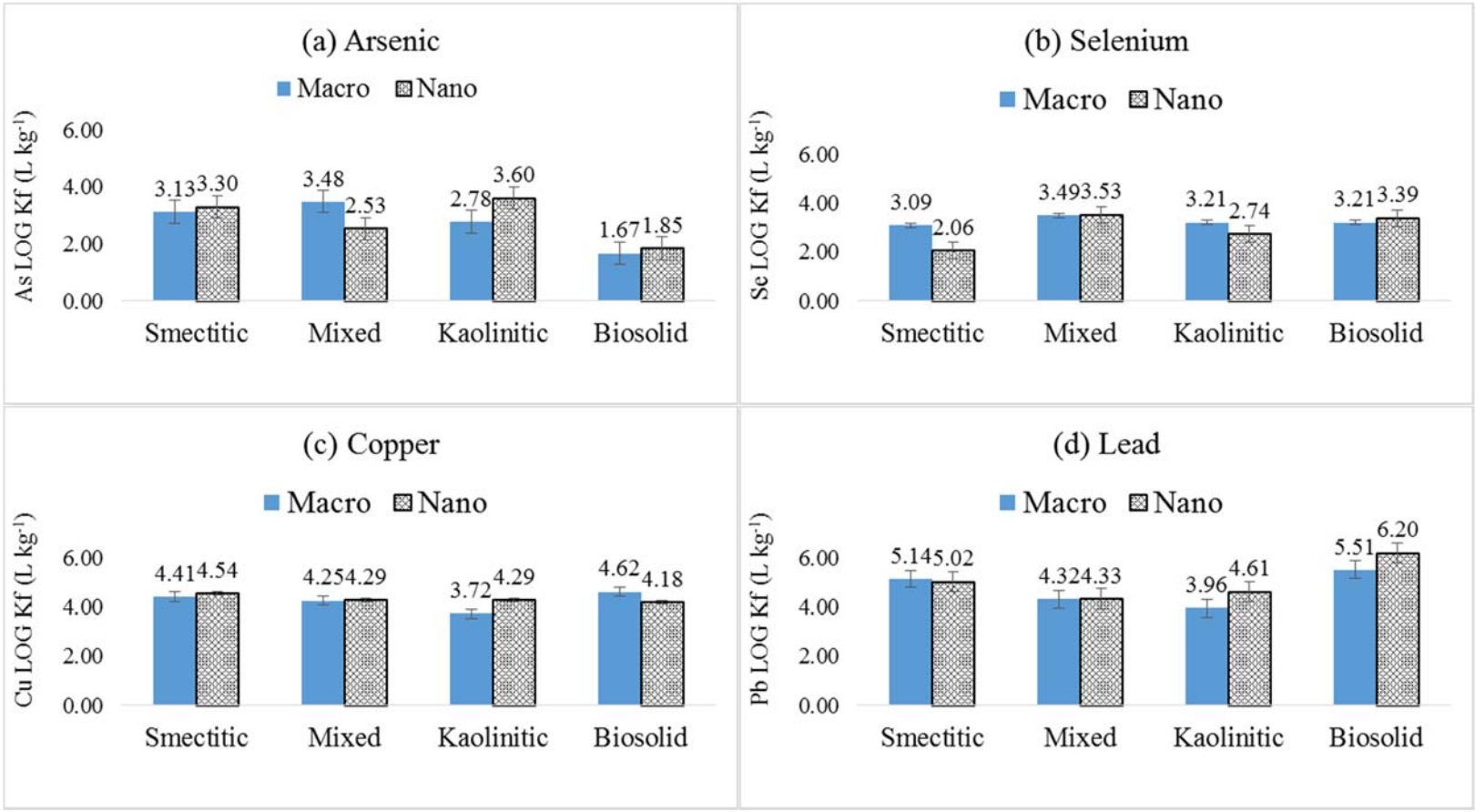

Typically, fractions dominated by kaolinitic minerals have greater anion (As) sorption capacities than those of illite or smectite (Violante, 2013). The biosolid colloids showed lower overall As affinity than the mineral colloids (Fig. 4.1), contrary to studies showing increased arsenate sorption in compositions with high organic matter (Balasoiu et al., 2001; Saada et al., 2003). This could be explained by the higher pH (Table 4.2) and phosphate content (data not shown) in the bio-colloids as compared to the mineral colloids. Phosphate has been shown to displace As, and arsenate sorption has been shown to decrease with increasing pH (Lui et al., 2001; Gao, 2008). There were no statistical differences in As sorption affinity between nano- or macro-sizes in the smectitic and the biosolid colloid fractions, however, significant differences with opposite trends were observed within the mixed and kaolinitic mineralogy colloids, with the kaolinitic nanocolloids and the mixed macrocolloids showing higher affinity than the other fractions (Fig. 4.1). Others have found both Fe-oxy-hydroxides and kaolinitic soils demonstrate high sorption capacities for arsenate (Bowell, 1994; Balasoiu et al., 2001), especially in the presence of humic acid surface coatings (Saada et al., 2003). In micaceous mineral fractions, surface hydroxyl-Al has been shown to contribute to sorption of arsenate, especially in particles less than 200 nm in size (Huang, 1975). Additionally, there was a weak correlation between As sorption affinities and surface area ($R^2 = 0.61$).

Next to As, Se also exhibited low sorption coefficients compared to those of Cu, and Pb (Fig. 4.1). Selenium in oxygenated soil environments typically occurs as the oxy-anion selenate, which can be sorbed via inner- and outer-sphere complexes, although it usually undergoes outersphere sorption (Ahlrichs and Hossner, 1987; Bar-Yosef and Meek, 1987; Neal and Sposito, 1989; Jackson and Miller, 1999; Peak and Sparks, 2002). Sorption affinities for Se within the macrocolloids showed no particular preference for composition, ranging from 3.09 to 3.49. The highest affinity was observed with the mixed mineralogy and the lowest with the smectitic colloids (Fig. 4.1, Table 4.1). There was more range within the nanocolloids (2.06 to 3.53) with the highest affinity representing the mixed mineralogy and the lowest the smectitic composition (Fig. 4.1, Table 4.1). The higher affinity of the mixed colloids for Se over the smectitic could be attributed to greater quantities of kaolinite and less smectite (Ahlrichs and Hossner, 1987; Bar-Yosef and Meek, 1987). Negative linear correlations observed between Se sorption affinities and the percentage of smectite minerals present are consistent with the anionic behavior of this contaminant ($R^2 = -0.42$) (Ahlrichs and Hossner, 1987; Bar-Yosef and Meek, 1987). Statistical differences in Se sorption affinity were observed only in the smectitic and kaolinitic nanofractions showing significantly lower sorption coefficients than their respective macro sizes (Fig. 4.1; p-value $< \alpha=0.05$). Selenate usually displays high affinity for goethite containing fractions through formation of inner- and outer-sphere complexes (Peak and Sparks, 2002; Waychunas et al., 2005). Another interesting relationship is the much higher affinity of the biosolid colloids (macros and nanos) for Se compared that shown for As (Fig. 4.1 p-value $< \alpha=0.05$). Despite predictions of stronger sorption of arsenate over selenate due to lower shared charge (Goh and Lim, 2004), greater Se sorption over As in the biosolids complimented findings in waste-amended soils by Jackson and Miller (1999).

Table 4.2. Physical and chemical characteristics of nano- and macro-colloids.

Properties	Colloids							
	Smectitic		Mixed		Kaolinitic		Biosolid	
Size Class	Macro	Nano	Macro	Nano	Macro	Nano	Macro	Nano
DLS † Mean Hydrodynamic Diameter (d_h) ±SD ‡ (nm)	487± 10	181±3	596± 21	205±4	545±25	187±4	4456±599	353±8
SEM/TEM ¶ Mean Smallest Particle Size ±SD ‡ (nm)	328±144	37±13	549±394	7±5	288±184	41±19	363±338	50±19
Surface Area ($m^2\ g^{-1}$) ±SD ‡	708±137	879±76	420±105	466±10	333±37	389±44	1674±70	1303±63
Electrical Conductivity (mmhos cm^{-1})	$3.93x10^{-3}$	$6.07x10^{-3}$	$2.91x10^{-3}$	$3.09x10^{-2}$	$2.87x10^{-3}$	$3.80x10^{-3}$	$1.56x10^{-2}$	$4.69x10^{-2}$
Ionic Strength § (mol L^{-1})	$4.99x10^{-5}$	$7.71x10^{-5}$	$3.70x10^{-5}$	$3.92x10^{-4}$	$3.64x10^{-5}$	$4.83x10^{-5}$	$1.97x10^{-4}$	$5.96x10^{-4}$
Natural pH	4.92	5.12	5.07	4.92	4.91	5.38	5.39	5.25
CEC ($cmol_c\ kg^{-1}$) #	35.05±12.84	42.19±15.12	8.89±1.62	10.51±1.67	6.94±1.85	13.12±2.84	37.61±14.85	70.99±22.98
OC (mg kg^{-1}) ‡‡	658	897	645	774	430	647	1.3K	16K
C:SA	0.93	1.02	1.54	1.66	1.29	1.66	0.78	12.28

† DLS = Dynamic Light Scattering was used to measure the mean intensity weighted hydrodynamic diameters (d_h, or z-average diameter).

‡ SD = Standard Deviation was calculated based on the averages of duplicate or triplicate measurements (see Methods section).

§ Ionic Strength (IS) = Estimated using Griffin and Jurinak's equation where IS (mol L^{-1}) = 0.0127 x Electrical Conductivity (millimhos cm^{-1}) (1973).

¶ SEM = Scanning Electron Microscopy, TEM= Transmission Electron Microscopy data represent the average smallest dimension of 300 representative particles from three to eight images of each size fraction as measured until the average and standard deviation values had less than 10% variation.

CEC = Cation Exchange Capacity by sum of cations.

‡‡ OC = Organic Carbon was derived by subtracting dissolved organic carbon from total carbon measurements. Due to low pH conditions and the typical absence of carbonates in the region, Inorganic carbon contributions were assumed to be minimal.

The lower sorption potentials of the kaolinitic and smectitic nano-fractions over corresponding macro-sizes despite larger surface areas may be evidence of less available sorptive surfaces due to nano-nano and nano-macro aggregation that may have been enhanced by organic carbon surface coatings (Table 4.2). Organic carbon can increase surface charge and reactivity with contaminants (Naidu et al., 1997; Lair et al., 2006), but in this case it may have induced lower sorption potentials in some of the nanocolloids by enhancing aggregation and decreasing available surface area for sorption (Redman et al., 2002; Cruz-Guzman et al., 2003). This is also evidenced by increases in size measurements between TEM/SEM crystallite particle sizes and d_h measured sizes, indicating particle aggregation (Table 4.2).

Generally, Cu sorption affinity by all colloid fractions was consistently higher than that demonstrated for As or Se (Fig. 4.1). Cation contaminants (Cu, Pb) tend to show ion exchange behavior on phyllosilicates, with electrostatic surface bonding and chemisorption to surface –SiOH and –AlOH groups (Violante, 2013). Sorption coefficients for Cu within the macrocolloids ranged from 3.72 to 4.62, with the highest affinity representing the biosolid composition and the lowest the kaolinitic (Fig. 4.1, Table 4.1). Copper has been shown to dominantly associate with mineralizable biosolid fractions in other studies (Donner et al., 2012), likely due to the presence of multi-ligand complexing systems through a variety of organic surface functional groups (Violante, 2013). In contrast, within the nanocolloid fractions, the highest affinity was associated with the smectitic (4.54) and the lowest (4.18) with the biosolid composition (Table 4.1). The opposite trend of Cu affinity observed in the smectitic and biosolid nanocolloids compared to the corresponding macrocolloids may be explained by greater C:SA ratios in the bio-nanocolloids that could potentially be aggregating and blocking sorption surface sites. The lower initial pH of the smectitic nanocolloid over the bio-nanocolloid (Table 4.2) may have enhanced sorption of Cu through interlayer spaces (Morton et al., 2001; Strawn et al., 2004) or through greater disassociation due to their lower pH, creating more available surface area for sorption. Additionally, smectite minerals can contribute to sorption because of their permanent charge and availability of internal and external surface areas (Morton et al., 2001). Statistical differences in Cu sorption affinity based on size were observed only between the kaolinitic macro- and nano-colloid fractions (Fig. 4.1; p-value $< \alpha=0.05$). Weak to moderate, negative linear correlations were found between Cu sorption affinities and the amount of kaolinite and HIV present in the sample (R^2 = -0.44 and -0.71, respectively), despite this, higher pH-dependent mineral fractions, such as those high in kaolinite, have been shown to contribute to preferential adsorption (Karathanasis, 1999).

Sorption affinities for Pb were the highest compared to other contaminants. Within the macrocolloids the highest coefficient (5.51) was associated with the biosolid composition and the lowest (3.96) with the kaolinitic (Table 4.1). Sorption affinities for Pb within the nanocolloids ranged from 4.33 to 6.20, with the highest value representing the biosolid composition and the lowest the mixed (Table 4.1). Statistical differences in affinity for Pb based on composition followed the trend: Biosolid (A) $\geq$ Smectitic (AB) $\geq$ Mixed (B) = Kaolinitic (B) (p-value $< \alpha=0.05$). These composition-based trends are complimentary to literature showing biosolids preferentially sorb Pb over other cation metals like Cu or Zn (Karathanasis et al., 2005), and smectitic minerals have shown increased affinity for Pb due to their permanent charge, and the availability of internal and external surface

area (Morton et al., 2001). Additionally, Pb (and most cation metals) have the ability to form inner sphere complexes with mineral surface –OH groups (Violante, 2013). Only the kaolinitic and biosolid colloids showed size sorption preferences, with the nanofractions being greater than the macro size fractions. Lead sorption affinities showed weak to moderate, negative correlations with the percentage of kaolinite and HIV minerals present (R^2 = -0.61 and -0.63, respectively); moderate to strong, positive relationships with the percentage of smectite present, CEC, and surface area (R^2 = 0.78, 0.92, and 0.73, respectively); and weak, positive relationships with organic carbon and carbon:surface area (R^2 = 0.56 and 0.46, respectively).

In summary, the mono-metal isotherm data normalized by surface area and organic carbon (not shown) did not give consistent or significant differences in size or composition-based trends. Despite this, all of the isotherm normalization methods showed cation contaminants (Cu, Pb) were preferentially sorbed over anion contaminants (As, Se), comparable to the findings of Echeverria et al. (1998), Smith et al. (2002) and Karathanasis and Johnson (2006). Altogether, the mono-metal isotherms had the following contaminant sorption preference: Pb (A) > Cu (B) > As (C) = Se (C) (Table 4.1; p-value < α= 0.05). Greater sorption of Pb than Cu is likely due to lead's lower hydrolysis constant (Heidmann et al., 2005; Sipos et al., 2008; Violante, 2013). The similar sorption of As to Se is contrary to other findings where arsenate has been shown to preferentially sorb over selenate (Goh and Lim, 2004), and may be explained by the bio-colloid's higher preference for Se, which may have overshadowed expected differences in anion sorption. There were surprisingly few sorption trends based on composition or size (Tables 4.1 and 4.3). Kaolinitic nano-colloids sorbed greater quantities of Pb, Cu, and As than corresponding macrocolloids, additionally, there was greater sorption of Pb by biosolid nanocolloids than macrocolloids and greater sorption of As by the mixed macrocolloids than nanocolloids (p-values < α=0.05). Finally, the smectitic and kaolinitic macroocolloids exhibited greater Se sorption affinities than did corresponding nanocolloids (Table 4.1; p-values < α=0.05).

Lack of greater sorption trends based on composition are surprising because kaolinite, for example, can have a greater capacity to sorb anions (including oxy-anions like Se and As) than illite or montmorillonite (Violante, 2013). Additionally, surface silanol and aluminol groups like those of montmorillonite and kaolinite tend to preferentially sorb cation contaminants such as Cu and Pb (Violante, 2013). The lack of greater sorption differences between size - and even composition - may be explained by the occurrence of nano-nano aggregation, and nano-macro aggregation; aggregation has been indicated to encapsulate contaminants within aggregates, with potential alterations to contaminant dispersal upon transport (Waychunas et al., 2005). Some studies show lower association of contaminants (from compost leachates) with nanocolloids compared to larger size fractions (Bolea et al., 2010), while others have indicated greater sorption and transport from smaller sized particles (Karathanasis, 2010).

Table 4.3. Mineralogical compositions of nano- and macro-colloids.

Properties	Colloids							
	Smectitic		Mixed		Kaolinitic		Biosolid	
Size Class	Macro	Nano	Macro	Nano	Macro	Nano	Macro	Nano
Kaolinite (%) ‡	29	30	42	46	52	55	NA §	NA §
Geothite (%) ‡	7	9	5	7	12	15	NA §	NA §
Gibbsite (%) ‡	0	0	0	0	5	6	NA §	NA §
Quartz (%) ‡	6	4	5	3	4	2	NA §	NA §
Mica (%) ‡	10	6	31	30	3	3	NA §	NA §
Smectite (%) ‡	48	51	0	0	0	0	NA §	NA §
MVI ¶ (%) ‡	0	0	7	7	0	0	NA §	NA §
HIV# (%) ‡	0	0	10	7	24	19	NA §	NA §

‡ Mineral percentage as determined using X-Ray Diffraction and Thermogravimentric Data (Karathanasis, 2008).

§ NA = Not Applicable

¶ MVI = Mica-Vermiculite Interstratified

HIV = Hydroxyinterlayered Vermiculite

4.3.2 Mixed-Metal Isotherms

Mixed-metal isotherms were generated for each colloid size and composition studied (smectitic, kaolinitic, mixed and biosolid nano- and macro-colloids) and normalized to colloid mass (Table 4.4), surface area, and organic carbon for the four contaminants (As, Se, Cu, Pb), because these parameters have been shown to affect sorption patterns (McKenzie, 1980; McBride, 1994; Naidu et al., 1997; Echeverria et al., 1998; Peak and Sparks, 2002; Lair et al., 2006; Seo et al., 2008). The various effects on competition for sorption between As, Se, Cu, and Pb after normalizing sorption to colloid mass, surface area, and colloid-surface organic carbon are detailed in the next few sections.

4.3.2.1 Mixed-metal Isotherms Normalized to Colloid Mass

Competition among As, Se, Cu and Pb sorption was established through mixed-metal isotherms for each colloid-size fraction. Sorption affinity was measured by Freundlich Kf values derived from plotting the equilibrium solution concentrations of contaminants (μmol L^{-1}) against calculated amounts of solid phase sorbed contaminants (μmol kg $colloid^{-1}$) (Table 4.4). The data conformed well to the Freundlich equation (Table 4.4). Most of the Freundlich 1/n values were <1, with the exception of those associated with As sorption by the smectitic, mixed, and kaolinitic macro- and nano-colloids and the biosolid macrocolloids, and Pb sorption by the smectitic and kaolinitic macro- and nano-colloids and the mixed macrocolloids, which had 1/n values >1 (Table 4.4). Freundlich 1/n values <1 probably indicate decreasing energy of sorption with increasing surface coverage (Karathanasis, 1999), while 1/n values >1 may suggest increasing energy of sorption or precipitation (Sparks, 2003). The 1/n values of the mixed isotherms were lower for Se and Cu than they were in the mono-metal isotherms. Seo et al. (2008) also showed lower sorption capacities for contaminants in mixed isotherms than in mono-metal. In the mixed isotherms, the bio-nanocolloid was the only colloid to have a 1/n value less than unity for As (Table 4.4). The mixed isotherm 1/n values indicated that all of the nanocolloids had smaller 1/n values than did the macrocolloids with the exception of the bio-nanocolloid 1/n value for Se.

There were no statistical differences in sorption affinities based on colloid composition or size despite differences in mineral compositions in the mineral colloids, as well as greater surface area and CEC in the nanocolloids over corresponding macrocolloid fractions (Table 4.2, 4.3 and 4.4). Sorption affinities for contaminants showed the following trends: Pb (A) = Cu (A) > Se (B) > As (C) (Table 4.4; p-value < α=0.05). The preferential sorption of the cation contaminants over anion contaminants is comparable to the findings of Echeverria et al., (1998), Smith et al. (2002) and Karathanasis and Johnson (2006), and is likely due to attractions of cations to the negatively charged colloid surfaces as well as due to greater charge-to-radius ratios of Cu and Pb to As and Se (McBride, 1994; Selim, 2012). While this study found statistically similar sorption affinities for Pb and Cu, others have reported conflicting sorption affinity exchanges between Cu and Pb (Schwertmann and Taylor, 1989; Seo et al., 2008).

Table 4.4. Freundlich equation parameters and statistical fitness for mixed isotherms normalized by colloid mass.

		LOG Kf (L kg^{-1})				1/*n*				R^2			
Colloid	Size	As	Se	Cu	Pb	As	Se	Cu	Pb	As	Se	Cu	Pb
Smectitic	Macro	3.04	4.12	5.04	4.55	1.62	0.79	0.54	1.44	0.92	0.69	0.64	0.95
	Nano	3.26	3.95	5.44	6.18	1.57	0.81	0.48	1.03	0.94	0.69	0.87	0.67
Mixed	Macro	3.32	3.85	5.30	5.67	1.43	0.94	0.39	1.52	0.98	0.86	0.63	0.68
	Nano	3.48	4.00	5.52	5.48	1.30	0.76	0.28	0.94	0.78	0.79	0.28	0.94
Kaolinitic	Macro	3.70	3.79	5.22	7.38	1.25	0.93	0.52	3.38	0.99	0.97	0.86	0.99
	Nano	3.39	4.03	5.16	4.54	1.24	0.71	0.50	2.02	0.76	0.95	0.79	0.80
Biosolid	Macro	3.78	4.22	5.62	6.57	1.02	0.68	0.41	0.71	0.78	0.72	0.83	0.80
	Nano	1.32	3.92	5.30	6.15	0.56	0.98	0.15	0.95	0.97	0.70	0.85	0.89

Some studies indicate Pb will preferentially sorb over Cu through inner sphere complexes due to a lower hydrolysis constant (Heidmann et al., 2005; Sipos et al., 2008), while others indicated Cu will preferentially sorb over Pb on geothite minerals due to copper's greater electronegativity and charge-to-radius ratio (McKenzie, 1980; McBride, 1994). Lead has also been indicated to sorb strongly to kaolinite, decreasing Cu sorption when both contaminants are present (Heidmann et al., 2005). Additionally, vermiculite has been shown to preferentially sorb Cu, while humic acid substances, and Fe- and Mn-oxides will sorb Pb and Cu (Violante, 2013). While the mixed-metal isotherms as normalized by colloid mass showed a preference for Se over As, Goh and Lim (2004) found preferential sorption of arsenate over selenate. Further competition for sorption could come from other cations and anions in solution, such as calcium, magnesium and sulfate or phosphate, when present (Liu et al., 2001; Gao, 2008; Violante, 2013). Mixed-metal isotherm data normalized by surface area and organic carbon (not shown) did not give consistent differences in size or composition-based trends. The mixed-metal isotherms normalized to surface area compositional based trends showed Kaolinitic (A) ≥ Mixed (AB) = Biosolid (AB) ≥ Smectitic (B), with sorption affinities for contaminants as follows: Pb (A) > Cu (B) > Se (C) = As (C) (data not shown). Meanwhile, the mixed-metal isotherms normalized to organic carbon indicated the following compositional based trends: Biosolid (A) ≥ Kaolinitic (AB) = Mixed (AB) ≥ Smectitic (B), with sorption affinities for contaminants as follows: Pb (A) = Cu (B) > Se (C) = As (C) (data not shown). Overall, the mixed isotherms had sorption trends based on the normalization method with the following trends: colloid mass (A) > colloid-surface organic carbon (B) > surface area (C). Aside from soil pH, organic carbon, and surface area have been shown in many studies to be key factors in understanding sorption patterns (McKenzie, 1980; McBride, 1994; Naidu et al., 1997; Echeverria et al., 1998; Peak and Sparks, 2002; Lair et al., 2006; Seo et al., 2008). Overall, across all three normalization methods for the mixed isotherms, the following contaminant sorption preferences were found: Pb (A) > Cu (B) > Se (C) > As (D) (Table 4.4; p-value < α=0.05). Overall, sorption preferences based on colloid compositions across all three normalization methods for the mixed-isotherms were as follows: Kaolinitic (A) = Biosolid (A) = Mixed (A) > Smectitic (B) (Table 4.4; p-value < α=0.05).

4.3.3 Effects of Surface Characteristics

In the single point zeta potential measurements, additions of 2 and 10 mg L^{-1} mixed contaminants resulted in nanocolloid zeta potentials which were more negative than those of their corresponding macrocolloids, with both sizes showing trends based on composition (Fig. 4.2). Overall, the mineral colloids had higher negative zeta potentials in the presence of 0, 2 and even 10 mg L^{-1} contaminant concentrations than did the bio-colloids (Fig. 4.2). While increasing ionic strengths of contaminants showed shifts towards less negative zeta potentials (Fig. 4.2), the nanocolloids maintained significantly more negative zeta potentials over their corresponding macrocolloids (Fig. 4.2). The macrocolloids did not show the same trends based on composition, and surprisingly, the smectitic macrocolloids had the smallest zeta potential after contaminant additions as compared to the other mineral (and even the biosolid) macrocolloids (Fig. 4.2).

Figure 4.2. Zeta potentials and pH measurements for each zeta potential measurement are shown for the nano- and macro-colloids in the presence and absence of equal parts (0, 2, and 10 mg L^{-1}) mixtures of each contaminant (As, Se, Cu and Pb; the sum of each contaminant totaled 2 and 10 mg L^{-1}). Error bars represent standard error between triplicate measurements taken on duplicate samples.

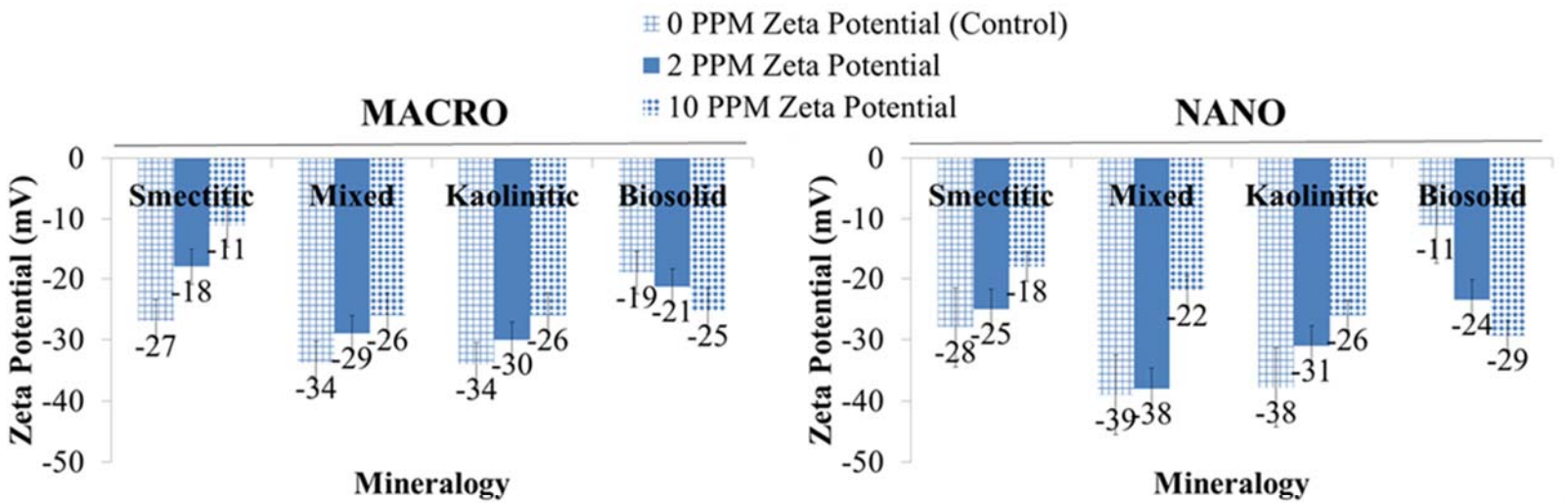

Macrocolloid pH of Zeta Potential Samples

	Smectitic	Mixed	Kaolinitic	Biosolid
0 PPM	4.60	5.50	4.98	5.11
2 PPM	4.67	4.45	4.96	5.42
10 PPM	4.38	4.24	4.40	5.18

Nanocolloid pH of Zeta Potential Samples

	Smectitic	Mixed	Kaolinitic	Biosolid
0 PPM	5.11	4.84	4.90	5.25
2 PPM	5.02	4.61	4.79	5.79
10 PPM	4.56	4.33	4.55	5.69

The large shift in zeta potential displayed by the smectitic macrocolloids upon addition of contaminants (-27 mV without contaminants shifting to -18, then -11 mV with 2 and 10 mg L^{-1} contaminant additions, respectively) indicates greater inner sphere cation contaminant attraction, likely due to to their larger initial negative zeta potential and surface area (Fig. 4.2). It is noted here that in order to mimic natural conditions, the pH of the zeta potential measurements was not constant (Fig. 4.2), hence, the change in zeta potential could reflect sorption of contaminants, or pH changes.

Overall, the mineral colloid zeta potentials became more positive with the increased addition of contaminants, indicating that the cations were out-competing the anions for inner sphere sorption (anions tend towards outer sphere sorption and would thus have little to no effect on the zeta potential values). Inner sphere bonding of Pb and Cu in the mineral colloid adsorption isotherm experiments was suggested through positive zeta potential shifts and pH reduction (from initial pH measurements to equilibrium at 24 hours) with increased metal loads (p-value < α=0.05, 95% CI) (Fig. 4.2) (McKenzie, 1980; Lair et al., 2006). Hydroxyl species of Cu and Pb can form monodentate inner sphere complexes (Violante, 2013). Outer sphere bonding was suggested in the biosolids by negative zeta potential shifts and pH increases with increased metal loads, suggesting a greater preference for anion contaminants.

Inner sphere sorption was also estimated by taking measurements of pH before contaminant additions and again at contaminant equilibrium concentration at 24 hours of interaction (data not shown). Drops in pH with increased metal load can indicate inner sphere sorption due to proton release after cation contaminant exchange on sorption sites, or could be due to "hydrolysis of metals in soil solution, and precipitation of metals" (Lair et al., 2006). Outer sphere bonding of the oxy-anion contaminants (As, Se) was indicated by increases in pH with increased contaminant loads. Anion pH was on average 0.32 units higher than the initial pH, while the cation pH was on average 0.31 units lower than the initial pH at the 0.05 probability level of significance (LSD=0.245, CV=3.38). Other studies have induced that the lower hydration energies of the cation metals helps to induce inner sphere bond formation; additionally, the negatively charged colloid surfaces attract the cations and repel the oxy-anion metals resulting in overall isotherm sorption preferences of Pb/Cu>Se/As (Sipos et al., 2008). The nanocolloids showed significantly larger changes in pH than did the macrocolloids upon the addition of contaminants (p-value < α=0.05). This indicates that the nanocolloids are able to form more inner sphere bonds than the macrocolloids or merely that they don't have the same buffering capacity as their larger-sized macrocolloid fractions. The biosolid colloids had significantly larger increases in pH units as compared to the soil colloids at a 0.05 level of significance, indicating more surface hydroxyl release and less buffering capacity.

4.4 Conclusions

The findings from this study demonstrate how comprehensive characterization of environmental nano- and macro-colloids and their interactions with contaminants can lead to a better understanding of the contaminant sorption and transport risks they pose to ground and surface waters. Overall, the sorption studies showed significant differences in surprisingly few fractions, including greater Pb, Cu and As sorption by kaolinitic nanocolloids over macrocolloids, greater Pb sorption by bio-nano-colloids, greater As sorption by mixed macrocolloids, and greater Se sorption by smectitic and kaolinitic macrocolloids over corresponding size fractions. Additionally, normalization to surface

area and organic carbon did not give consistent or significant trends as compared to those based on colloid mass. Overall, the mono-metal isotherms did not indicate sorption preferences based on composition, but showed contaminant sorption preferences of Pb (A) > Cu (B) > As (C) = Se (C). However, the mixed-metal isotherms did indicate sorption preferences based on composition in the following order: Kaolinitic (A) = Biosolid (A) =Mixed (A) > Smectitic (B), and contaminant sorption preferences of Pb (A) > Cu (B) > Se (C) > As (D). Surface properties such as cation exchange capacity, organic carbon, carbon:surface area and surface area were found to affect sorption properties amongst the differing colloid compositions. The sorption and surface characterization studies showed that the adhesion of nanocolloids to surfaces of macrocolloids may be enhancing macrocolloid reaction and sorption of contaminants, while higher organic carbon coatings on the nanocolloids may be inducing aggregation and limiting available surfaces for sorption. Nano-nano and macro-nano aggregation also suggests potential encapsulation of contaminants with unknown effects on transport and release of contaminants. Suggested inner sphere bonding of the cation metals indicated the nanocolloids can form lasting bonds with contaminants, giving them the potential for further transport via colloid surfaces, while suggested outer sphere bonding likely formed between oxy-anion contaminants and colloid surfaces would result in localized mobilization of the contaminants. This study is important for water quality professionals and environmental consulting agencies undertaking remediation tasks who strive to understand contaminant reaction and potential movement in subsurface media and groundwater as well as to developers of engineered nanoparticles who seek to better understand the interaction and potential behavior of nanoparticles in the environment as a basis for their model.

Chapter Five - Soil and Biosolid Nanocolloids and Macrocolloids Transport Behavior in the Presence of Lead, Copper, Arsenic and Selenium Contaminants

5.1 Introduction

Recent studies have shown that environmental nanoparticles with their high surface area and reactivity may enhance the transport of contaminants in surface waters, and through soil media into the groundwater (Seta and Karathanasis, 1997; Karathanasis and Johnson, 2006). The transport of nanoparticles in surface waters, in subsurface media, as well as groundwater is affected by competitive sorption processes from ions in solution, organic matter, surface hydrophobicity and functional groups, as well as the dissolution of binding agents. Additionally, the transport of nanoparticles is a function of their stability, preferential flow paths and particle size (Seta and Karathanasis, 1997; McCarthy and McKay, 2004; Madden et al., 2006; Maurice and Hochella, 2008; Waychunas and Zhang, 2008).

The interaction of nanoparticles with pollutants could be altered by changes to their surface properties. Nanoparticles are vehicles for the movement of trace elements in surface and shallow subsurface environments. This process involves complex biogeochemical interactions, such as those seen in the mobilization of Zn, Pb, As and Cu from acid mine drainage over hundreds of kilometers in the Clark Fork River drainage basin in Montana (Madden et al., 2006; Maurice and Hochella, 2008). The mobilization of the metals resulted from their incorporation into nanocrystalline vernadite-like nanominerals onsite. The nanomineral formed was the result of catalytic oxidation of aqueous manganese on ferrihydrite surfaces, a great example of nanoscale biogeochemical reaction influencing contaminant transport in water (Madden et al., 2006; Maurice and Hochella, 2008).

Water near surfaces is known to be ordered. However, as water attempts to have a tetrahedral bond network, the ordering can become frustrated, forcing different bond angles and local density. This process can create unusual aggregation of nanoparticles, sorption, or other chemical effects such as the dissipation of surface charges. Nanoparticles can repel one another or at pH values differing from point of zero charge, they might be able to approach one another (Waychunas and Zhang, 2008). Aggregation, sorption or dissipation of surface charges will affect the mobility of the particles and therefore the likelihood of contaminant transport.

The transport of nanoparticles in soil environments is affected by Brownian motion rather than gravitational settling. In soil environments, the transport of nanoparticles can occur through macro- or micro-pores in soil. Sequestration within these pores could greatly affect nanoparticle mobility. However, nanoparticles may be present in aggregates that are too large for the micropores, and thus travel through the macropores. Nanoparticle sorption to non-mobile particles may limit their mobility, while sorption to mobile particles could increase mobility. Nanoparticles may also adsorb to the air-water interface, which may affect their transport in the unsaturated zone (Maurice and Hochella, 2008).

In previous colloid leaching experiments (Seta and Karathanasis, 1997a; Seta and Karathanasis, 1997b), the infusion of colloid suspensions (average colloid diameter of 220-1050 nm) into undisturbed soil monoliths produced eluted nanocolloids with a mean diameter range of 50 – 120 nm. This suggests that nanocolloids can mobilize through soil media and into subsurface media or groundwater. In reviews of particle transport in porous media, McCarthy and McKay (2004) pointed out that groundwater colloids were capable of enhancing transport of contaminants with high sorption affinities to aquifer solids. Studies have shown that radionucleotides can be

transported over several kilometers via nanoparticles in groundwater over short time periods, defying thermodynamic predictions. For example, near a nuclear waste plant in Mayak, Russia, plutonium transport in groundwater was shown to be occurring via ferric oxide nanoparticles less than 15 nm in size (Hochella, 2008; Hochella, et al., 2008).

Natural systems have complex chemistries, including mixed colloidal phases. Colloidal stability can be affected by interactions between other nanocolloids or solutes in the system. At the microscopic scale, nanocolloidal transport is affected by "the arrangement and nature of surface functional groups, surface hydrophobicity and roughness, as well as by the physical arrangement of the colloidal phases relative to the larger grains and pore spaces" (McCarthy and McKay, 2004). The spatial distribution of physical and chemical features along a flow path in an aquifer will also affect nanocolloid transport (McCarthy and McKay, 2004).

The question arises however, of how the nanoparticle fraction is mobilized into groundwater in the first place. While the previously mentioned soil transport studies show that nanoparticles and colloids are capable of leaching through soil horizons, the likelihood of particle movement through both the soil root and vadose zone seems highly unlikely. However, nanocolloids can infiltrate groundwater by moving from the vadose or root zone when there is a large influx during storms or during snow melt events. The same events occur for bacterial populations whose migration into groundwater from the soil vadose zone shows that other similarly sized particulates, (such as nanoparticles) could do the same (McCarthy and Zachara, 1989).

Mobile nanocolloids in groundwater could also be the result of the formation of colloid suspensions in pore water. A few possibilities include the homogenous nucleation of inorganic solids in the fluid phase, or the release of colloidal material from geologic matrices. Nanocolloid precipitates could be the result of geochemical gradients that are common byproducts of the differing chemical properties of contaminant plumes and the associated uncontaminated groundwater nearby (McCarthy and Zachara, 1989). These precipitates would result in suspended and mobilized nanocolloids in groundwater.

Additionally, nanoparticles can be mobilized in groundwater if inorganic cementing agents binding them to larger sized grains dissolve or if the aggregates are deflocculated by an influx of certain cations (McCarthy and Zachara, 1989). This is especially true with consideration to iron oxide cementation. At decreasing environmental pH's (often a result of contaminant loading) iron oxides will dissolve, thus releasing out bound colloidal fractions and associated contaminants. Siliceous colloidal material can be released from calcareous environments due to dissolution of carbonate cementing agents after infiltration of water. Finally, microorganisms possess the ability to transport nanoparticles and their associated contaminants via ingestion of the particles as they mobilize throughout the water column.

The spatial distribution of physical and chemical features along a flow path in an aquifer will also affect nanocolloid transport (McCarthy and McKay, 2004). In their reviews, McCarthy and McKay (2004) pointed out that groundwater colloids were capable of enhancing the transport of contaminants with high sorption affinities to aquifer suspended solids. Subsurface environments are not usually favorable for nanocolloidal deposition because of the electrostatic repulsion between the generally negatively charged nanocolloids and subsurface media. Nanocolloid transport should therefore be characterized by the surface charge of the nanocolloids and aquifer surfaces. However, the average surface charge (zeta potential) of nanocolloids or nanoparticles

can become irrelevant to transport predictions through spatial heterogeneity (McCarthy and McKay, 2004).

Nanocolloids, with their high adsorption capacities, reactivity, and immense surface area are expected to transport larger amounts of contaminants than the larger size fractions of soil. Due to their prolonged stability in suspension and contaminant sorption capacities, nanocolloids are likely contaminant transport vectors in surface waters, unsaturated subsurface media, and in groundwater. There is currently a deficiency of research available for natural nanoparticle facilitated contaminant transport in subsurface environments. In order to ensure the future safety of drinking water supplies, it is imperative that the scientific community addresses this deficiency, especially in relation to emerging contaminants, such as the heavy metals Se, As, Cu and Pb.

The objectives of this study were to evaluate the potential of soil- and biosolid-derived nano- and macro-colloids to sorb and transport As, Cu, Pb, and Se contaminants through soil media. Due to their small size and large surface area, high surface energy and reactivity, we hypothesize that nanocolloids will sorb and transport greater quantities of contaminants *in situ* than corresponding macrocolloids.

5.2 Materials and Methods

5.2.1 Colloid Generation and Characterization

Three Kentucky soil Bt horizons were used to generate the mineral colloids: Caleast-variant (fine, smectitic, mesic mollic Hapludalf), Tilsit (fine-silty, mixed, mesic Typic Fragiudult), and Trimble (fine-loamy, siliceous, mesic Typic Paleudult), referred to as smectitic, mixed, and kaolinitic nano- and macro-colloids, respectively. Biosolid nano- and macro-coloids were derived from an aerobically digested municipal sewage sludge (Jessamine County, Kentucky). Centrifugation was used to fractionate colloids into two size classes (nanocolloids <100 nm and macrocolloids 100-2000 nm) using a Centra GP8R Model 120 centrifuge (ThermoIEC) in deionized water (resistivity of 1 μΩcm at 25°C) (Karathanasis, 2010). All collected sample suspensions were then diluted to 50 mg L^{-1} concentrations for additional analysis.

Primary particle size of the nano- and macro-colloids were determined using transmission electron microscopy (TEM-EDS; JEOL 2010F, Tokyo, Japan) (Zhu and Lu, 2010; Nemeth et al., 2011), and scanning electron microscopy, respectively (SEM-EDS; Hitachi S-4300, Tokyo, Japan) (Goldstein et al., 1992; Deng et al., 2009). Dynamic light scatter was used to determine hydrodynamic diameters (d_h) on a Malvern Zetasizer Nano ZS (Malvern, United Kingdom). Surface area was measured using the Ethylene Glycol Monoethyl Ether (EGME) method. A Denver Instruments Model 250 pH*ISE*electrical conductivity meter measured pH and electrical conductivity (Arvada, CO). Cation exchange capacity (CEC) was determined using an adapted version of the ammonium acetate method. A Flash EA 1112 Series NC Soil Analyzer (Thermo Electron Corporation) with a Mettler Toledo MX5 microbalance was used to determine organic C (OC). Mineralogical characterizations were completed using X-ray diffraction (XRD) and Thermogravimetric analysis (TG) on a Phillips PW 1840 diffractometer and PW 1729 x-ray generator (Mahwah, NJ), and a Thermal Analyst 2000 (TA Instruments) equipped with a 951 Thermogravimetric Analyzer (DuPont Instruments), respectively (Karathanasis et al., 2005; Karathanasis, 2008).

Mixed-metal adsorption isotherms evaluated the competitive affinity of each nano- and macro-colloid suspension for Cu, Pb, Se, and As contaminants, as analyzed using inductively coupled

plasma mass spectroscopy *(*ICP-MS) (Essington, 2004). The following reagents were used to prepare all contaminant concentrations used in this study: Aqueous solutions of Pb, Cu, As and Se were prepared from $PbCl_2$ (98% purity, Aldrich Chemicals, Milwaukee, WI), $CuCl_2$ (>99% purity, Sigma Chemical Company, St. Louis, MO), arsenic acid $Na_2HAsO_4 \cdot 7H_2O$(98% purity, Sigma Chemical Company, St. Louis, MO), and sodium selenate decahydrate $Na_2SeO_4 \cdot 10H_2O$ (99.9% purity, Sigma Chemical Company, St. Louis, MO).
Select characterizations are displayed in Table 5.1.

5.2.2 Soil Monolith Preparation and Characterization

Twenty-two intact soil monoliths (D-18x H-30 cm) representing the Bt horizon of a KY Ashton soil series (Fine-silty, mixed, active, mesic Mollic Hapludalfs) were encased in PVC columns and sealed with Poly-U-Foam to decrease preferential flow. Four extra monoliths were collected for characterization. Soil bulk density (D_b) was determined from triplicate oven dried cores collected with a bulk density probe. Hydraulic conductivity was determined on measurements taken at 10 minute intervals for one hour at upper and lower boundaries set first at -10 cm and then at -5 cm prior to leaching experiments. A representative monolith sample was air dried, ground, homogenized and analyzed for mineralogy, pH, EC, OC and CEC using the methods described in the colloid chemical characterization section. Particle size analysis was completed using the pipette method.

5.2.3 Colloid Leaching Experiments

Colloid-contaminant suspensions of 2 mg L^{-1} As, Cu, Se and Pb with 50 mg L^{-1} colloid were infused through duplicate columns using an unsaturated, steady state, unit gradient, downward percolation experiment at h=-5 cm, referring to K=5.57 mm h^{-1}, representing a 10-day KY rainstorm with a 2-year frequency of reoccurrence. Infusions occurred over four continuous pore volumes. Soil measurement systems infiltrometers attached to baseplates at the top of the monolith controlled the upper boundary while a marriote device at the bottom of the monolith (an inverted flask attached to a baseplate) controlled the lower boundary. Collection vials allowed sample collection at the outlet of the marriote device at the lower boundary. Control columns were infused with DI Water solutions of 2 mg L^{-1} As, Cu, Se and Pb. Blank columns were infused with DI Water. A 0.02 M solution of KBr acted as a conservative tracer.

5.2.3.1 Monolith Eluent Characterization

Eluted colloid concentrations were determined using a colorimetric procedure on a Molecular Devices Versa Max Microplate Reader at 450 nm alongside a standard colloid curve. The pH and EC were measured using a Denver Instruments Model 250 pH*ISE*electrical conductivity meter (Arvada, CO). DOC was determined on 20 mL samples with 50 µL of concentrated HCl addition on a Flash EA 1112 Series NC Soil Analyzer (Thermo Electron Corporation) with a Mettler Toledo MX5 microbalance. Eluted colloid mineralogy was determined using XRD and TG analysis and checked against the composition of colloids from the stock suspension. This comparison allowed assessment of colloid contamination from the column matrix and preferential filtration of specific minerals (Seta and Karathanasis, 1997; Karathanasis and Johnson, 2006). Total, soluble, and sorbed metals were analyzed using Millipore filtration systems set up with 0.025 µm nitrocellulose filters. Blanks consisted of 30 mL of double-deionized water passed through and analyzed for As, Cu, Pb, and Se. Next, 15 mL aliquots of eluent samples were filtered and the collected solution was analyzed for soluble As, Se, Cu and Pb. Finally, a 15 mL 1N trace metal grade solution of nitric acid was passed through the filter

and analyzed for sorbed metals. Filtered samples were preserved with 1% nitric acid, stored in polyethylene vials, and analyzed within 24 hours via inductively coupled plasma mass spectroscopy (ICP-MS).

5.2.4 Statistics

Significant differences between means were tested using Analysis of Variance (ANOVA) (SAS PROC GLM) and the Fisher's protected least significant difference test (LSD) in SAS 9.3 (SAS Institute Inc., Cary, NC, USA). The statistical significance level used was $\alpha = 0.05$.

5.3 Results and Discussion

5.3.1 Soil Monolith Characteristics

Twenty two soil monoliths were collected and used for the leaching experiments, representing depths of 5 cm to 35 cm below the surface. Monoliths had neutral pH (7.07), 1.45% OC, and 42% porosity (Table 5.2). The pH of the monoliths (7.07) was considerably higher compared to the colloid suspensions (4.92 to 5.39) (Table 5.1 and 5.2). Analysis of representative monolith depths had a loam texture class, and a CEC (8.12) that was typical for a mixed mineralogy soil (Table 5.2). The CEC of the monoliths is comparable to that of the mixed and kaolinitic colloid suspensions, but significantly lower than that of the smectitic and biosolid colloids (Table 5.1 and 5.2). The proximity of the monolith CEC to that of the mixed and kaolinitic colloids, especially for the macro-fractions, indicates potential similarities in sorption capacities between the colloids and the monolith matrix. The loam texture class, 42% porosity, and granular surface and subangular blocky subsurface structures suggest adequate potential for subsurface flow and pathways for transport (Table 5.2).

5.3.2 Eluent Solution Characteristics

Eluents were collected over four, continuous pore volume cycles and analyzed for physico-chemical and mineralogical characteristics. Overall, eluent pH's (Fig. 5.1) were higher than the initial colloid-contaminant suspension pHs (Table 5.1) suggesting significant buffering by the soil matrix. All colloid PZC values were indicated to be lower than pH 4, so any pH above that would likely enhance stability and mobility of colloids (Karathanasis and Johnson, 2006). The lower initial suspension pH, combined with the higher monolith and eluent pH indicates enhanced colloid stability and mobility (Seta and Karathanasis, 1996; Karathanasis, 1999; Karathanasis and Johnson, 2006), especially within the smectitic nanocolloids and mixed macrocolloid fractions, which showed pH ranges between 7.51-8.02 and 7.01-8.24, respectively (Fig. 5.1). The higher than 7.07 eluent pH values are probably the result of carbonate dissolution within the soil matrix during the leaching cycle.

Table 5.1 Characteristics of nano- and macro-colloid suspensions.

Properties	Colloids							
	Smectitic		Mixed		Kaolinitic		Biosolid	
Size Class	Macro	Nano	Macro	Nano	Macro	Nano	Macro	Nano
% Water Dispersible Colloid Recovered from Bulk Sample	33.41	0.67	37.17	0.33	11.00	0.07	4.95	0.03
SEM/TEM Mean Smallest Particle Size ±SD ‡ (nm)	328±144	37±13	549±394	7±5	288±184	41±19	363±338	50±19
DLS Mean Particle Size (d_H) ±SD ‡ (nm)	487±10	181±3	596±21	205±4	545±25	187±4	4456±599	353±8
Surface Area ($m^2\ g^{-1}$) ±SD ‡	708±137	879±76	420±105	466±10	333±37	389±44	1674±70	1303±63
Electrical Conductivity (mmhos cm^{-1})	$3.93x10^{-3}$	$6.07x10^{-3}$	$2.91x10^{-3}$	$3.09x10^{-2}$	$2.87x10^{-3}$	$3.80x10^{-3}$	$1.56x10^{-2}$	$4.69x10^{-2}$
Ionic Strength (mol L^{-1})	$4.99x10^{-5}$	$7.71x10^{-5}$	$3.70x10^{-5}$	$3.92x10^{-4}$	$3.64x10^{-5}$	$4.83x10^{-5}$	$1.97x10^{-4}$	$5.96x10^{-4}$
Natural pH	4.92	5.12	5.07	4.92	4.91	5.38	5.39	5.25
CEC ($cmol_c\ kg^{-1}$) #	35.05±12.84	42.19±15.12	8.89±1.62	10.51±1.67	6.94±1.85	13.12±2.84	37.61±14.85	70.99±22.98
Ca^{2+} ($cmol_c\ kg^{-1}$)	27.60	32.64	3.80	4.00	4.40	7.12	31.60	51.68
Mg^{2+} ($cmol_c\ kg^{-1}$)	6.27	8.00	3.40	3.47	1.60	3.73	3.60	12.13
K^{+} ($cmol_c\ kg^{-1}$)	0.57	0.78	1.15	2.80	0.45	1.23	1.64	3.98
Na^{+} ($cmol_c\ kg^{-1}$)	0.61	0.77	0.54	0.24	0.49	1.04	0.77	3.20
OC ($mg\ kg^{-1}$) ‡‡	658	897	645	774	430	647	1.3K	16K
Kaolinite (%)	29	30	42	46	52	55	NA §	NA §
Geothite (%)	7	9	5	7	12	15	NA §	NA §
Gibbsite (%)	0	0	0	0	5	6	NA §	NA §
Quartz (%)	6	4	5	3	4	2	NA §	NA §
Mica (%)	10	6	31	30	3	3	NA §	NA §
Smectite (%)	48	51	0	0	0	0	NA §	NA §
MVI ¶ (%)	0	0	7	7	0	0	NA §	NA §
HIV# (%)	0	0	10	7	24	19	NA §	NA §

‡ SD = Standard Deviation was calculated from duplicate or triplicate measurements (see Methods section).

CEC = Cation Exchange Capacity by sum of cations.

†† SAR = Sodium Adsorption Ratio

‡‡ OC = Organic Carbon was derived by subtracting dissolved organic carbon from total carbon measurements. Due to low pH conditions and the typical absence of carbonates in the region, inorganic carbon contributions were assumed to be minimal.

§ NA = Not Applicable

¶ MVI = Mica-Vermiculite Interstratified

HIV = Hydroxyinterlayered Vermiculite

Table 5.2. Soil monolith characteristics.

pH	7.07
Total C	1.45%
Bulk Density g cm^{-3}	1.54
Porosity	42%
Texture	Loam
Hydraulic Conductivity (mm h^{-1})	5.57
CEC $cmol_c\ kg^{-1}$	8.12
Na^{+} $cmol_c\ kg^{-1}$	0.01
Ca^{2+} $cmol_c\ kg^{-1}$	8.06
Mg^{2+} $cmol_c\ kg^{-1}$	1.52
K^{+} $cmol_c\ kg^{-1}$	0.23
Clay Mineralogy Class	Mixed
Kaolinite %	35
Mica %	20
HIV# %	15
Goethite %	12
MVI ¶ %	10
Quartz %	5
Feldspar %	3

¶ MVI = Mica-Vermiculite Interstratified

HIV = Hydroxyinterlayered Vermiculite

Figure 5.1. Eluent pH for macro- and nano-colloids.

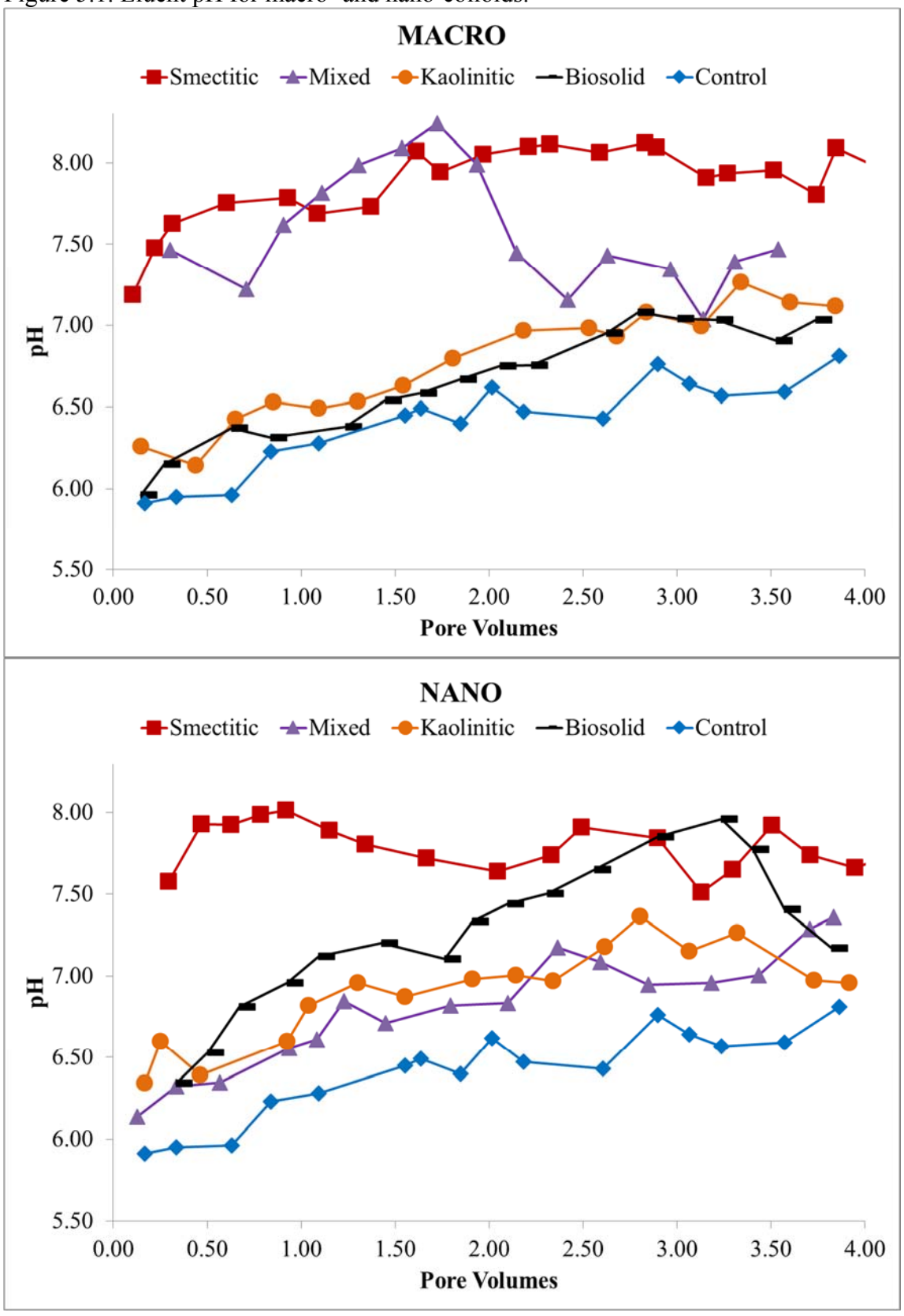

The lowest eluent pH's were associated with the biosolid macrocolloids and mixed nanocolloids, showing 5.96-7.08 and 6.14-7.36, respectively (Fig. 5.1). Overall, the colloid-associated monoliths had higher associated eluent pH's than that of the control (5.91-6.81). Colloid-associated eluent pH's ranged from 5.96- 8.24, with the lowest pH from the bio-macrocolloids and the highest from the mixed macrocolloids (Fig. 5.1). Spikes in eluent pH and electrical conductivity (EC) (Fig. 5.2) can be both an indicator of colloid stability as well as used to corroborate colloid breakthrough in eluents. Electrical conductivity remained constant or decreased slightly over time except for the nano-biocolloid fraction which showed a more than 2-fold increase by the end of the leaching cycle. This increase may have been caused by carbonate dissolution, as corroborated by the significant pH rise and may have contributed to drastic elution fluctuations (Fig. 5.4). The nanocolloid eluents had higher dissolved organic carbon (DOC) concentrations than did the macrocolloid eluents, with the exception of the mixed and biosolid macrocolloids which were higher (Fig. 5.3). This corresponds to greater OC measured in the nanocolloid-suspensions prior to leaching (Table 5.1). Studies have indicated that 83-99% of all TOC will be leached as DOC (Kjaergaard et al., 2004). The high initial DOC colloid concentrations may have also induced the instantaneous breakthrough curves displayed by the colloids (Fig. 5.4), which has usually been associated with greater facilitated transport (Karathanasis, 1999).

Statistical correlations between colloid-suspension characteristics, eluent suspension characteristics and colloid-mediated transport of contaminants indicated weak correlations between colloid-mediated transport and the percentages of initial colloid-suspension percentages of kaolinite, mica, and hydroxyl-interlayered vermiculite. Significantly greater elutions were found to occur in association with nanocolloids as compared to macrocolloids. Additionally, correlations were analyzed between colloid-mediated transport and eluent sample characteristics. Eluent sample DOC, pH and EC were indicated to significantly affect differences in colloid mobility and transport (p-value $< \alpha=0.05$). Eluents were analyzed for mineralogy to estimate contamination from the monolith matrix. The eluted colloids showed similar mineralogical composition to the infused colloids, suggesting very little preferential filtration or contamination by the monolith matrix.

Figure 5.2. Eluent Sample electrical conductivity (EC).

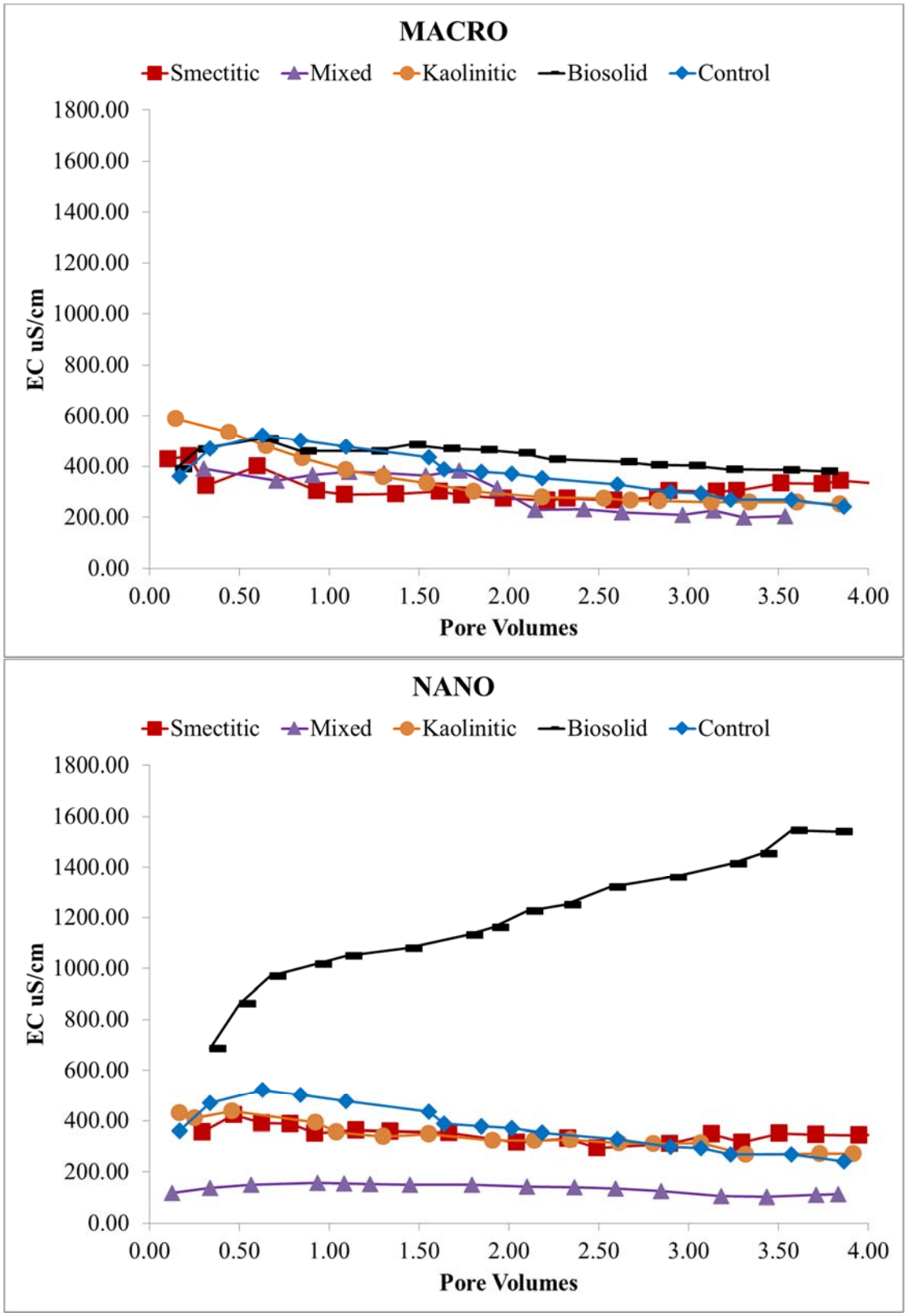

Figure 5.3. DOC for macro- and nano-colloid associated eluents.

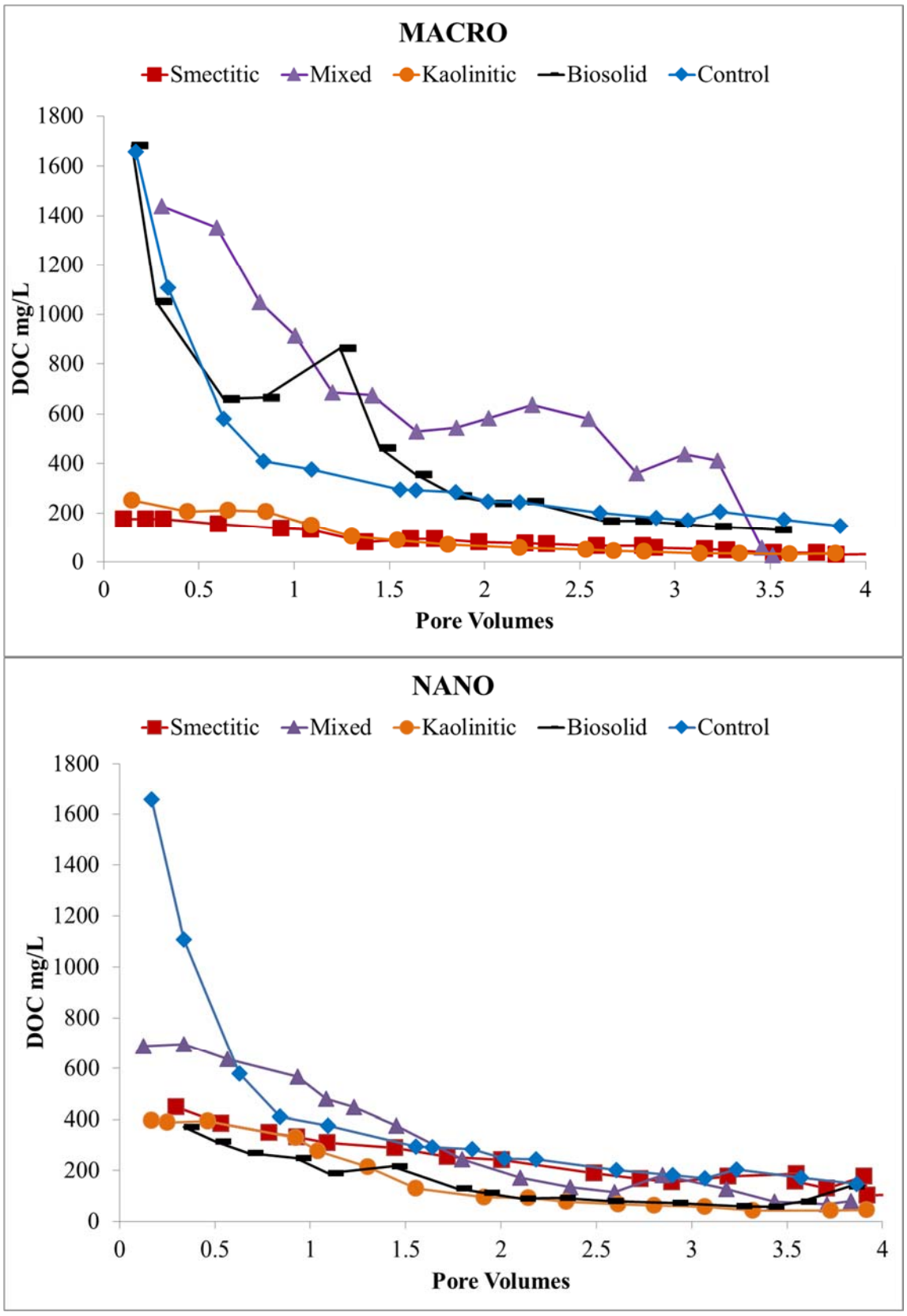

Figure 5.4. Soil monolith eluent colloid concentration (C/Co) for the (a) smectitic, (b) mixed, (c) kaolinitic, and (d) biosolid macro- and nano-colloids. Data is representative of the average of duplicate columns.

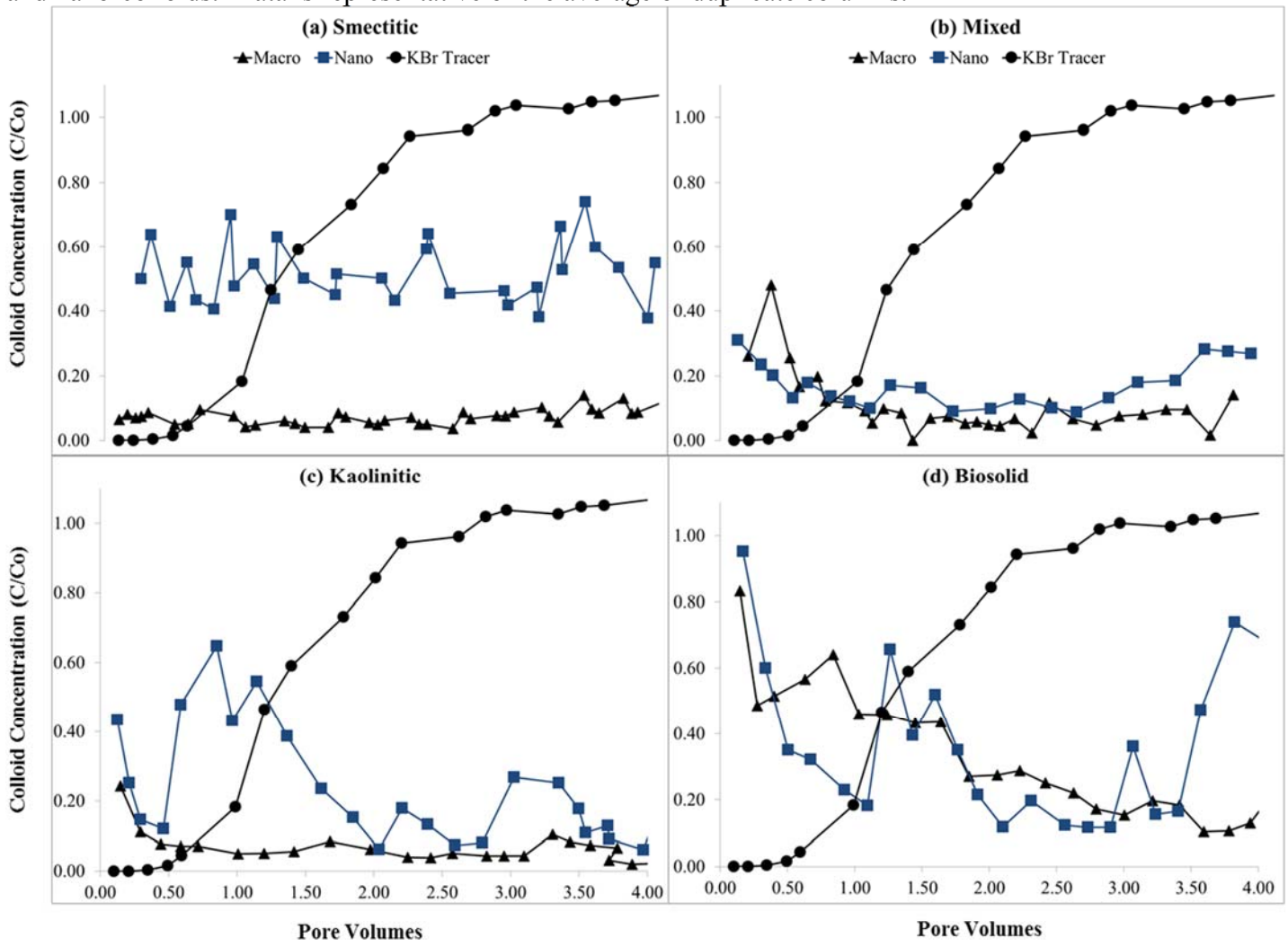

5.3.3 Eluent Colloid Breakthrough Curves

Eluents from monoliths receiving nano- and macro-colloid-contaminant suspensions portrayed irregular colloid breakthrough curves (BTC; Fig. 5.4), indicating cluster transport and deposition of the colloids (Jacobsen et al., 1997; Karathanasis and Johnson, 2006). Resurgences of colloids are indicated by spikes in eluent concentrations, potentially from biological activity creating new flow paths, or flushing of clogged pores from backed up water pressure (Barton and Karathanasis, 2003; Karathanasis, 2010). This is evidenced in the erratic kaolinitic and biosolid nanocolloid BTCs, where initial large and immediate concentrations declined until pore volumes of about 0.6 and 1.1 (kaolinitic and biosolid, respectively) where abrupt spikes indicated release of blocked pores (Fig. 5.4 c and d). The smectitic nanocolloids had even more erratic BTCs, with maxima and minima ranging from around 40-75% C/Co (Fig. 5.4a). Despite their likely transport in clusters, nanocolloids eluted significantly greater concentrations of colloids, showing as much as 44 and 23% more elutions than corresponding macro-fractions (smectitic and kaolinitic nanocolloids, respectively; Fig. 5.5).

Colloid BTCs also indicated instantaneous breakthrough ahead of the conservative KBr tracer, suggesting both ion and size exclusion resulting in preferential flow as the dominant colloid transport mechanisms (Seta and Karathanasis, 1997; Karathanasis and Johnson, 2006; Karathanasis et al., 2007; Karathanasis, 2010). Ion exclusion is likely the result of blocked pores inhibiting transport pathways to the tracer. Size exclusion would likely enhance colloid transport through larger pores - whose flow paths are more conductive - likely resulting in faster transport than conservative solute tracers (Simunek et al., 2006). Lower macrocolloid than nanocolloid elutions are attributed to greater matrix straining due to their larger size (Harris et al., 1989), with the exception of the bio-macrocolloids which eluted greater concentrations than corresponding nanocolloids (Fig. 5.4). Despite this, the biosolid, mixed, and kaolinitic macrocolloids best portraying this phenomena with high initial concentrations somewhat erratically falling in concentration throughout the leaching process (Fig. 5.4d).

Preferential flowpaths were suggested by the faster and higher initial breakthroughs of nanocolloid eluents as compared to macrocolloids (Fig. 5.4; Karathanasis, 2010), with nano elutions showing average colloid C/Co concentrations as high as 51% (smectitic nanocolloids, Fig. 5.5). The mixed colloids eluted 1.7 times more nanocolloids than their corresponding macro-fraction (Fig. 5.5). The greater initial BTC of the nanocolloids (Fig. 5.4) combined with greater average colloid concentrations (Fig. 5.5) highlight the greater mobility of nanocolloids over corresponding macrocolloids. The bio-colloids were an exception, showing macrocolloids eluted an average of 5% greater colloid concentrations than the bio-nanocolloids (Fig. 5.5).

Additionally, enhanced nanocolloid transport may be attributable to Brownian motion controlling their mobility, likely resulting in increased interactions with other colloids and solutes in the system (Tsao et al., 2011). These enhanced interactions could cause greater repulsion phenomena, and thus enhanced stability and mobility, especially if they are being conducted through faster flow paths (macropores) due to size exclusion and preferential flow phenomena (Karathanasis, 2010; Tsao et al., 2011). Finally, while unsaturated colloid transport can be retarded by thin water films and preferential deposit in the air-water interface, it would appear that nanocolloids are less affected than macrocolloids (Wan and Wilson, 1994).

Figure 5.5. Means analysis of concentration C/Co.

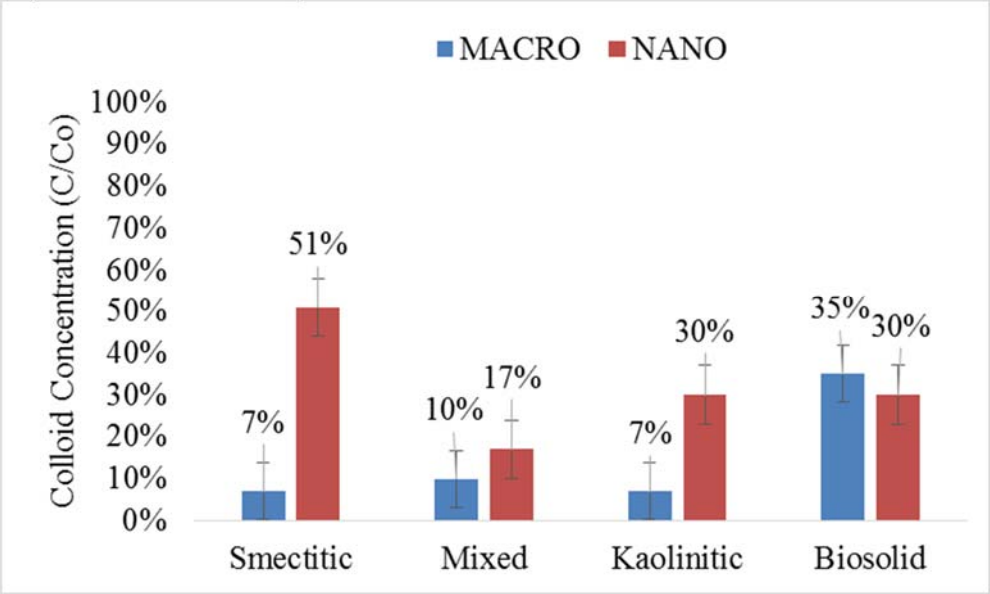

Overall, composition trends were present based on size, with nanocolloids showing the following sequence: Smectitic (A) > Kaolinitic (B) = Biosolid (B) > Mixed (C), while the macrocolloids sequence portrayed: Biosolid (A) > Mixed (B) = Smectitic (B) = Kaolinitic (B) (Fig. 5.4 and 5.5; p-value < α=0.05). Based on averages across both sizes, composition trends for colloid concentrations eluted indicated the following trends: Biosolid (A) = Smectitic (A) > Kaolinitic (B) = Mixed (B) (Fig. 5.5; p-value < α=0.05). Of the four nanocolloid compositions, the smectitic colloids were the most mobile, with instantaneous breakthroughs (Fig. 5.4a) peaking around 75% C/Co and average elution concentrations of 51% (Fig. 5.4a). Karathanasis (2010) also indicated both instantaneous breakthrough and greater eluted concentrations from smectitic nanocolloids as compared to nanocolloids of mixed and kaolinitic mineralogies (51, 17 and 30%, respectively). Other studies have shown similar kaolinitic recoveries, but indicated greater recoveries of smectitic and mixed colloids, which may be attributed to greater input concentrations of the colloid-suspensions (Seta and Karathanasis, 1997; Karathanasis, 2010). The lowest mobility by nanocolloids came from the mixed composition, with an average colloid recovery of 17% (Fig. 5.5), with elutions ranging from around 15-35% C/Co with more moderate BTCs than other the compositions (Fig. 5.4). The lower elution of the mixed nanocolloids could be attributed to their higher initial EC (Table 5.1), which can destabilize colloids (Seta and Karathanasis, 1997).

Within the macrocolloids, the biosolid colloids were the most mobile (35% average colloid recovery, Fig. 5.5), while the lowest mobility's were shown by the smectitic and kaolinitic colloids (7% for both; Fig. 5.5). The low mobility of the smectitic macrocolloids was surprising, but may be explained by their higher goethite content, which has a PZC near the pH of the eluents (~8) (Karathanasis, 2010). The macrocolloid BTCs were less irregular as compared to those of the nanocolloids - insinuating more matrix straining than nanocolloids due to their larger size (Gang and Flury, 2005) - but still showed instantaneous breakthrough ahead of the conservative KBr tracer (Fig. 5.4). The eluted colloids showed similar mineralogical composition to the infused colloids, suggesting very little preferential filtration or contamination by the monolith matrix. The instantaneous breakthrough of the colloids (Fig. 5.4) indicated that preferential flow is the mechanism controlling colloid transport. Additionally, the colloid breakthrough prior to the KBr tracer (Fig. 5.4) suggests that size exclusion also plays a significant role in the transport process (Seta and Karathanasis, 1997). The greater mobility of the nanocolloids is likely a result of higher DOC concentrations in some fractions as well as smaller sizes bypassing matrix filtration processes (Fig. 5.3; Barton and Karathanasis, 2003), despite irregular BTCs likely resulting from irregular flushing due to occurrences of nano-nano aggregates (Jacobsen et al., 1997; Kjaergaard et al., 2004) (Table 5.1). The irregular BTCs of the macro- and nano-colloid eluents are corroborated by the irregular pH and EC of the eluted colloid suspensions, DOC and in some cases, EC (Fig. 5.2) as compared to the control. Despite indications of enhanced transport with decreasing particle size (Figs. 5.4 and 5.5; Harris et al., 1989; Karathanasis, 2010), DLS measurements of eluted colloids indicated some aggregation, as evidenced by larger d_h sizes compared to those of colloid-suspensions prior to leaching (Fig. 5.6).

Figure 5.6. DLS measured particle sizes (d_h) from the colloid-suspensions prior to leaching (Before) and from eluent suspensions (After) from columns receiving macro- or nano-colloid contaminant suspensions. Error bars represent standard error.

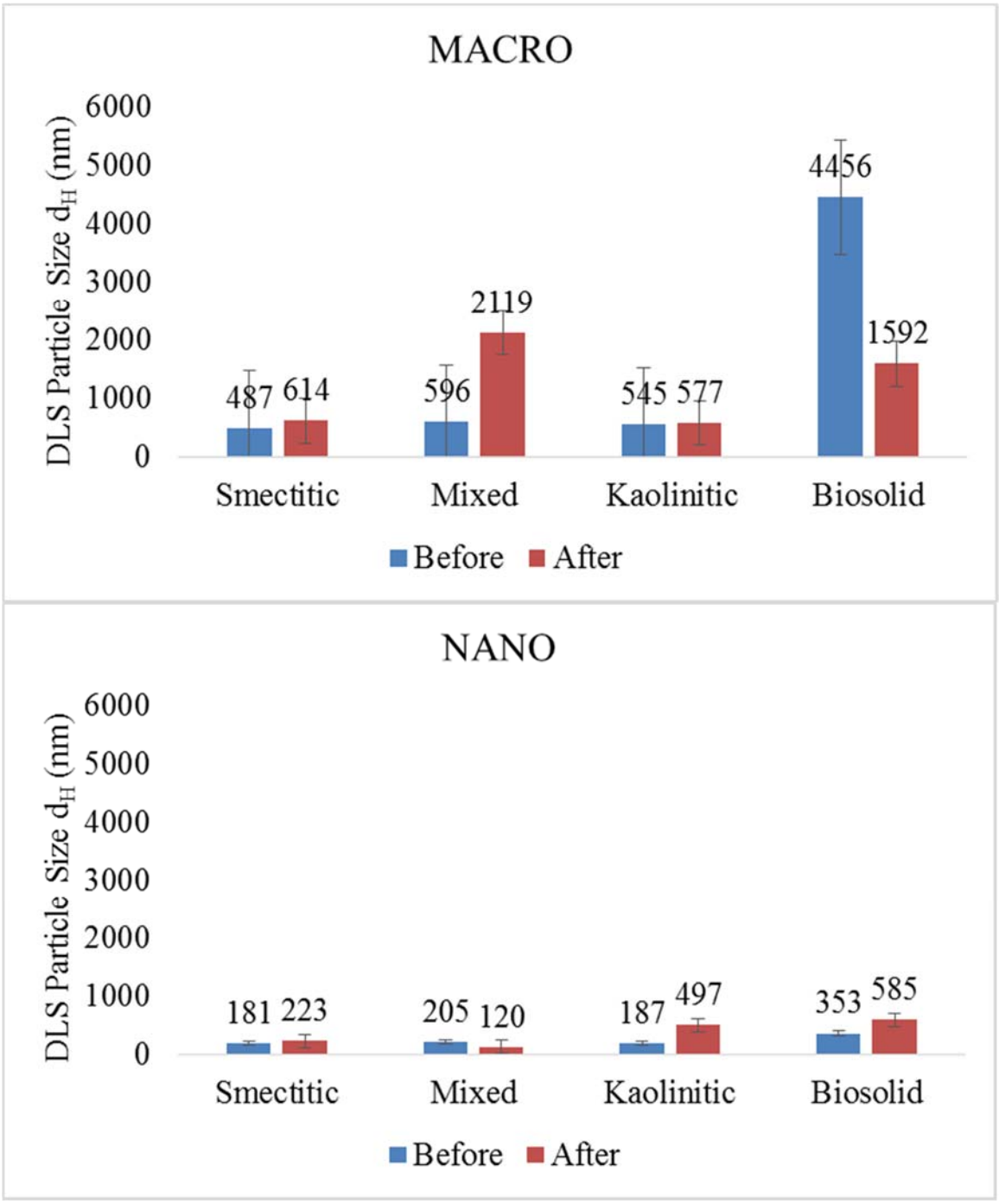

The largest average size increase in colloid eluents was associated with the mixed macrocolloids (2119 vs. 596 nm) and the smallest with the kaolinitic macrocolloids (577 vs. 545 nm), respectively (Fig. 5.6). Within the nanocolloids the largest eluted sizes were associated with the biosolid composition (585 nm), and the smallest from the mixed nanocolloids (120 nm; Fig. 5.6). Most colloid sizes eluted were larger than the measured DLS sizes of the suspensions prior to adding them to the monoliths with the exception of the mixed nanocolloid eluent and biosolid macrocolloid eluents. The occurrence of larger DLS sizes in most eluents as compared to those measured on colloid suspensions prior to leaching might indicate that colloids are transporting as aggregates (Kjaergaard et al., 2004). However, DLS measurements do not necessarily portray individual particle sizes, but are representative of the average hydrodynamic diameter size. Therefore, one or just a few large particles detached from the monolith matrix may distort the overall measurement. Despite this, the irregular colloid breakthrough patterns in Fig. 5.4 further demonstrate that colloids are likely transported in clusters, rather than as individual particles. Further, the similar mineralogy between infused and eluted colloids suggests that such contamination of eluted colloids was not a significant factor. Hence, aggregation of particles during the transport within the monoliths is the most likely scenario.

5.3.4 Contaminant Elution Breakthrough Curves

5.3.4.1 Eluted Total Contaminant Loads

Figures 5.7 a-d show the total contaminant elutions (where total equals sorbed plus soluble contaminants eluted) of Cu, As, Pb and Se by colloid composition and size. Colloid-mediated transport of Cu, As, and Pb contaminants were suggested by significantly greater elutions of Cu, As, and Pb in the presence of colloids over that of the control (p-values = <0.0001, 0.0094, and <0.0001, respectively). Colloids have been shown to enhance contaminant transport through surface complexation and co-precipitation mechanisms (Karathanasis, 2010). Overall, the total contaminant elutions of Cu, As, and Pb were as erratic as the colloid concentration BTCs (Figs. 5.7 a-d and 5.4). In contrast, total Se elutions showed BTCs that steadily increased throughout the leaching cycle, suggesting anion exclusion resulting in preferential flow of Se contaminants (Simunek et al., 2006). Total contaminant BTCs differed based on composition and size, showing contaminant elutions in association with the smectitic and mixed colloids were more irregular than the kaolinitic and biosolid breakthrough curves (Fig. 5.7). Nanocolloids were associated with higher total elutions of contaminants than were macrocolloids (p-value=0.045). Individual contaminant trends in association with each colloid composition and size are discussed in more detail below.

The smectitic nanocolloids were more effective at transporting all four contaminants than were corresponding macrocolloids, showing erratic BTCs for each contaminant (Fig. 5.7a). Macrocolloid BTCs of Cu, Pb and As had high initial concentrations that were minimized over the course of the leaching cycle in an erratic fashion, indicating maxima of 47% for Cu, 16% for Pb, and 5% for As (Fig. 5.7a). In comparison, the nanocolloid Cu, Pb and As patters were more erratic throughout the entire leaching cycle, with multiple minima and maxima ranging from around 5-90% for Cu, and 0-20% for As and Pb, that did not necessarily decrease over the course of the leaching cycle like those of the macrocolloids.

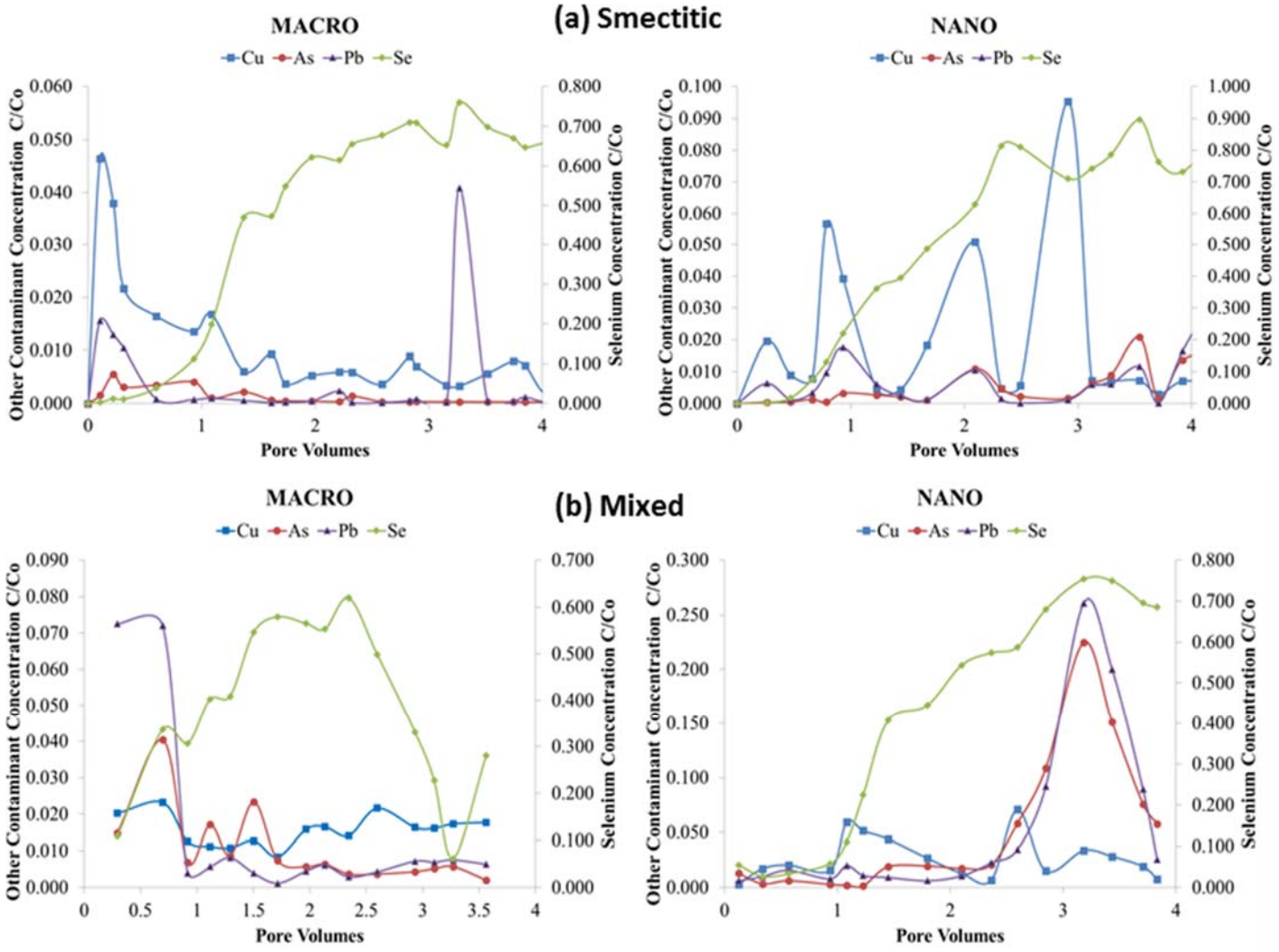
(a) Smectitic
MACRO
NANO
(b) Mixed
MACRO
NANO
Cu As Pb Se
Other Contaminant Concentration C/Co
Selenium Concentration C/Co
Pore Volumes

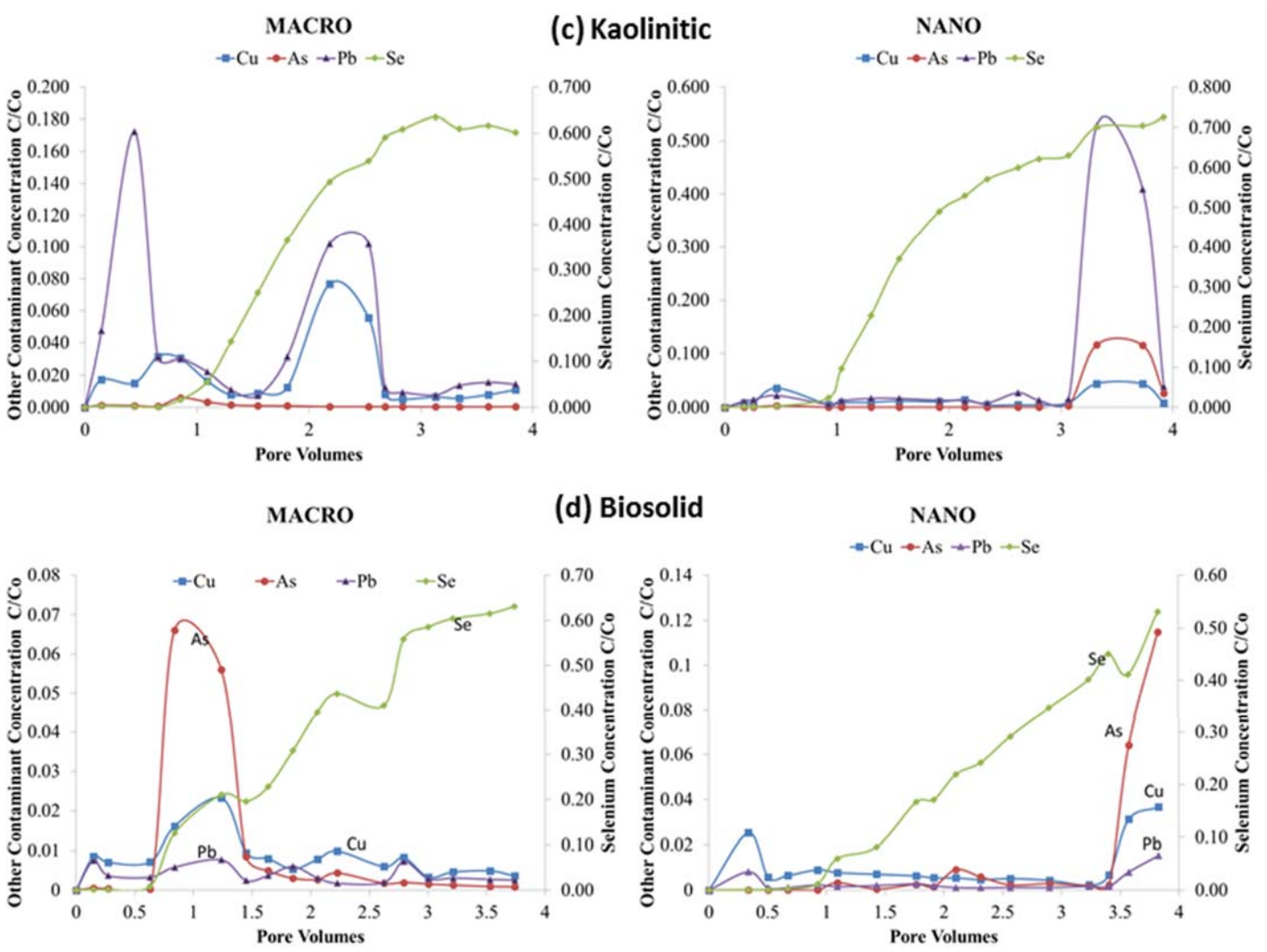
(c) Kaolinitic
MACRO
NANO
Cu As Pb Se
Other Contaminant Concentration C/Co
Selenium Concentration C/Co
Pore Volumes
(d) Biosolid
MACRO
NANO
Cu As Pb Se
As
Se
Cu
Pb
Other Contaminant Concentration C/Co
Selenium Concentration C/Co
Pore Volumes

Figure 5.7. Soil monolith eluent total metal concentrations (C/Co) eluted by pore volume for the (a) smectitic, (b) mixed, (c) kaolinitic, and (d) biosolid macro- and nano-colloids.

Total elutions of Selenium were so high they were given their own y-axis, showing maxima for the macro- and nano-colloids as high as 55 and 90%, respectively (Fig. 5.7a), highlighting the mobility of Se through soil profiles. The irregular patterns corroborated well with colloid elution and suggested numerous clogging and flushing cycles (Jacobsen et al., 1997; Karathanasis and Johnson, 2006). The erratic yet gradual decrease of As, Pb and Cu contaminants in association with the macrocolloids indicates that as the leaching cycles progressed, the larger sized colloids may have been physically excluded from smaller or blocked pores, resulting in a gradual decrease in elution of contaminants, as indicated by lower overall maxima (Barton and Karathanasis, 2003; Karathanasis and Johnson, 2006). Additionally, the higher pH matrix may have provided more competition for sorption of contaminants. Finally, it is possible that nanocolloids eluted greater quantities of contaminants because soil matrix sites reached sorption capacity and no longer provided competition for sorption. The more numerous flushing cycles evidenced in nanocolloid-associated contaminant BTCs could be due to less physical exclusion due to their smaller size, or due to greater continued interaction with contaminants along the flow path due to Brownian motion affects (Karathanasis, 2010). Within the mixed colloids, the nanocolloids showed higher overall maxima than corresponding macrocolloids (Fig. 5.7b). Nanocolloid associated total transport of Cu peaked at around 5%, while macrocolloids showed maxima of only 2% (Fig. 5.7b). For As, nanocolloids peaked at around 20% in the third pore volume, while macrocolloids showed maxima before the first pore volume at only 4% (Fig. 5.7b). Lead transport affinity was higher within the nanocolloids, ranging from 2 to 25%, versus ranges of less than 1 to 7% for macrocolloids (Fig. 5.7b). Selenium was consistently higher from the first pore volume to the end of the leaching cycle for the nanocolloids (maxima of 75%), but was more irregular for macrocolloids, with maxima at 75% but falling to less than 10% just after the third pore volume (Fig. 5.7b). The greater overall spikes in contaminants in the nanocolloid BTCs, especially after the second pore volumes, indicates significant clogging occurred, resulting in large flushing events late in the leaching cycle. Despite this, nanocolloids eluted greater total concentrations of contaminants, showing total elutions of As, Cu and Pb to be almost 3.5 times greater than corresponding macrocolloids (Fig. 5.7a). Additionally, leaching of As complimented DOC elutions in the mixed colloids, indicating organo-complex associations with transport (Fig. 5.3; Karathanasis, 2010).

The kaolinitic BTCs were not as irregular as those of the mixed or smectitic BTCs, but still indicated some clogging and flushing through spikes in total contaminant concentrations eluted (Fig. 5.7c). Overall, nanocolloids were associated with higher elutions of contaminants than macrocolloids, despite initially lower concentrations of Cu, As and Pb contaminants than macrocolloids until the third pore volume. Nanocolloids showed C/Co values that were less than 10% until the third pore volume when Pb and As spike to 55 and 12%, respectively (Fig. 5.7a). Selenium shows about 10% greater total elutions in the nanocolloids than the macrocolloids, although macrocolloids show a faster initial breakthrough. The macrocolloids showed immediate breakthroughs of as much as 17% Pb, with Cu showing maxima of 8% in the second pore volume. Arsenic stays at less than 2% total elutions for the macrocolloids. Kaolinitic colloid BTCs indicated greater fluctuations than did the contaminant BTCs, which suggests that dissolved

organic ligands may be responsible for carrying more of the load than the colloids themselves (Karathanasis and Miller, 2011).

Biosolid nanocolloids did not show significant breakthroughs in contaminants until 3.5 pore volumes, with even Se showing a slow linear increase in elution throughout the leaching cycle (Fig. 5.7d). Macrocolloids showed faster spikes in contaminant breakthroughs at the end of the first pore volume, with maxima reaching 7% for As, 2.5% for Cu and 1% for Pb. Nanocolloids showed spikes after the third pore volume with maxima of 11% for As, 4% for Cu and 2% for Pb (Fig. 5.7d). This may indicate that the organic functional groups available on these particular bio-colloids are not as competitive for sorption as those present in the DOC fraction or soil matrix, or could be due to released salts from the bio-colloids as evidenced by increased eluent EC values (Fig. 5.2) (Karathanasis et al., 2005).

The lower overall total contaminant elutions of the macrocolloids emphasizes the role of colloid size in contaminant transport, and highlights the greater mobility of environmental nanocolloids. Despite greater overall total contaminant elutions (Fig. 5.9) and faster initial colloid concentration BTCs (Fig. 5.4) by nanocolloids, macrocolloid BTCs indicate faster initial breakthrough times of about half a pore volume for contaminants than nanocolloids. The later breakthroughs of contaminants observed in the mixed, kaolinitic and biosolid nanocolloid fractions indicate contaminant elution increased once the soil matrix sites were saturated (Karathanasis and Johnson, 2006). The faster breakthroughs of the smectitic nanocolloids in association with contaminant elutions highlights their more reactive surfaces and greater potential for sorption competition over the other nanocolloids. It may also be that the lower nanocolloid suspension pHs inhibit initial mobility of contaminants until dissolution of carbonates from the monoliths creates a spike in eluent pH, creating greater colloid mobility and thus interaction with contaminants.

5.3.4.2 Individual Contaminant Elutions

Soluble and colloid-bound elution trends for each individual contaminant (As, Se, Cu, and Pb) are shown in Fig. 5.8. With the exception of Se, the presence of colloids enhanced contaminant elutions above that of the control treatment (contaminants added without colloids, Fig. 5.8; p-value <0.0001). Overall, there were greater colloid-bound than soluble associations for Pb and Cu contaminants, and greater soluble contaminant associations for As, and especially for Se contaminants than colloid-bound associations. Greater colloid-bound associations are likely due to attraction of the cation contaminants to the negatively charged colloid surfaces enhancing surface chemisorption as well as possible co-precipitation mechanisms (Karathanasis, 2010). Greater soluble contaminant loads could be due to repulsion of the oxy-anions from negatively charged colloid surfaces, or due to physical and chemical exclusion processes encountered during transport (Karathanasis et al., 2007; Karathanasis, 2010). Physical exclusion processes contributing to soluble loads include pore blockage from migrating colloids resulting in preferential flow of contaminants through larger available pore spaces and less interaction with either soil pore sites or migrating colloids.

(a)

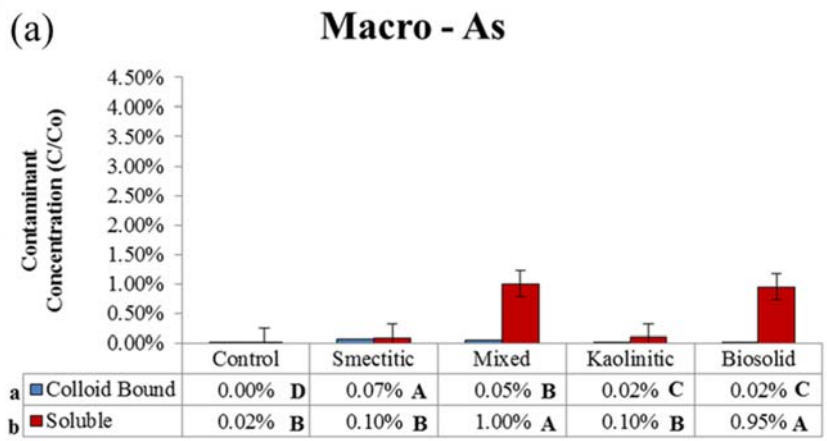

		Control	Smectitic	Mixed	Kaolinitic	Biosolid
a	Colloid Bound	0.00% **D**	0.07% **A**	0.05% **B**	0.02% **C**	0.02% **C**
b	Soluble	0.02% **B**	0.10% **B**	1.00% **A**	0.10% **B**	0.95% **A**

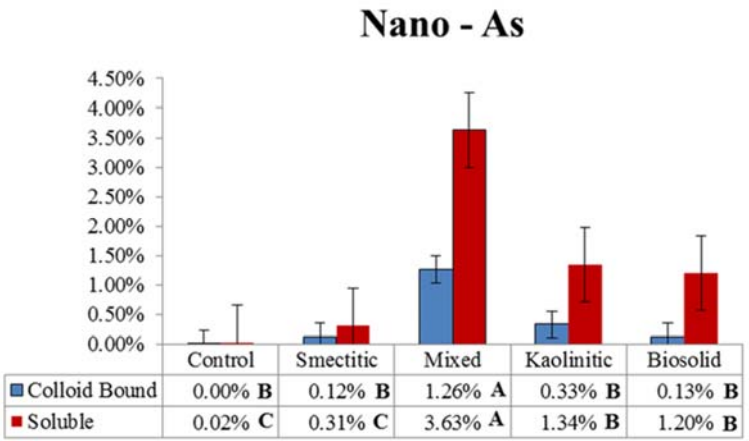

	Control	Smectitic	Mixed	Kaolinitic	Biosolid
Colloid Bound	0.00% **B**	0.12% **B**	1.26% **A**	0.33% **B**	0.13% **B**
Soluble	0.02% **C**	0.31% **C**	3.63% **A**	1.34% **B**	1.20% **B**

(b)

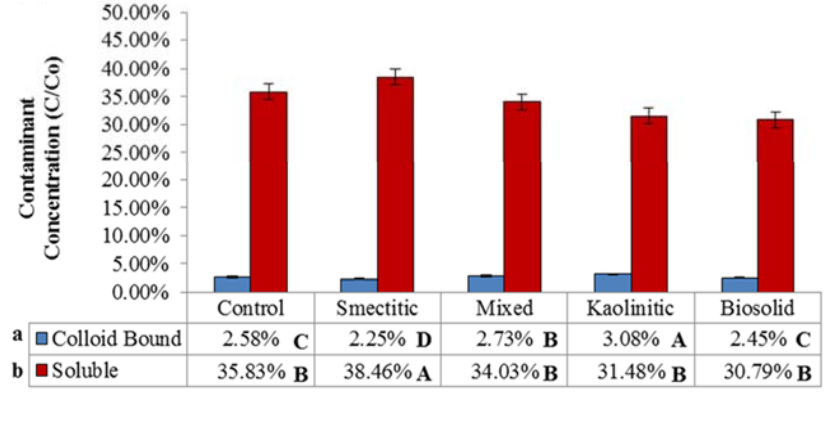

		Control	Smectitic	Mixed	Kaolinitic	Biosolid
a	Colloid Bound	2.58% **C**	2.25% **D**	2.73% **B**	3.08% **A**	2.45% **C**
b	Soluble	35.83% **B**	38.46% **A**	34.03% **B**	31.48% **B**	30.79% **B**

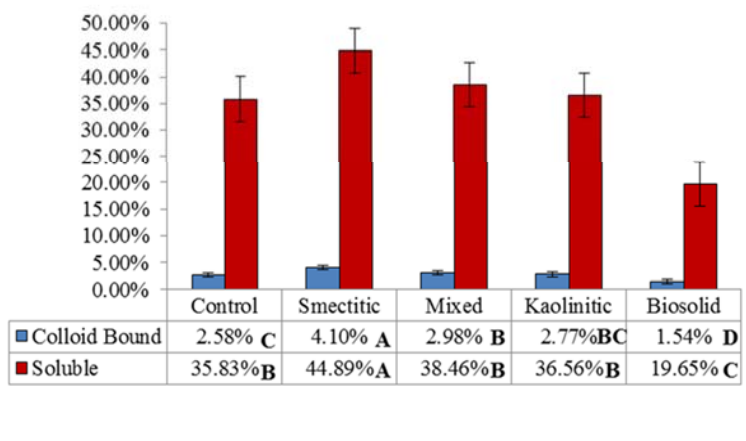

	Control	Smectitic	Mixed	Kaolinitic	Biosolid
Colloid Bound	2.58% **C**	4.10% **A**	2.98% **B**	2.77% **BC**	1.54% **D**
Soluble	35.83% **B**	44.89% **A**	38.46% **B**	36.56% **B**	19.65% **C**

(c)

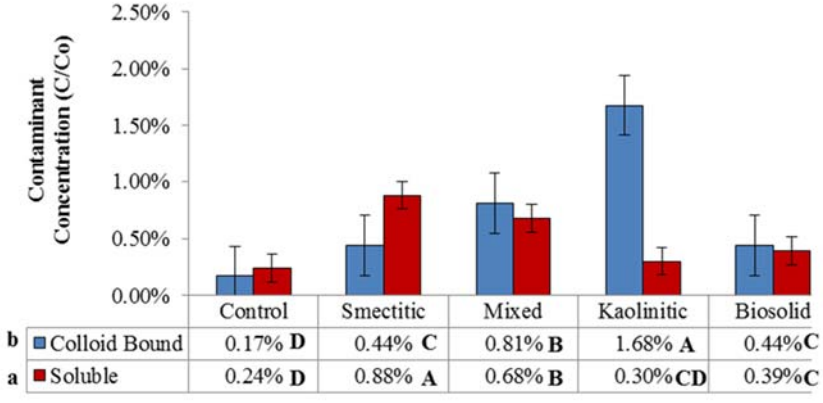

		Control	Smectitic	Mixed	Kaolinitic	Biosolid
b	Colloid Bound	0.17% **D**	0.44% **C**	0.81% **B**	1.68% **A**	0.44% **C**
a	Soluble	0.24% **D**	0.88% **A**	0.68% **B**	0.30% **CD**	0.39% **C**

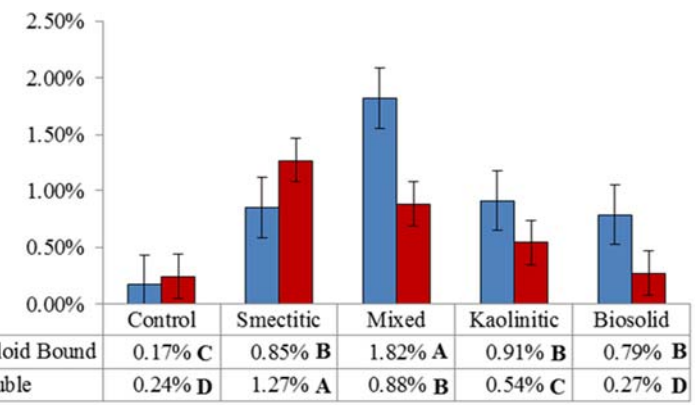

	Control	Smectitic	Mixed	Kaolinitic	Biosolid
Colloid Bound	0.17% **C**	0.85% **B**	1.82% **A**	0.91% **B**	0.79% **B**
Soluble	0.24% **D**	1.27% **A**	0.88% **B**	0.54% **C**	0.27% **D**

(d)

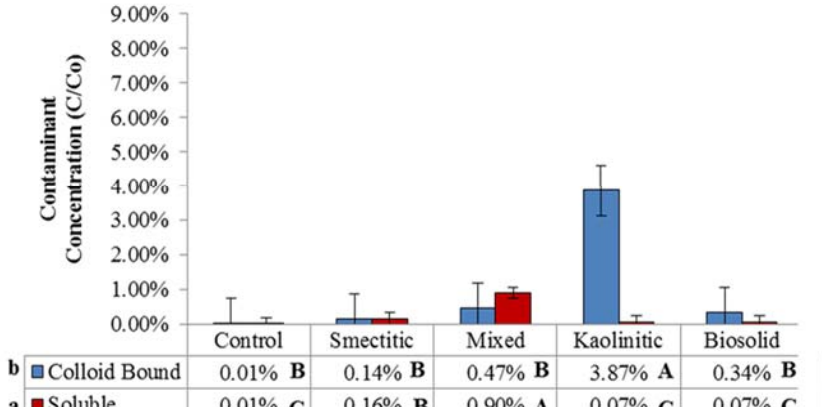

		Control	Smectitic	Mixed	Kaolinitic	Biosolid
b	Colloid Bound	0.01% **B**	0.14% **B**	0.47% **B**	3.87% **A**	0.34% **B**
a	Soluble	0.01% **C**	0.16% **B**	0.90% **A**	0.07% **C**	0.07% **C**

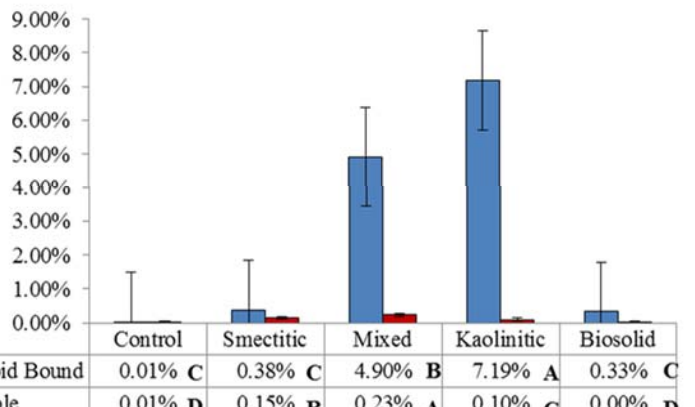

	Control	Smectitic	Mixed	Kaolinitic	Biosolid
Colloid Bound	0.01% **C**	0.38% **C**	4.90% **B**	7.19% **A**	0.33% **C**
Soluble	0.01% **D**	0.15% **B**	0.23% **A**	0.10% **C**	0.00% **D**

Figure 5.8. Soil monolith eluent colloid-bound and soluble contaminant concentrations (C/Co) for the macro- and nano-colloids are shown for (a) arsenic, (b) selenium, (c) copper, and (d) lead. Data represents averages of samples collected from all four pour volumes from duplicate columns. Error bars represent standard error. Significant differences (α=0.05) in between compositions for data table rows of soluble and colloid-bound metals are indicated in capital letters, lower case letters indicate differences between colloid-bound and soluble contaminants eluted for both size fractions combined.

Chemical exclusion processes that may contribute to soluble contaminant loads include inactive pore wall sites due to contaminant-colloid associations, which may be inhibiting any further interactions with soluble contaminants, exchange of contaminants on pore sites or colloid surfaces with anions or cations (such as phosphate ligand exchange mechanisms that complete for arsenic sorption and thus enhance soluble arsenic fractions), and finally, soluble loads may increase due to associations with colloid diffuse layers (Karathanasis et al., 2007; Gao, 2008; Karathanasis, 2010). A major mechanism contributing to soluble loads is ion exclusion from matrix sites blocked by migrating or attached colloid particles. Overall, colloid co-transport of both soluble and colloid-bound contaminants indicated the following overall sequence: Se (A) > Pb (B) = Cu (B) ≥ As (BC) (Fig. 5.8; p-value < α=0.05), with trends based on composition and size for the colloid-bound and soluble transport of each contaminant discussed below.

Macro- and nano-colloid transported soluble As fractions were significantly higher than colloid-bound fractions (Fig. 5.8a). This is typical behavior for As in soil environments, where it likely occurs as the negatively charged oxy-anion arsenate (Violante, 2013). Any colloid-bound As would likely sorb through bridging between surface organic carbon or (if present) between Fe/Al-OH groups (Violante, 2013). The highest elutions of soluble As were associated with the mixed and biosolid macrocolloids, and the mixed nanocolloids (Fig. 5.8a). Despite having 15 times more soluble As associated with the smectitic nanocolloids and 5 times more with the kaolinitic and smectitic macrocolloids over the control, they failed to differ statistically, likely due to larger standard error values incurred from extensive ranges in data values (Fig. 5.8a). However, colloid-bound As was higher for the smectitic and mixed macrocolloids, with all colloid additions eluting greater colloid-bound associations than the control (Fig. 5.8a). Within the nanocolloids the only colloid-bound As to exceed that of the control was the mixed composition (Fig. 5.8a), despite fractions showing more than 15 times that of the control (Fig. 5.8a). The consistent association of As with the mixed colloid fractions is likely due to their large mica content (Table 5.1), which has been shown to possess As retention properties (Huang, 1975).

Colloid-mediated transport of anionic As contaminants in subsurface soil environments is likely through the formation of solubilized or organo-complexed bridging formations (Karathanasis and Johnson, 2006). Sorption and transport of As has also been shown to preferentially associate with humic acid in soils through organo-complexation or to Fe-oxides and hydroxides (Smith et al., 2002; Voegelin and Hug, 2003; Han, 2009). The high DOC content associated with the mixed colloid elutions could contain humic materials that may be enhancing As transport as well (Fig. 5.3). Overall, co-transport of As showed composition based trends, with overall averages of soluble and colloid-bound contaminants of both macro- and nano-colloid eluents showing the following preferences: Mixed (A) > Biosolid (B) = Kaolinitic (B) ≥ Smectitic (BC) ≥ Control (C) (Fig. 5.8a; p-value < α=0.05). Additionally, monoliths with additions of nanocolloids eluted greater concentrations of As than did those with macrocolloid additions (Fig. 5.8a), likely due to greater Al/Fe:Si ratios (evidenced in EDS data), formation of bridging complexes (Karathanasis and Johnson, 2006), or larger organic surface carbon and C:SA ratios (Table 5.1).

Despite its occurrence as an oxy-anion similar to As, colloid-mediated transport of Se was different (Table 5.8b). The highest Se-soluble elutions came from monoliths with

both smectitic macro- or nano-colloid associations, while the other compositions failed to show significant differences from the control, or in the case of the bio-nanocolloids eluted lower concentrations than the control (Fig. 5.8b). This indicates that the addition of bio-nanocolloids to mixed mineral soil environments may inhibit the transport of solubilized Se by enhancing affinity for Se within the soil matrix. Other studies have indicated that Se is highly mobile in the environment and more likely to be quickly leached through soils as an oxy anion (Wang and Zhang, 1997; Jackson and Miller, 1999; Goh and Lim, 2004). Despite this, a few fractions showed surprisingly high associations of colloid-bound Se (Fig. 5.8b). Colloid-bound Se was as highest in the kaolinitic and mixed macrocolloids, as well as in the smectitic and mixed nanocolloids (Fig. 5.8b). The other fractions failed to show significant differences from the control, and in the case of the smectitic macrocolloids and biosolid nanocolloids, they eluted lower concentrations than the control (Fig. 5.8b). The occurrence of colloid-bound anionic contaminants suggests formation of weak outer sphere bonds through surface bridging mechanisms, potentially through organic surface coatings on colloids (Karathanasis and Johnson, 2006; Violante, 2013). Further, the greater DOC concentrations of the smectitic nanocolloids may explain their enhanced Se contaminant transport (Fig. 5.3 and 5.8) (Violante, 2013). Additionally, studies have shown that Se can form surface complexes with Al and Mn hydroxide and oxide surfaces, if present (Foster, 1999).

Copper, unlike Se or As, occurs as a cation. The highest associations of eluted soluble Cu were with the smectitic macro- and nano-colloids, showing 0.88 and 0.44% C/Co, respectively (Fig. 5.8c). Overall, macrocolloids showed 1.6-3.7 times greater soluble C/Co over the control, with the exception of the kaolinitic fraction, which did not show statistically higher soluble Cu (Fig. 5.8c). Overall, the mineral nanocolloids had higher soluble Cu associations, emphasizing their capacity over macrocolloids to facilitate contaminant transport. This could be attributed to lower initial pH's of nanocolloid suspensions compared to that of macrocolloids (Table 5.1), which likely induced carbonate dissolution in the soil columns and enhanced the formation of metal-organo complexes in the soluble fraction. This phenomena is evidenced at pHs above 6, such as that evidenced in the higher eluent pHs (Fig. 5.1, Karathanasis et al., 2005). Despite multiple studies citing bio-colloid mediated transport of Cu (Karathanasis et al., 2005; Karathanasis, 1999), and high affinities between Cu and the bio-colloids in sorption experiments, the biosolid nanocolloids failed to show significantly greater soluble-Cu elution from the control (Fig. 5.8c). This could indicate that the bio-colloids enhanced sorption of Cu within the monolith soil matrix. Typically, cation contaminants such as Cu, are associated in greater quantities with colloid-bound fractions or sorb to the soil matrix, especially when the soil matrix has a higher pH (McBride and Blasiak, 1979; Karathanasis et al., 2005).

All of the macro- and nano-colloids exhibited significantly higher colloid-bound elutions of Cu over the control (Fig. 5.8c), with the highest associated with the kaolinitic macrocolloids and the mixed nanocolloids (1.68 and 1.82% C/Co, respectively). Despite colloid-bound Cu being as much as 11 times higher than the control, C/Co values still ranged between only 0.44 and 1.82%, with other studies showing ranges of 7-87% colloid-bound Cu (Karathanasis and Miller, 2010). Other studies have indicated biosolid and mineral colloids of smectitic and mixed composition to have high affinity and colloid-mediated transport potential for Cu (Karathanasis, 1999). The weaker association

found in this study could be attributed to both lower inputs of colloid and contaminant concentrations used (others used inputs with 2.5 times greater contaminant concentrations and 4 times as much colloid concentration, Karathanasis et al., 2005; Karathanasis and Miller, 2010). Additionally, the lower colloid-bound fractions suggests some sorption competition with the monolith matrix, likely due to the higher pH (7.07) as compared to that of the colloid-suspensions (<5.36) (Karathanasis et al., 2005). Copper is known to have strong sorption affinity and low solubility at higher pHs, and may have preferentially sorbed to the column matrix due to a higher pH (McBride and Blasiak, 1979). Finally, additional competition for Cu sorption may have occurred between dissolved organic ligand complexes in the soluble fraction (Karathanasis et al., 2005). Lead is a cation contaminant similar to Cu. Copper soluble fractions, similar to findings by others, were higher than those associated with Pb (Karathanasis et al., 2005). Greater soluble Pb elutions were associated with the mixed and smectitic macro- and nano-colloids, showing as much as 90 times more soluble Pb over the control (Fig. 5.8d). The biosolid nanocolloids, and the biosolid and kaolinitic macrocolloids failed to show significantly different soluble Pb elutions from the control, despite the macrocolloids showing as much as 7 times more soluble Pb than the control (Fig. 5.8d). This is attributed to high standard error values from a large spread in data in the macrocolloid soluble Pb analysis, with ranges from 0.07 to 0.90% (Fig. 5.8d). Other studies found lower soluble Pb fractions, especially when other contaminants were added at the same time (Karathanasis et al., 2005). Lower soluble Pb associations are attributed to higher sorption affinity of Pb to both soil matrix and colloid surfaces. Additionally, Pb can be complexed into organic colloid-OH groups, Pb-carboxylic or Pb-phenolic groups (Karathanasis et al., 2005), which are all functional groups indicated to be present on the colloid surfaces in the DRIFT patterns from chapter 1.

Despite this, the only colloid-bound associations of Pb that were greater than the control were within the kaolinitic and mixed nanocolloids, and the kaolinitic macrocolloid fractions (Fig. 5.8d). The smectitic, mixed and bio-macrocolloids and the smectitic and bio-nanocolloid fractions failed to show significantly different colloid-bound fractions of Pb from the control, despite showing between 14 and 47 times greater colloid-bound Pb associations (Fig. 5.8d). The lack of significant differences from the control here is again attributed to large standard error values from ranges in data showing average maxima and minima of 4.90 and 0.14% C/Co (Fig. 5.8d). Despite the presence of Pb complexing organic groups on colloid surfaces, it is possible that the soil matrix or DOC fraction of the eluents have greater affinity for Pb (McBride and Blasiak, 1979; Karathanasis et al., 2005), or potential co-precipitation mechanisms (Karathanasis, 2010). At such high pHs, precipitation of Pb as cerrusite or chloropyromorphite minerals is possible (Gao, 2008). It is not surprising the colloids were out competed for Pb sorption by a higher pH soil matrix (Fig. 5.8d). This insinuates that high pH and DOC environments in conjunction with smectitic and mixed minerals may be used to remediate or dilute transport of Pb.

5.3.4.3 Anionic versus Cationic Contaminant Elutions

The average trends for cation and anion contaminant loads eluted through the monoliths are displayed in Fig. 5.9. Greater colloid-bound anionic contaminants occurred in association with the smectitic, mixed and biosolid macrocolloids than was expected (Fig. 5.9), indicating potential OC or cation bridging effects (Karathanasis and Johnson, 2006).

Figure 5.9. Soil monolith eluent concentrations (C/Co) for colloid-bound and soluble contaminants, as averaged across all four contaminants, are shown for the macro- and nano-colloids. Error bars represent standard error. Significant differences (α=0.05) amongst the four composition types for each size fraction are shown using capital letters for soluble contaminants and lower case letters for colloid-bound contaminants eluted.

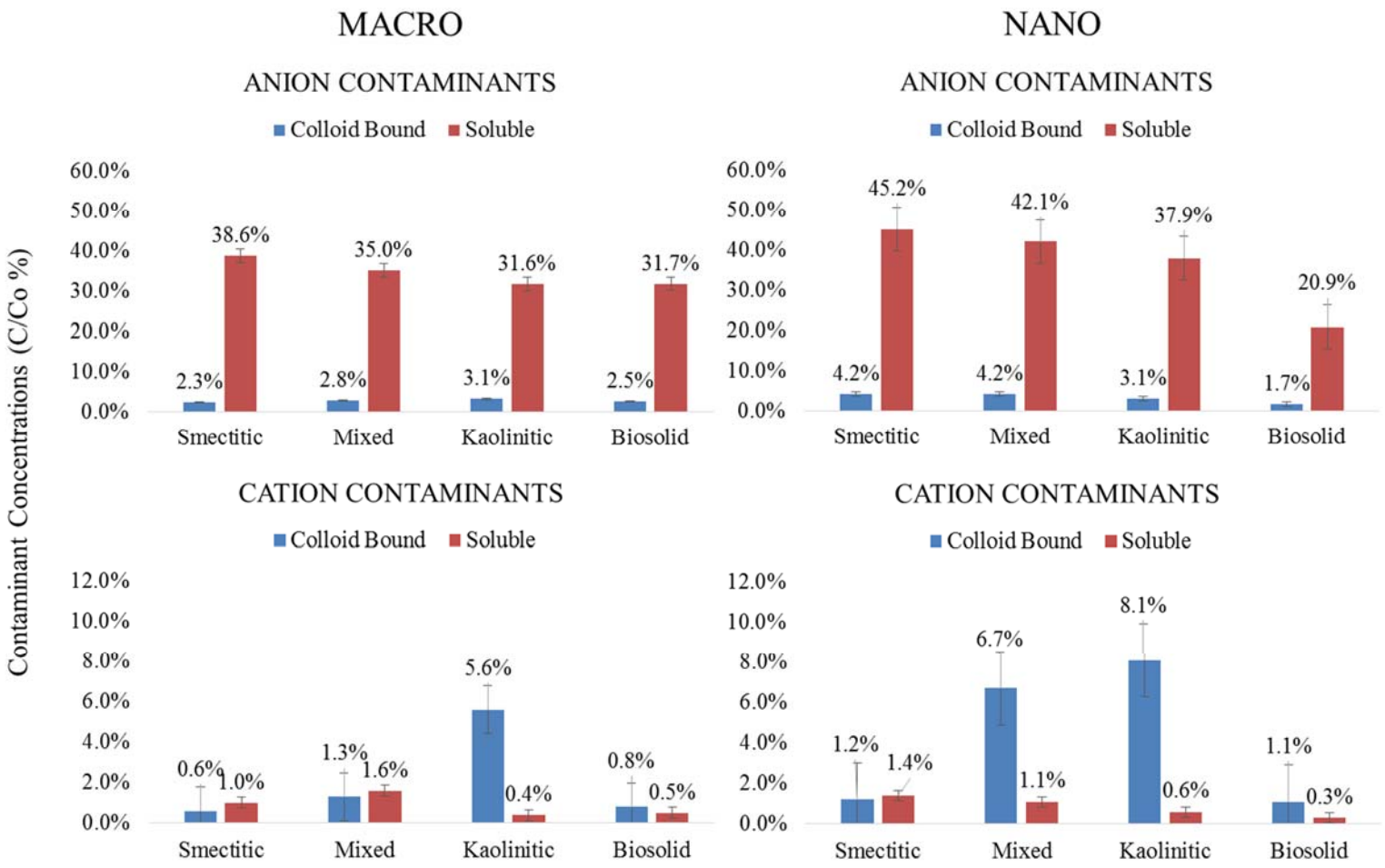

However, the kaolinitic macrocolloids had greater associations with cationic contaminants than anionic, likely due to direct formation of surface complexes through attraction of opposite charges (Fig. 5.9; Violante, 2013). Enhanced negative surface charges in the kaolinitic macrocolloids is supported by eluent pH increases as leaching progressed (Fig. 5.1). The smectitic and biosolid nanocolloids were the most effective anionic contaminant carriers, showing higher colloid-bound fractions as opposed to the mixed and kaolinitic nanocolloids, which were associated with greater cationic colloid-bound contaminants than anionic (Fig. 5.9). The greater associations of colloid-bound anion contaminants in the smectitic and biosolid nanofractions could be attributed to bridging through their higher initial OC and Ca^{2+} concentrations (Table 5.1; Karathanasis and Johnson, 2006).

However, when Se was excluded, the colloid-bound fractions of As anion contaminants were smaller than those of the cation contaminants (Cu, Pb, Fig. 5.8), similar to findings comparing anion and cation contaminants by Seta and Karathanasis (1997), and Karathanasis (1999). Colloid-bound Se was larger than expected, and in most cases larger than that of Cu and Pb (Fig. 5.8). As and Se contaminants are oxy-anion contaminants, anion contaminants are usually repelled by the negatively charged colloid surfaces, however, colloid-mediated transport could occur through soluble or organically-complexed forms (Karathanasis and Johnson, 2006). Overall, the anion contaminants had greater soluble load elutions than did cation contaminants, probably due to physical and chemical exclusion processes (Papelis, 2001; Karathanasis and Johnson, 2006). Additionally, greater soluble load elutions in association with colloids are probably associated with ion exclusion from matrix sites blocked by migrating or attached colloid particles.

Mineral colloids showed greater anionic contaminant associations, eluting 17-24% more anionic contaminants than the bio-colloids (Fig. 5.9). The most effective elutions of soluble anionic contaminants occurred in association with the smectitic and mixed macro- and nano-colloids, ranging from 35 to 39% C/Co (smectitic macro- and nano-colloids, respectively, Fig. 5.9). Conversely, the macrocolloids did not indicate trends based on composition for soluble anionic contaminant elutions, with average soluble anionic elutions ranging from 32-39% (biosolid and smectitic fractions, respectively; Fig. 5.9). Compared to the anions, nanocolloid elutions of soluble cation contaminants were small, ranging from 0.3-1.4% (biosolid and smectitic fractions, respectively; Fig. 5.9). Soluble cation elutions in association with macrocolloids ranged from 0.5-1.6%, represented by the biosolid and mixed compositions, respectively (Fig. 5.9). Greater soluble elutions of cation contaminants were associated with the smectitic and mixed macro- and nano-colloids as compared to the other compositions (Fig. 5.9). The overall lower soluble elutions of cation contaminants indicated significant competition for sorption by the soil matrix, likely attributable to the higher soil matrix pH compared to input suspension pH's (Table 5.2 and 5.1) (McBride and Blasiak, 1979; Karathanasis et al., 2005).

On average, the bio-nanocolloids had the lowest soluble and colloid-bound associations with anionic and cationic contaminants, with the bio-macrocolloids having the second lowest soluble and colloid-bound elutions after the smectitic and kaolinitic colloid-bound and soluble fractions, respectively (Fig. 5.9). This is contrary to the findings of

Karathanasis and Miller (2011), who indicated overall greater bio-colloid co-transport of contaminants, but also showed lower colloid-bound fractions (with the exception of Pb). The range of contaminant transport increase in the presence of colloids was dependent upon colloid size, composition, and contaminant type. Contaminant co-transport in the presence of colloids was higher in nanocolloids than corresponding macrocolloids. Even though sorption isotherms indicated differences in sorption amongst only a select few fractions based on size, it is likely that greater co-transport of contaminants occurs in association with nanocolloids because they are not as subject to the matrix straining processes than their larger size counterparts, making them more mobile in subsurface environments (Seta and Karathanasis, 1997; Karathanasis, 1999). The likely mechanisms attributing to greater colloid-bound and soluble loads over control treatments were size and ion exclusion. Greater nanocolloid mobility was indicated by greater nanocolloid concentrations in eluents (Fig. 5.4 and 5.5), corresponding to greater elutions of smaller sized particles in other column transport studies (Karathanasis, 2010). The greater mineral colloid-associations with contaminants over bio-colloids was corroborated by the mixed isotherm experiments, although other studies have indicated higher contaminant transport potential of bio-colloids (Karathanasis et al., 2005; Karathanasis and Johnson, 2006).

5.4 Conclusion

The findings from this study demonstrate that smaller size nanocolloids are greater threats to groundwater quality than are larger, corresponding macro-colloid fractions. Despite only a select few size-based sorption differences in isotherms, monolith studies indicated significantly greater colloid-bound and soluble transport for As, Se, Cu and Pb contaminants in association with nanocolloids than with macrocolloids. This was likely because their smaller size and greater mobility allows for less straining and restriction from soil matrices compared to that of the larger macrocolloids. Transport trends were surprising, indicating elutions of contaminants in the following order: Se>Cu, Pb and As. Mineral colloids were associated with greater overall contaminant transport as compared to bio-colloids, with contaminant preferences based on composition. Greater Se was associated with the smectitic colloids, while greater quantities of Pb and Cu were associated with the kaolinitic and mixed nano-fractions. Finally, mixed colloids, particularly the nanos, were associated with greater quantities of As. The higher column pH matrix as compared to that of the input colloid suspensions probably enacted as a remediatory medium, resulting in less than expected transport of Cu and Pb. Nevertheless, anionic contaminants indicated indirect attachment through organic and cation bridging formations while cations indicated more direct complex formation to colloid surfaces. Overall, colloids were suggested as dual contaminant carriers and facilitators through enhanced colloid-bound and soluble elutions in the presence of colloids. Greater elutions of soluble contaminant loads compared to control treatments are likely due to ion exclusion from matrix sites that were blocked by migrating or attached colloids. The lack of prediction through sorption affinities for colloid facilitated transport highlights the importance of transport experiments in assessing the complexities of contaminant transport. Most colloids eluted greater overall contaminants than did the control, underlining their potential as contaminant transport vectors and emphasizing the threat they pose to groundwater quality.

Chapter Six – Conclusions

The findings from this study demonstrate that smaller size nanocolloids are greater threats to groundwater quality than are larger, corresponding macro-colloid fractions, and that comprehensive characterization of environmental nano- and macro-colloids and their interactions with contaminants can lead to a better understanding of the contaminant sorption and transport risks they pose to ground and surface waters. Surface properties such as cation exchange capacity, organic carbon, carbon:surface area and surface area were found to affect sorption properties amongst the differing colloid compositions, while mineralogy and size were shown to affect stability and transport.

Greater surface reactivity was indicated by nanocolloids larger, more negatively charged surface areas, but aggregation induced from OC surface coatings likely decreased available surface area, masking differences in sorption. Despite this, nanocolloids were also shown to have enhanced stability, even in the presence of contaminants. The sorption and surface characterization studies showed that the adhesion of nanocolloids to surfaces of macrocolloids may be enhancing macrocolloid reaction and sorption of contaminants, while higher organic carbon coatings on the nanocolloids may be inducing aggregation and limiting available surfaces for sorption. Nano-nano and macro-nano aggregation also suggests potential encapsulation of contaminants with unknown effects on transport and release of contaminants.

Despite showing only a few select sorption differences in isotherms, monolith studies indicated significantly greater colloid-bound and soluble transport of As, Se, Cu and Pb contaminants in association with nanocolloids than with macrocolloids. This was likely because their smaller size and greater mobility allows for less straining and restriction from soil matrices compared to that of the larger macrocolloids. Mineral colloids were associated with greater overall contaminant transport as compared to bio-colloids, with contaminant preferences based on composition. Greater Se was associated with smectitic minerals, while greater quantities of Pb and Cu were associated with kaolinitic colloids. Finally, mixed colloids were associated with greater quantities of As. Overall contaminant transport indicated Se was transported in greater quantities than was Pb, Cu and finally, As. The higher column pH matrix as compared to that of the input colloid suspensions enacted an almost remediatory-type situation, resulting in less than expected transport of Cu and Pb, despite this, colloids eluted greater overall contaminants than did the control, indicating their basis as contaminant transport systems and emphasizing the threat they pose to groundwater quality.

The results from this study emphasize the importance of considering multiple physicochemical and mineralogical parameters in contaminant transport models in order to accurately assess environmental pollution risks and develop efficient remediation strategies. This study is important for water quality professionals and environmental consulting agencies undertaking remediation tasks who strive to understand contaminant reaction and potential movement in subsurface media and groundwater as well as to developers of engineered nanoparticles who seek to better understand the interaction and potential behavior of nanoparticles in the environment as a basis for their model. Finally, the role of both facilitated and associated transport of contaminants via colloids, especially of smaller, nanocolloids over macrocolloids indicates their vast potential to transport contaminants into ground and surface waters.

References

1. Ahlrichs, J.S. and L.R. Hossner. 1987. Selenate and selenite mobility in overburden by saturated flow. J. Environ. Qual. 16: 95-98.
2. Baes, A.U. and P.R. Bloom. 1989. Diffuse reflectance Fourier transform infrared (DRIFT) spectroscopy of humic and fulvic acids. Soil Sci. Soc. Am. J. 53: 695-700.
3. Balasoiu, C.F., G.J. Zagury and L. Deschênes. 2001. Partitioning and speciation of chromium, copper, and arsenic in CCA-contaminated soils: influence of soil composition. Sci. Total Environ. 280: 239-255. doi:http://dx.doi.org/10.1016/S0048-9697(01)00833-6.
4. Bar-Yosef, B. and D. Meek. 1987. Selenium sorption by kaolinite and montmorillonite. Soil Sci. 144: 11-19.
5. Barton, C.D., and A.D. Karathanasis. 2003. Influence of soil colloids on the migration of atrazine and zinc through large soil monoliths. Water, Air, Soil Poll. 143: 3-21.
6. Bertsch, P.M. and J.C. Seaman. 1999. Characterization of complex mineral assemblages: Implications for contaminant transport and environmental remediation. Proc. Natl. Acad. Sci. USA 6: 3350-3357.
7. Bolea, E., F. Laborda and J.R. Castillo. 2010. Metal associations to microparticles, nanocolloids and macromolecules in compost leachates: Size characterization by assymetrical flow field-flow fractionation coupled to ICP-MS. Anal Chim Acta 661: 206-214.
8. Borchardt, G.A. 1977. Montmorillonite and other smectite minerals. p. 293-330. In Dixon, J.B. and S.B. Weeds (eds.) Minerals in soil environments (2nd Edition). Soil Sci. Soc. Am. Book 1, Madison, WI.
9. Bowell, R.J. 1994. Sorption of arsenic by iron oxides and oxyhydroxides in soils. Appl. Geochem. 9: 279-286.
10. Bradford, S.A. and S. Torkzaban. 2008. Colloid transport and retention in unsaturated porous media: A review of interface-, collector-, and pore-scale processes and models. Vadose Zone J. 7: 667-681.
11. Bradford, S.A., S. Torkzaban and S.L. Walker. 2007. Coupling of physical and chemical mechanisms of colloid straining in saturated porous media. Water Research 41: 3012-3024.
12. Bryant, J.P. and J.B. Dixon. 1963. Clay mineralogy and weathering of red-yellow podzolic soil from quartz mica schist in the Alabama Piedmont. Clays Clay Miner. 12: 509-521.
13. Calabi-Floody, M., J.S. Bendall, A.A. Jara, M.E. Welland, B.K.G. Theng, C. Rumpel, et al. 2011. Nanoclays from an Andisol: Extraction, properties, and carbon stabilization. Geoderma 161: 159-167.
14. Carroll-Webb, S.A. and J.V. Walther. 1988. A surface complexion reaction model for the pH-dependence of corundum and kaolinite dissolution rates. Geochim Cosmochim Ac 52: 2609-2623.
15. Carter, D.L., M.D. Heilman and C.L. Gonzalez. 1965. Ethylene glycol monoethylene ether for determining surface area of silicate minerals. Soil Sci. Soc. Am. J. 100: 356-360.
16. Carter, D.L., M.M. Mortland and W.D. Kemper. 1986. In Ch. 16, p. 413, Methods of soil analysis, Part 1. Physical and mineralogical methdos - Agronomy

monograph no. 9. American Society of Agronomy - Soil Science Society of America.
17. Chefetz, B., P.G. Hatcher, Y. Hadar and Y. Chen. 1996. Chemical and biological characterization of organic matter during composting of municipal solid waste. J. Environ. Qual. 25: 776-785.
18. Cheshire, M.V., C. Dumat, A.R. Fraser, S. Hillier and S. Staunton. 2000. The interaction between soil organic matter and soil clay minerals by selective removal and controlled addition of organic matter. Eur. J. Soil Sci. 51: 497-509.
19. Chorover, J. and G. Sposito. 1995. Colloid chemistry of kaolinitic tropical soils. Soil Sci. Soc. Am. J. 59: 1558-1564.
20. Christian, P., F. Von der Kammer, M. Baalousha and T. Hofmann. 2008. Nanoparticles: structure, properties, preparation and behaviour in environmental media. Ecotoxicology 17: 326-343.
21. Covelo, E.F., F.A. Vega and M.L. Andrade. 2007. Competitive sorption and desorption of heavy metals by individual soil components. J. Hazard. Mater. 140: 308-315.
22. Cruz-Guzman, M., R. Celis, M.C. Hermosin, P. Leone, M. Negre and J. Cornejo. 2003. Sorption-desorption of lead (II) and mercury (II) by model associations of soil colloids. Soil. Sci. Soc. Am. J. 67: 1378-1387.
23. De Momi, A. and J.R. Lead. 2008. Behaviour of environmental aquatic nanocolloids when separated by split-flow thin-cell fractionation (SPLITT). Sci. Total Environ. 405: 317-323.
24. Deng, Y., N. White and J.B. Dixon. 2009. Soil Mineralogy Laboratory Manual Texas A&M.
25. Dixon, J.B. 1966. Quantitative analysis of kaolinite and gibbsite in soils by differential thermal and selective dissolution methods. Clays Clay Miner. 14: 83-90.
26. Dixon, J.B. 1989. Kaolin and serpentine group minerals. p. 467-525. In Dixon, J.B. and S.B. Weeds (eds.) Minerals in soil environments (2nd Edition). Soil Sci. Soc. Am. Book 1, Madison, WI.
27. Donner, E., C.G. Ryan, D.L. Howard, B. Zarcinas, K.G. Scheckel, S.P. McGrath, et al. 2012. A multi-technique investigation of copper and zinc distribution, speciation and potential bioavailability in biosolids. Environmental Pollution 166: 57-64. doi:http://dx.doi.org/10.1016/j.envpol.2012.02.012.
28. Dupuy, N. and F. Douay. 2001. Infrared and chemometrics study of the interaction between heavy metals and organic matter in soils. Spectrochim. Acta. A 57: 1037-1047.
29. Echeverria, J.C., M.T. Morera, C. Mazkiaran and J.J. Garrido. 1998. Competitive sorption of heavy metals by soils. Isotherms and fractional factorial experiments. Environ Pollut 101: 275-284.
30. Essington, M.E. 2004. Soil and water chemistry: An integrative approach. CRC Press LLC, Boca Raton, FL, USA.
31. Farley, K.J., D.A. Dzombak and F.M.M. Morel. 1985. A surface precipitation model for the sorption of cations on metal oxides. J. Colloid Interf. Sci. 106: 226-242.

32. Farmer, V.C. 1974. Vibrational spectroscopy in mineral chemistry. In V.C. Farmer (ed.) The infrared spectra of minerals. Mineralogical Society Monograph 4, London.
33. Foster, A.L. 1999. Partitioning and transformation of arsenic and selenium in natural and laboratory systems. Ph.D., Stanford University, Ann Arbor.
34. Frey, E. and G. Lagaly. 1979. Selective coagulation in mixed colloidal suspensions. J. Colloid Interf. Sci. 70: 46-55.
35. Gang, C. and M. Flury. 2005. Retention of mineral colloids in unsaturated porous media as related to their surface properties. Colloids Surf. A. Physicochem. Eng. Asp. 256: 207-216.
36. Gao, X. 2008. Speciation and geochemical cycling of lead, arsenic, chromium, and cadmium in a metal-contaminated histosol (Doctoral Dissertation). Retrieved from ProQuest Dissertations and Thesis (Accession Order No. 3294674).
37. Gilbert, B., F. Huang, H. Zhang, G.A. Waychunas and J.F. Banfield. 2004. Nanoparticles: Strained and stiff. Science 305: 651-654.
38. Goh, K. and T. Lim. 2004. Geochemistry of inorganic arsenic and selenium in a tropical soil: effect of reaction time, pH, and competitive anions on arsenic and selenium adsorption. Chemosphere 55: 849-859.
39. Goldberg, S. and R.A. Glaubig. 1987. Effect of saturating cation, pH, and aluminum and iron oxides on the flocculation of kaolinite and montmorillonite. Clays Clay Miner. 35: 220-227.
40. Goldstein, J.I., D.E. Newbury, P. Echlin, D.C. Joy, C. Fiori and E. Lifshin. 1992. Scanning Electron Microscopy and X-ray microanalysis. 2nd ed. Plenum Press, New York. 820 pp.
41. Griffin, R.A. and J.J. Jurinak. 1973. Estimation of activity coefficients from the electrical conductivity of natural aquatic systems and soil extracts. Soil. Sci. 116: 26-30.
42. Grund, S.C., K. Hanusch and H.U. Wolf. 2005. Arsenic and arsenic compounds. Ullmann's Encyclopedia of Industrial Chemistry, Weinheim: Wiley-VCH, doi:10.1002/14356007.a03_113.pub2.
43. Haering, K.C. and G.K. Evanylo. 2006. Mid-Atlantic Nutrient Management Handbook. CSREES Mid-Atlantic Regional Water Quality Program. MAWQP #06-02 [online], last verified January 11, 2012. Available [online]: http://www.mawaterquality.org/capacity_building/ma_nutrient_mgmt_handbook.html.
44. Han, D.S. 2009. Sorption of arsenic, mercury, selenium onto nanostructured adsorbent media and stabilization via surface reactions. Ph.D., Texas A&M University, Ann Arbor.
45. Harris, W.G., K.A. Hollien, and V.W. Carlisle. 1989. Pedon distribution of minerals in coastal plain Paleudults. Soil Sci. Soc. Am. J. 53: 1901-1906.
46. Harron, W.R.A., G.R. Webster and R.R. Cairns. 1983. Relationship between exchangeable sodium and sodium adsorption ratio in a solonetzic soil association. Can. J. Soil Sci. 63: 461-467.
47. Hassellov, M. and F. Von der Kammer. 2008. Iron oxides as geochemical nanovectors for metal transport in soil-river systems. Elements 4: 401-406. doi:DOI 10.2113/gselements.4.6.401.

48. Heidmann, I., I. Christl, C. Leu and R. Kretzschmar. 2005a. Competitive sorption of protons and metal cations onto kaolinite: experiments and modeling. J. Colloid Interf. Sci. 282: 270-282. doi:10.1016/j.jcis.2004.08.019.
49. Heidmann, I., I. Christl, C. Leu and R. Kretzschmar. 2005b. Sorption of Cu and Pb to kaolinite-fulvic acid colloids: Assessment of sorbent interactions. Geochim Cosmochim Ac 69: 1675-1686.
50. Hesterberg, D. and A.L. Page. 1990. Flocculation series test yielding time-invariant critical coagulation concentrations of sodium illite. Soil Sci. Soc. Am. J. 54: 729-735.
51. Hochella, M.F., Jr. 2008. Nanogeosciences: From origins to cutting-edge applications. Elements 4: 373-379.
52. Hochella, M.F., Jr., S.K. Lower, P.A. Maurice, R.L. Penn, N. Sahai, D.L. Sparks, et al. 2008. Nanominerals, mineral nanoparticles, and earth systems. Science 319: 1631-1635.
53. Huang, P.M. 1975. Retention of arsenic by hydroxy-aluminum on surfaces of micaceous mineral colloids. Soil. Sci. Soc. Am. J. 39: 271-274.
54. IUPAC. 1997. IUPAC compendium of chemical terminology, 2nd ed., A.D. McNaught and A. Wilkinson (Eds.). Blackwell Science Publications, Oxford, UK.
55. Jackson, B.P. and W.P. Miller. 1999. Soluble arsenic and selenium species in fly ash/organic waste-amended soils using ion chromatography - inductively coupled plasma mass spectrometry. Environ. Sci. Technol. 33: 270-275.
56. Jacobsen, O.H., P. Moldrup, C. Larsen, L. Konnerup and L.W. Petersen. 1997. Particle transport in macropores of undisturbed soil columns. Journal of Hydrology 196: 185-203. doi:http://dx.doi.org/10.1016/S0022-1694(96)03291-X.
57. Judy, J.D., J.M. Unrine and P.M. Bertsch. 2011. Evidence of biomagnification of gold nanoparticles within a terrestrial food chain. Environ. Sci. Technol. 45: 776-781.
58. Kaplan, D., P.M. Bertsch, D.C. Adriano and W.P. Miller. 1993. Soil-borne mobile colloids as influenced by water flow and organic carbon. Environ. Sci. and Technol. 27: 1192-1200.
59. Kaplan, D.I., P.M. Bertsch and D.C. Adriano. 1997. Mineralogical and physicochemical differences between mobile and nonmobile colloidal phases in reconstructed pedons. Soil Sci. Soc. Am. J. 61: 641-649.
60. Karathanasis, A.D. 1999. Subsurface migration of copper and zinc mediated by soil colloids. Soil Sci. Soc. Am. J. 63: 830-838.
61. Karathanasis, A.D. 2008. Thermal Analysis of Soil Minerals, Chapter 5, pp. 117-160, In A. L. Ulery and L. R. Drees (eds.) Methods of Soil Analysis, Part 5-Mineralogical Methods. Soil Sci. Soc. Am. Book 5, Madison, WI.
62. Karathanasis, A.D. 2010. Composition and transport behavior of soil nanocolloids in natural porous media. Ch. 4, In F.H. Frimmel and R. Nießner (eds.), Nanoparticles in the water cycle. Springer-Verlag Berlin Heidelberg.
63. Karathanasis, A.D., and D.M.C. Johnson. 2006a. Stability and transportability of biosolid colloids through undisturbed soil monoliths. Geoderma 130: 334-345.
64. Karathanasis, A.D. and D.M.C. Johnson. 2006b. Subsurface transport of Cd, Cr, and Mo mediated by biosolid colloids. Sci. Total. Environ 354: 157-169. doi:10.1016/j.scitotenv.2005.01.025.

65. Karathanasis, A.D., D.M.C. Johnson and C.J. Matocha. 2005. Biosolid colloid-mediated transport of copper, zinc, and lead in waste-amended soils. J. Environ. Qual. 34: 1153-1164.
66. Karathanasis, A.D., D.M.C. Johnson and C.J. Matocha. 2007. Subsurface transport of heavy metals mediated by biosolid colloids in waste-amended soils. Ch. 7, pp. 175-201, In: F. Frimmel, F. von der Kammer, and H.C. Flemming, (eds.), Colloidal Transport in Porous Media. Springer, Cambridge, Mass.
67. Karathanasis, A.D., and J.O. Miller. 2011. Ch. 5, Colloid-associated transport and metal speciation at reclaimed mine sites following biosolid application. p. 129-145. In H.M. Selim (ed.) Dynamics and bioavailability of heavy metals in the rootzone. CRC Press, Boca Raton, FL.
68. Kjaergaard, C., H.C.B. Hansen, C.B. Koch and K.G. Villholth. 2004. Properties of water-dispersible colloids from macropore deposits and bulk horizons of an Agradalf. Soil Sci. Soc. AM. J. 68: 1844-1852.
69. Kjaergaard, C., P. Moldrup, L.W. de Jonge and O.H. Jacobsen. 2004. Colloid mobilization and transport in undisturbed soil columns. II. The role of colloid dispersibility and preferential flow. Vadose Zone J. 3: 423-433.
70. Kretzschmar, R., M. Borkovec, D. Grolimund and M. Elimelech. 1999. Mobile subsurface colloids and their role in contaminant transport. Adv. Agron 66: 121-194.
71. Kretzschmar, R.W., W.P. Robarge and S.B. Weed. 1993. Flocculation of kaolinitic clays: Effects of humic substances and iron oxides. Soil Sci. Soc. Am. J. 57: 1277-1283.
72. Lado, M. and M. Ben-Hur. 2004. Soil mineralogy effects on seal formation, runoff and soil loss. App. Clay Sci. 24: 209-224.
73. Lair, G.J., M.H. Gerzabek, G. Haberhauer, M. Jakusch and H. Kirchmann. 2006. Response of the sorption behavior of Cu, Cd, and Zn to different soil management. J. Plant Nutr. Soil Sci. 169.
74. Lowry, G.V., S. Majetich, K. Matyjaszewski, D. Sholl and R. Tilton. 2006. Transport, targeting, and applications of metallic functional nanoparticles for degredation of DNAPL chlorinated organic solvents. Technical Report, Carnegie Mellon University, Pittsburgh, PA.
75. Lui, F., A.D. Cristofaro, and A. Violante. 2001. Effect of pH, phosphate and oxalate on the adsorption, desorption of arsenate on/from goethite. Soil Sci. 166: 197-208.
76. Madden, A.S., M.F. Hochella, Jr. and T.P. Luxton. 2006. Insights for size-dependent reactivity of hematite nanomineral surfaces through Cu2+ sorption. Geochim Cosmochim Ac 70: 4095-4104. doi:DOI 10.1016/j.gca.2006.06.1366.
77. Madejova, J. 2003. FTIR techniques in clay mineral studies. Vib. Spectrosc. 31: 1-10.
78. Maurice, P.A. and M.F. Hochella, Jr. 2008. Nanoscale particles and processes: A new dimension in soil science. Adv. Agron. 100: 123-153.
79. McBride, M.B. 1994. Environmental chemistry of soils. Oxford University Press, New York.
80. McBride, M.B. and J.J. Blasiak. 1979. Zinc and copper solubility as a function of pH in an acid soil. Soil Sci. 43: 866-870.

81. McCarthy, J.F. and L.D. McKay. 2004. Colloid transport in the subsurface: Past, present, and future challenges. Vadose Zone J. 3: 326-337.
82. McCarthy, J.F. and J.M. Zachara. 1989. Subsurface transport of contaminants. Environ. Sci. Technol. 23: 496-502.
83. McKenzie, R.M. 1980. The adsorption of lead and other heavy metals on oxides of manganese and iron. Aust. J. Soil Res. 18: 61-73.
84. Miller, J.O., A.D. Karathanasis and O.B. Wendroth. 2010. In situ colloid generation and transport in 30-year-old mine soil profiles receiving biosolids. Int J. Mining Recl. Environ. 24: 95-108.
85. Morton, J.D., J.D. Semrau and K.F. Hayes. 2001. An X-ray absorption spectroscopy study of the structure and reversibility of copper adsorbed to montmorillonite clay. Geochim Cosmochim Ac 65: 2709-2722.
86. Naidu, R., R.S. Kookana, M.E. Sumner, R.D. Harter and K.G. Tiller. 1997. Cadmium sorption and transport in variable charge soils: A Review. J. Environ. Qual. 26: 602-617.
87. Neal, R.H. and G. Sposito. 1989. Selenate adsorption on alluvial soils. Soil Sci. Soc. Am. J. 53: 70-74.
88. Nemeth, T., J. Jimenez-Millan, P. Sipos, I. Abad, R. Jimenez-Espinosa and Z. Szalai. 2011. Effect of pedogenic clay minerals on the sorption of copper in a Luvisol B horizon. Geoderma 160: 509-516.
89. Niemeyer, J., Y. Chen and J.M. Bollag. 1992. Characterization of humic acids, composts, and peat by Diffuse Reflectance Fourier-Transform Infrared Spectroscopy. Soil Sci. Soc. Am. J. 56: 135-140.
90. NRCS. 1996. Soil survey laboratory methods manual. Soil Survey Invest. Rep. 42. Version 3.0. USDA, National Soil Survey Center, Lincoln, NE.
91. Ottofuelling, S., F. Von der Kammer and T. Hofmann. 2011. Commercial titanium dioxide nanoparticles in both natural and synthetic water: Comprehensive multidimensional testing and prediction of aggregation behavior. Environ. Sci. Technol. 45: 10045-10052.
92. Ouyang, Y., D. Shinde, R.S. Mansell and W. Harris. 1996. Colloid-enhanced transport of chemicals in subsurface environments: a review. Crit. Rev. Env. Sci. Tec. 26: 189-204.
93. Papelis, C. 2001. Cation and anion sorption on granite from the project Shoal Test Area, near Fallon, Nevada, USA. Adv. Environ. Res. 5: 151-166.
94. Peak, D. and D.L. Sparks. 2002. Mechanisms of selenate adsorption on iron oxides and hydroxides. Environ. Sci. Technol. 36: 1460-1466.
95. Pennell, K.D., S.A. Boyd and L.M. Abriola. 1995. Surface area of soil organic matter reexamined. Soil. Sci. Soc. Am. J. 59: 1012-1018.
96. Qu, F., R.H. Oliveira and P.C. Morais. 2004. Effects of nanocrystal shape on the surface charge density of ionic colloidal nanoparticles. J. Magn. Magn. Mater. 272-276: 1668-1669.
97. Redman, A.D., D.L. Macalady and D. Ahmann. 2002. Natural organic matter affects arsenic speciation and sorption onto hematite. Environ. Sci. Technol. 36: 2889-2896.

98. Saada, A.D., D. Breeze, C. Crouzet, S. Cornu and P. Baranger. 2003. Adsorption of arsenic (V) on kaolinite and on kaolinite-humic acid complexes. Role of humic acid nitrogen groups. Chemosphere 51: 757-763.
99. Saleh, N., K. Sirk, Y. Liu, T. Phenrat, B. Dufour, K. Matyjaszewski, et al. 2007. Surface modifications enhance nanoiron transport and NAPL targeting in saturated porous media. Environ. Eng. Sci. 24: 45-57. doi:10.1089/ees.2007.24.45.
100. Schwertmann, U. and R.M. Taylor. 1989. Iron oxides. p. 145-180. In Dixon, J.B. and S.B. Weeds (eds.) Minerals in soil environments (2nd Edition). Soil Sci. Soc. Am. Book 1, Madison, WI.
101. Selim, H.M. 2012. Competitive sorption and transport of heavy metals in soils and geological media. CRC Press, Boca Raton, FL. p. 426.
102. Seo, D.C., K. Yu and R.D. DeLaune. 2008. Comparison of monometal and multimetal adsorption in Mississippi River alluvial wetland sediment: Batch and column experiments. Chemosphere 73: 1757-1764. doi:http://dx.doi.org/10.1016/j.chemosphere.2008.09.003.
103. Seta, A.K. and A.D. Karathanasis. 1996. Water dispersible colloids and factors influencing their dispersibility from soil aggregates. Geoderma 74: 255-266.
104. Seta, A.K. and A.D. Karathanasis. 1997a. Atrazine adsorption by soil colloids and co-transport through subsurface environments. Soil. Sci. Soc. Am. J. 61: 612-617.
105. Seta, A.K. and A.D. Karathanasis. 1997b. Stability and transportability of water-dispersible soil colloids. Soil Sci. 61: 604-611.
106. Shen, Y.H. 1999. Sorption of humic acid to soil: The role of mineralogical composition. Chemosphere 38: 2489-2499.
107. Shroeder, P.A. 2002. Infrared spectroscopy in clay science. pp. 181-206. In A. Rule and S. Guggenheim, (eds.), CMS workshop lectures, Vol. 11, Teaching Clay Science. The Clay Mineral Society, Aurora, CO.
108. Signes-Pastor, A., F. Burlo, K. Mitra and A.A. Carbonell-Barrachina. 2007. Arsenic biogeochemistry as affected by phosphorus fertilizer addition, redox potential and pH in a west Bengal (India) soil. Geoderma 137: 504-510.
109. Simunek, J., C. He, L. Pang, and S.A. Bradford. 2006. Colloid-facilitated transport in variably saturated porous media: Numerical model and experimental verification. Vadose Zone J. 5 (3): 1035-1047.
110. Sipos, P., T. Nemeth, V.K. Kis and I. Mohai. 2008. Sorption of copper, zinc and lead on soil mineral phases. Chemosphere 73: 461-469. doi:10.1016/j.chemosphere.2008.06.046.
111. Smith, E., R. Naidu and A.M. Alston. 2002. Chemistry of inorganic arsenic in soils: II. Effect of phosphorus, sodium, and calcium on arsenic sorption. J. Environ. Qual. 31: 557-563.
112. Sparks, D.L. 2003. Environmental soil chemistry. Academic Press, (Elsevier Science), San Diego, CA.
113. Sposito, G. 1984. The surface chemistry of soils. Oxford University Press, Oxford, New York.
114. Strawn, D.G., N.E. Palmer, L.J. Furnare, C. Goodell and J.E. Amonette. 2004. Copper sorption mechanisms on smectites. Clay Clay Miner. 52: 321-333.
115. Su, C. and D.L. Suarez. 2000. Selenate and selenite sorption on iron oxides: An infrared and electrophoretic study. Soil Sci. Soc. Am. J. 64: 101-111.

116. Theng, B.K.G. and G.D. Yuan. 2008. Nanoparticles in the Soil Environment. Elements 4: 395-399. doi:DOI 10.2113/gselements.4.6.395.
117. Tsao, T.M., Y.M. Chen and M.K. Wang. 2011. Origin, separation, and identification of environmental nanoparticles: a review. J. Environ. Monitor. 13: 1156-1163.
118. Tsunekawa, S., S. Ito, T. Mori, K. Ishikawa, Z.-Q. Li and Y. Kawazoe. 2000. Critical size and anomalous lattice expansion in nanocrystalline BaTiO3 particles. Phys. Rev. B 62: 3065-3070.
119. Unrine, J.M., P.M. Bertsch and S. Hunyadi. 2008. Bioavailability, trophic transfer and toxicity of manufactured metal and metal oxide nanoparticles in terrestrial environments. Chapter 14, pp. 345-360. In Grassian, V.H. (Ed.), Nanoscience and Nanotechnology Environmental and Health Impacts. John Wiley and Sons.
120. Violante, A. 2013. Chapter Three - Elucidating Mechanisms of Competitive Sorption at the Mineral/Water Interface. In: L. S. Donald, editor Advances in Agronomy. Academic Press. p. 111-176.
121. Voegelin, A. and S.J. Hug. 2003. Catalyzed oxidation of arsenic (III) by hydrogen peroxide on the surface of ferrihydrite: An in situ ATR-FTIR study. Environ. Sci. Technol. 37: 972-978.
122. Wan, J., and J.L. Wilson. 1994. Visualization of the role of the gas-water interface on the fate and transport of colloids in porous media. Water Resour. Res. 30: 11-23.
123. Wang, C.B. and W. Zhang. 1997. Synthesizing nanoscale iron particles for rapid and complete dechlorination of TCE and PCBs. Environmental Science & Technology 31: 2154-2158.
124. Waychunas, G.A., C.S. Kim and J.A. Banfield. 2005. Nanoparticulate iron oxide minerals in soils and sediments: Unique properties and contaminant scavenging mechanisms. J. Nanopart. Res. 7: 409-433.
125. Waychunas, G.A. and H.Z. Zhang. 2008. Structure, chemistry, and properties of mineral nanoparticles. Elements 4: 381-387. doi:DOI 10.2113/gselements.4.6.381.
126. Weng, L., E.J.M. Temminghoff and W.H. Van Riemsdijk. 2001. Contribution of individual sorbents to the control of heavy metal activity in sandy soil. Environ. Sci. Technol. 35: 4436-4443.
127. White, J.L. 1971. Interpretation of infrared spectra of soil minerals. Soil Sci. 112: 22-31.
128. Zhu, R. and S. Lu. 2010. A high-resolution TEM investigation of nanoparticles in soils. pp. 282-284, In Molecular Environmental Soil Science at the Interfaces in the Earth's Critical Zone, Session 4 Springer Berlin Heidel.

Vita

Jessique L. Ghezzi

EDUCATION AND EMPLOYMENT

Educational Background

- B.S. (2007), California Polytechnic State University, San Luis Obispo, Animal Science, Concentration in Pre-Veterinary Medicine and Beef Production, Minor in Rangeland Management
- M.S. (2010), California Polytechnic State University, San Luis Obispo, Agriculture, Concentration in Soil Science

Employment Record

- Graduate Research Assistant, Dept. of Plant and Soil Sciences, University of Lexington, KY 2010-present
- Staff Soil Scientist, Equipoise Environmental Corporation, San Clemente, CA, 2010
- Research & Development Laboratory Technician, Creation's Garden Natural Products, Inc., Valencia, CA, 2009-2010
- Graduate Teaching and Research Assistant, California Polytechnic State University, San Luis Obispo, CA, 2007-2009
- GIS Intern, San Luis Obispo County Public Works Department, San Luis Obispo, CA, 2005-2009
- Ranch Manager, California Polytechnic State University, San Luis Obispo, CA, 2003-2006

PROFESSIONAL RECOGNITION

Awards and Honors

- Lyman T. Johnson Fellowship Recipient 2011, 2012, 2013
- Gamma Sigma Delta Honor Society of Agriculture Member 2013
- Minorities in Agriculture, Natural Resources and Related Sciences
  2014 Alessandra Wayne Memorial 110% Member Award Recipient
  2013 and 2014 Chapter of the Year
  2013 National Graduate Research Poster Contest, 2nd Place
  2013 Regional Impromptu Public Speaking Contest, 3rd Place
  2013-2014 Region 6 Graduate Student Vice President
  2013 University of Kentucky Chapter E-board Member
- Soil Science Society of America
  2013 Early Career Committee Member, as appointed by Society President
  2013 International SSSA-CSA-ASA Conference Presiding Officer of Minerals in the Environment Session I
  2012 International SSSA-CSA-ASA Conference 2nd Place Soil Chemistry Division S2 Graduate Student Poster Competition
  2012 International SSSA-CSA-ASA Conference Presiding Officer of the Solid-Solution Interface Chemistry Session I
- 2008 NASA Develop Program Internship recipient
- Assistant Coach, Soil Judging Team 2008-2011; Awarded 1st Place Group at 2008 Nationals
- 2007 Animal Science Department Outstanding Senior Award

RESEARCH PUBLICATIONS

Refereed Journal Articles

Ghezzi, J.L., A.D. Karathanasis, J. Unrine, C. Matocha, and Y.L. Thompson. 2013. Characterization of environmental nano- and macro-colloid particles extracted from selected soils and biosolids. Applied Environmental Soil Science. 2014: 1-13. doi: 10.1155/2014/506482.

Ghezzi, J.L., A.D. Karathanasis, J. Unrine, C. Matocha, and Y.L. Thompson. 2013. Soil and biosolid nanocolloid and macrocolloid stability characteristics in their natural state and in the presence of lead, copper, arsenic, and selenium contaminants. *Submitted to Applied Environmental Soil Science in March, 2014.*

Published Symposia & Proceedings

Ghezzi, J.L., L.E. Moody, A.F. Garcia and W. Preston. 2009. Influence of clay mineralogy on soil dispersion behavior and water quality. Proceedings, Soil Science Society of America International Annual Conference (No. 251-6), Pittsburgh, PA.

Ghezzi, J.L. May 8, 2011. Seminar: Clays as water quality perpetrators. Plant and Soil Sciences Department, University of Kentucky, Lexington, KY.

Ghezzi, J.L., A.D. Karathanasis, J. Unrine, C. Matocha and Y.L. Thompson. 2011. Properties and interaction of environmental nanocolloids with selected metal contaminants. Proceedings, Soil Science Society of America International Annual Conference (No. 284-4), San Antonio, TX.

Ghezzi, J.L., A.D. Karathanasis, J. Unrine, C. Matocha, and Y.L. Thompson. 2012. Soil and biosolid nanocolloid properties and metal contaminant transport behavior. Proceedings, Soil Science Society of America International Annual Conference (No. 386-4), Cincinnatti, OH.

Ghezzi, J.L., A.D. Karathanasis, J. Unrine, C. Matocha, and Y.L. Thompson. 2013. Environmental nanocolloid properties, contaminant interaction, and transport behavior. Proceedings, Minorities in Agriculture, Natural Resources and Related Sciences National Conference (No. B4), Sacramento, CA.

Ghezzi, J.L., A.D. Karathanasis, J. Unrine, C. Matocha, and Y.L. Thompson. 2013. Soil and biosolid nano- and macrocolloid properties and contaminant interaction. Proceedings, International Conference on the Biogeochemistry of Trace Elements (No. 112), Athens, GA.

Ghezzi, J.L., A.D. Karathanasis, J. Unrine, C. Matocha, O. Wendroth, and Y.L. Thompson. 2013. Transport of Se, As, Cu and Pb contaminants in the presence of soil and biosolid nano- and macro-colloids through undisturbed soil monoliths. Proceedings, Soil Science Society of America International Annual Conference (No. 139-9), Tampa, FL.

Other

Ghezzi, J.L., L.E. Moody, A.F. Garcia and W.Preston. 2010. Influence of clay mineralogy on soil dispersion behavior and water quality. Cal Poly Digital Commons [online]. Published online: doi: http://digitalcommons.calpoly.edu/theses/289